



Università degli Studi di Cagliari

DOTTORATO DI RICERCA

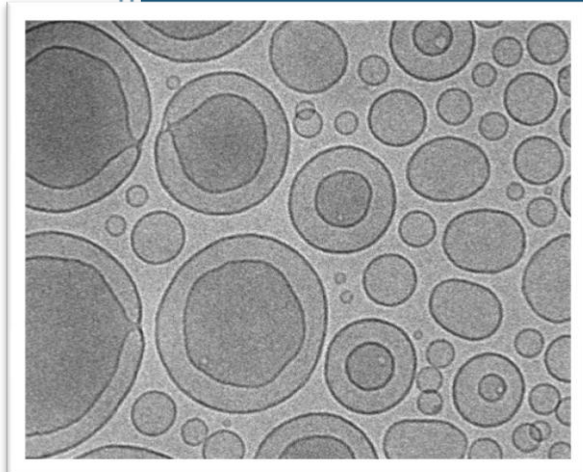
Scuola di dottorato in Scienze e Tecnologie Chimiche e Farmaceutiche

Indirizzo/Corso in Scienze e Tecnologie Chimiche

Ciclo XXV

TITOLO TESI

**Nanostructures for protection and vehiculation of
bioactive molecules**



Settore scientifico disciplinare di afferenza
CHIM/02 Chimica Fisica

Esame finale anno accademico 2011 – 2012

Dottorando: Maura Carboni

Coordinatore Dottorato:

Prof. Mariano Casu

Tutor/Relatori:

Prof. Maura Monduzzi

Dr. Sergio Murgia



Università degli Studi di Cagliari

DOTTORATO DI RICERCA

Scuola di dottorato in Scienze e Tecnologie
Chimiche e Farmaceutiche
Indirizzo/Corso in Scienze e Tecnologie Chimiche
Ciclo XXV

TITOLO TESI

**Nanostructures for protection and vehiculation of
bioactive molecules**

Settore scientifico disciplinare di afferenza
CHIM/02 Chimica Fisica

Presentata da:	<i>Maura Carboni</i>
Coordinatore Dottorato:	Prof. Mariano Casu
Tutor/Relatori:	Prof. Maura Monduzzi Dr. Sergio Murgia

Esame finale anno accademico 2011 – 2012

Summary Index

<i>List of Publications</i>	7
<i>Acknowledgements</i>	8
<i>Abstract</i>	9
1 Chapter	11
1.1 General Background	11
1.1.1 Surfactants	11
1.1.2 The Packing Parameter	12
1.1.3 Liquid crystalline phases	14
1.2 Liquid Crystalline nanoparticles	17
1.2.1 Liposomes.	17
1.2.2 Vesicle lipid gels.	19
1.3 Emulsions	21
1.3.1 Creaming and Sedimentation	22
1.3.2 Flocculation	23
1.3.3 Ostwald Ripening	23
1.3.4 Coalescence	23
1.3.5 Phase Inversion	23
1.3.6 Liquid crystals and emulsions	23
1.4 The monoolein (MO) - water system	24
1.5 The Lecithin (LCT) - water system	25
1.6 Skin delivery	27
1.7 Franz cell	29
1.8 Micrococcus lysodeikticus assay	30
2 Chapter	32
2.1 Theoretical background	32
2.1.1 Introduction	32
2.2 Dinamic Light Scattering	32
2.2.1 Introduction	32
2.2.2 Light Scattering Theories	33

2.2.3	Optical Configuration of a Dynamic Light Scattering Instrument.	35
2.3	Zeta-potential	37
2.3.1	Introduction	37
2.3.2	Electric double layer	37
2.3.3	Measuring ζ -potential	38
2.4	Small angle X-Ray Scattering (SAXS)	39
2.5	Transmission Electron Microscopy (TEM)	43
2.5.1	Cryo-TEM	43
2.6	Rheology	43
2.6.1	Shear Viscosity	44
2.6.2	Shear Induced Structure (SIS)	44
2.6.3	Theory	44
2.6.4	The rheometer	48
2.7	Optical Microscopy	50
2.8	Nuclear Magnetic Resonance (NMR)	51
2.8.1	^2H NMR Quadrupolar Splittings in Anisotropic LC	51
3	Chapter	53
3.1	MO-based formulations	53
3.1.1	Introduction	53
3.2	Materials and methods	56
3.2.1	Materials	56
3.2.2	Formulations preparation	56
3.2.3	Dynamic Light Scattering (DLS) and Zeta (ζ)-Potential Experiments	56
3.2.4	Small-Angle X-ray Scattering (SAXS) Experiments	56
3.2.5	Biological assay	57
3.2.5.1	Cell Cultures and Treatments	57
3.2.5.2	Fluorescence Microscopy and Image Analysis	57
3.2.5.3	MTT Assay for Cell Viability	58
3.2.5.4	Statistics	58
3.2.6	In vitro Release	58
3.2.6.1	Gel Preparation	58
3.2.6.2	Drug Loading Efficiency (E%)	58
3.2.6.3	Deformability Measurements	59

3.2.6.4	Ex Vivo Skin Penetration and Permeation Studies	59
3.2.7	Rheology	59
3.3	Physicochemical, Cytotoxic, and Dermal Release	
	Features of a Novel Cationic Liposome Nanocarrier.	61
3.3.1	Characterization of the Nanocarrier	61
3.3.2	Cytotoxicity Assays	63
3.3.3	Lipid Droplet Evaluation	66
3.3.4	Characterization of the Drug Loaded Nanocarrier	67
3.3.5	Ex Vivo Skin Penetration and Permeation Tests	69
3.4	Physicochemical and rheological properties of a novel monoolein-based vesicle gel	71
3.4.1	From vesicles to vesicle gel and back	71
3.4.2	Rheological characterization of VLG	75
3.5	Conclusions	80
4	Chapter	108
4.1	Emulsions stabilized by liquid crystals	108
4.1.1	Introduction	108
4.1.2	Experimental section	83
4.2	Drug delivery system based on liquid crystals stabilized emulsion .	116
4.2.1	In-vitro release experiments	118
	Bibliography	123

List of Publications

This thesis is based on the following papers:

- 1) ***Physicochemical, Cytotoxic, and Dermal Release Features of a Novel Cationic Liposome Nanocarrier.***
M. Carboni, A. M. Falchi, C. Sinico, M. L. Manca, S. Murgia, S. Lampis, J. Schmidt, Y. Talmon, M. Monduzzi, .
Advanced Healthcare Materials , DOI: 10.1002/adhm.201200302
- 2) ***Physicochemical and rheological properties of a novel monoolein-based vesicle gel.***
R. Angelico, M. Carboni, S. Lampis, J. Schmidt, Y. Talmon, M. Monduzzi, S. Murgia.
Soft Matter, 2013,**9**, 921-928
- 3) ***Lysozyme delivery system based on liquid crystals stabilized emulsion.***
M. Carboni, S. Lampis, M. Monduzzi, S. Murgia, D. Steri.
Manuscript

Other paper not included in the thesis:

Characterization of sodium dodecylsulphate and dodecylphosphocholine mixed micelles through NMR and dynamic light scattering.

G. Manzo, M. Carboni, A. C. Rinaldi, M. Casu, M. A. Scorciapino
Magnetic Resonance in Chemistry, Vol 51, Issue 3, start page 176

Acknowledgements

I would like to express my deep gratitude to Prof. Maura Monduzzi and Dr. Sergio Murgia, my research supervisors, for their patient guidance and useful critiques of this research work.

I would also like to thank Dr. S. Lampis, for introducing me to SAXS and for her advice and assistance in making measurements.

I would like to thank all the co-authors of the publications included in this thesis, in particular Dr. C. Sinico and Dr. M. L. Manca for the precious collaborations during the in vitro release studies, and Dr. A. M. Falchi for the biological assays.

Thanks also to Prof. Y. Talmon for cryo-TEM experiments and analysis.

My grateful thanks are extended to Dr. R. Angelico for rheological measurements and his support in the writing of the rheological section.

I wish to thank Daniela Steri for her contribution to this project.

Special thanks are due to Prof. M. Casu group, particularly to Dr. A. Scorciapino, for the offer of a fruitful collaboration in their research field.

I would also like to extend my thanks to Dr. Andrea Salis and my colleagues Francesca, Luca, Sandrina, Daniela, Elisabetta, and to the whole “Sala dottorandi” crew: I will always remember the good time spent with them in last three years.

Thanks are due to CSGI for partial financial support. Sardegna Ricerche Polaris is thanked for free access to the instruments belonging to the Nanobiotechnology laboratories.

Finally, I wish to thank my parents and my boyfriend Marcello, for their support and encouragement throughout my study.

Abstract

Advances in nanostructured materials and nanotechnologies play a crucial role in engineering innovative systems useful in nanomedicine applications. For example, the most promising drug delivery systems belong to the colloidal domain and, particularly, to the soft matter. Indeed, a growing effort in the discovery of innovative therapies has led to an increasing demand for drug delivery vehicles whose capability should go far beyond the task for which they were originally designed for, that is the simple transport and indiscriminate release of the drug. In principle, every newly formulated nanocarrier should be able to selectively release the drug. Mainly, overcoming the biological barriers that prevent the drug to reach the pathologic site represents the strictest requirement. Thus, a major objective of formulation chemistry is to improve bioavailability, stability, and, last but not least, convenience to the patient.

Lipids, along with proteins and nucleic acids, are essential biomolecules for the structure and function of living matter. Most lipids are fats and waxes, but many others have unique structural features due to their amphiphilic character. The choice of polar lipid based systems to build nanostructured architectures to entrap, protect, and release therapeutic agents with hydrophilic, lipophilic, or amphiphilic nature, appears a good strategy since polar lipids such as phospholipids or monoglycerides are generally friendly toward biological membranes and favor bioadhesion.

The physico-chemical characterization of structure and stability of three different lipid based formulations intended for drug delivery is the central issue in this thesis. The main contents here discussed are outlined as follows. General features of amphiphiles and their behavior in aqueous solutions will be presented in Chapter 1. Chapter 2 is a theoretical review that describes the main techniques used throughout this study. Chapter 3 reports on two different formulations where monoolein, a natural monoglyceride, and lauroylcholine chloride are the main components. Finally, Chapter 4 presents a third formulation: a water-in-oil emulsion stabilized by a liquid crystalline lamellar phase consisting of a technical grade soy lecithin (LCT), triolein (GTO) and water (W).

The first system investigated is a novel cationic liposome nanocarrier, having interesting performance in topical drug delivery. Both monoolein and lauroylcholine chloride, due to their high biocompatibility, can be regarded as strong penetration enhancers. They are combined to rapidly formulate (15 min) a cationic liposome nanostructure endowed of excellent stability (> 6 months) and skin penetration ability, along with low short-term cytotoxicity, as evaluated via the MTT test. Cytotoxicity tests and lipid droplet analysis give a strong indication that monoolein and lauroylcholine synergistically endanger long-term cells viability. The physicochemical features, investigated through SAXS, DLS, and cryo-TEM techniques, reveal that the nanostructure is retained after loading with diclofenac in its acid (hydrophobic) form. The drug release performances are studied using intact newborn pig skin. Analysis of the different skin strata proves that the drug mainly accumulates into the viable epidermis with almost no deposition into the derma. Indeed, the flux

of the drug across the skin is exceptionally low, with only 1% release after 24 h. These results validate the use of this novel formulation for topical drug release when the delivery to the systemic circulation should be avoided.

The second formulation is strictly related to the first one, since it concerns an innovative vesicle-based gel essentially obtained by concentrating the system previously described. A number of vesicular formulations were prepared, in the range of 4–14 wt% of the dispersed phase, to investigate the system evolution from the dilute unilamellar vesicle dispersion (the first formulation) to a vesicle lipid gel. Morphology, thermal stability up to 55 °C, and viscoelastic properties, along with the effect of acid diclofenac inclusion within the formulation, were evaluated by cryo-TEM, SAXS, and rheological measurements. Moreover, the nanostructure of the vesicle dispersion obtained upon gel dilution in water was assessed by cryo-TEM and SAXS, while DLS was used to monitor the formulation stability (size and ζ -potential). All the collected results lead to the conclusion that this new vesicle-based gel displays all the requirements needed for application in the pharmaceutical and cosmetic fields.

The LCT/GTO/W partial phase diagram was investigated by visual inspection and optical microscopy in polarized light, SAXS, and ^2H NMR spectroscopy to define the type of phases and characterize their structural parameters. Ternary LCT/GTO/W mixtures prepared with 85/15 and 90/10 constant mass ratio and increasing amounts of water were investigated. Particularly, it was found that the dominant hexagonal liquid crystalline phase identified at low water content evolves toward an emulsion region stabilized by a lamellar liquid crystalline phase for water content greater than 15% wt/wt. The emulsion having composition LCT/GTO/W = 58/11/31 was chosen to encapsulate the bioactive molecules lysozyme (LSZ) and caffeine. The thermal stability was assessed by means of SAXS in the temperature range 4–55 °C. The drug release performances were studied using Franz cell apparatus and a synthetic membrane made by cellulose acetate. After 24 h, the percentage of protein detected in the release media was equal to 10% of the nominal content of the formulation, while in the case of caffeine 80% of the initial content was released after 15 hours. In both cases, due to the use of a liquid crystalline phase as dispersing medium, burst release of the biomolecules from the formulations is prevented. Evaluation of the residual activity of the released protein was also carried out using the *Micrococcus lysodeikticus* assay. Approximately 30% of the released LSZ retains its enzymatic activity. The full biocompatibility of the formulation ingredients along with the absence of burst release for the investigated cases allow suggesting this formulation as a promising topical drug carrier for sustained release. Indeed, this formulation presents other advantages over conventional creams and ointments such as higher storage stability, good production feasibility, higher kinetic stability and, in particular, the absence of organic solvents in the preparation.

1 Chapter

1.1 General Background

1.1.1 Surfactants

Surfactants are amphiphilic molecules which possess a hydrophilic (water-loving) head group and a hydrophobic (water-hating) tail. The hydrophobic group in a surfactant molecule is usually a hydrocarbon chain but may be a fluorocarbon or siloxane chain.

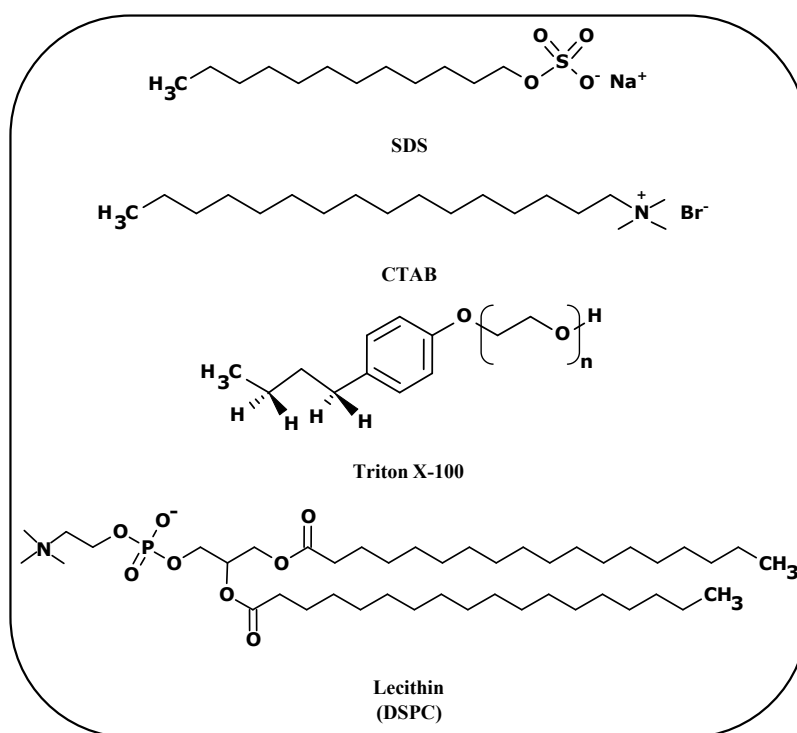


Figure 1.1: Some examples of surfactants molecules.

The hydrophilic group is polar and may be either ionic or nonionic. Depending on the nature of the hydrophilic head, major surfactants can be divided into anionic, cationic, catanionic, zwitterionic and non ionic classes.^{1,2} Some examples are reported in figure 1.1.

Due to hydrophobic/hydrophilic competitions, surfactant molecules tend to migrate to interfaces or surfaces and orientate so that the polar group lies in water and the apolar group is placed out of it, and eventually in oil. In this way surfactants are able to lower the surface tension of a liquid;³ that is why the surfactant name: “**surface active agent**”. Surfactant molecules can also assemble in the bulk solution thus forming aggregates such as micelles and vesicles (see fig. 1.2). The concentration at which surfactants begin to form micelles is known as the critical micelle concentration (CMC).

Depending on temperature - there is a narrow temperature range , referred as Krafft point, above which the solubility of a surfactant rises sharply - type and concentration of the solvents, there may exist direct or

inverted molecular aggregates. In direct systems, the polar solvent is a continuous medium, while in the case of inverted systems, the polar solvent is confined in closed regions.

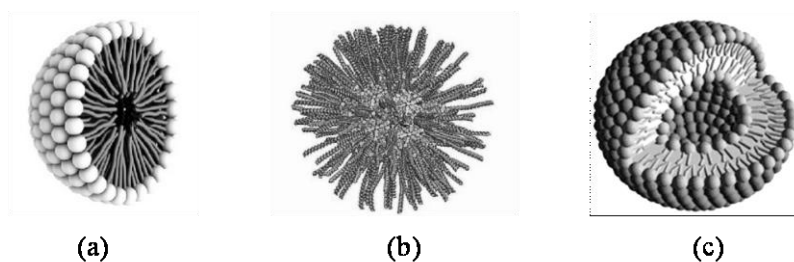


Figure 1.2: Structure of direct (a) and inverted (b) micelles and a cross section of a liposome (c).

Depending on surfactant shape, at a concentration very close to the CMC the micelles can be spherical. As the concentration is increased, the micelles may remain spheroidal or grow and become elongated, cylindrical or disk like. Indeed, rod-like or disk-like micelles are commonly observed.⁴ Surfactants may also form liquid crystalline phases (LC).

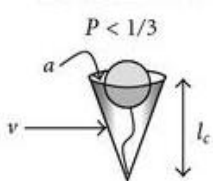
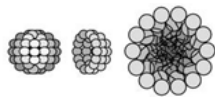

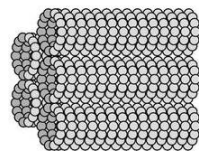

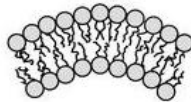



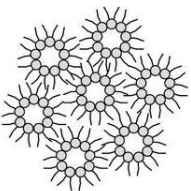
1.1.2 The Packing Parameter

The self-assembly of surfactants in solutions has been widely investigated both experimentally and theoretically, because numerous practical applications take advantage of the resulting aggregates. The structure of these aggregates influences the properties of surfactant solutions, such as, for example, their solubilization capacity for hydrophobic substances or their viscous and viscoelastic properties, and consequently, the performance of surfactants in various applications. To select molecules that would yield desired structures such as spherical, globular or rodlike micelles, or spherical bilayer vesicles, it is necessary to know how the molecular structure of the surfactant controls the shape and size of the resulting aggregate. The molecular packing parameter⁵ allows a simple and intuitive insight into the self-assembly phenomenon. The molecular packing parameter P is defined as:

$$P = \frac{v}{al} \quad \text{Eq 1.1}$$

where v and l are the volume and the length of the surfactant tail and a is the surface area of the hydrophilic head group.

⁶**Table 1.1** Molecular shapes and association structures of surfactants

Packing shape	Packing parameter	Phase formed	Lipid examples
<p>CONE</p> 	<p>< 1/3 (spheres)</p>		<p>Lysophospholipids (e.g. LPC, LPE, etc.)</p>
<p>TRUNCATED CONE</p> 	<p>1/3-1/2 (Rods)</p>		<p>Free fatty acids (e.g. oleate, stearate, etc)</p>
<p>TRUNCATED CONE</p> 	<p>1/2 – 1 (lamellar, flexible bilayers, vesicles)</p>		<p>Double-chained lipids with large head group areas and fluid chains</p>
<p>CYLINDER</p> 	<p>~ 1 (lamellar, planar bilayers)</p>		<p>Double-chained lipids with small head group areas, anionic lipids and saturated chains</p>
<p>INVERTED TRUNCATED CONE</p> 	<p>> 1 (hexagonal HII, micellar reverse)</p>		<p>Double-chained lipids with small head group areas, non-ionic lipids and polyunsaturated chains</p>

The magnitude of this parameter can be estimated for simple hydrocarbon amphiphiles from molecular dimensions, by using Tanford's formulae.⁴ For a saturated chain with n carbon atoms, volume and lengths are given by the following relationships:

$$v = (27.4 + 26.9 n) \text{ \AA}^3 \quad \text{Eq.1.2}$$

$$l_{max} = (1.5 + 1.26 n) \text{ \AA} \quad \text{Eq.1.3}$$

while the magnitude of the head-group area depends on the amphiphile, as well as on the degree of hydration and temperature.

The packing parameter is related to the mean and Gaussian curvatures of the aggregate, respectively H and K , on the basis of the following equation derived from the differential geometry⁷:

$$\frac{v}{al} = 1 + HI + \frac{KI^2}{3} \quad \text{Eq.1.4}$$

Depending on the P value, different arrangements can arise from the surfactants' molecules into structured aggregates. Table 1.1 shows the expected structure for different P values. Which structure is formed depends not only on the molecular structure of the lipid. Indeed it is possible to affect the phase behavior by mixing different lipids, by changing the hydration level and environmental conditions, such as temperature, pressure, pH, ionic strength and types of additives.

1.1.3 Liquid crystalline phases

Liquid crystals can be divided into thermotropic and lyotropic phases. The phase transitions of thermotropic liquid crystals, which form exclusively as a result of their molecular shapes and mutual interactions, depend on temperature, while those of lyotropic liquid crystals, which form in the presence of solvents, depend on both temperature and concentration. A brief overview of lyotropic liquid crystals will be given here.

LAMELLAR PHASES. In the lamellar phase, amphiphilic molecules are arranged in bilayer sheets separated by layers of water (see fig. 1.3). Different types of lamellar phases, such as L_α , L_β , L_c have been observed in lyotropic mixtures. The lamellar phase is characterized by a one-dimensional periodicity.

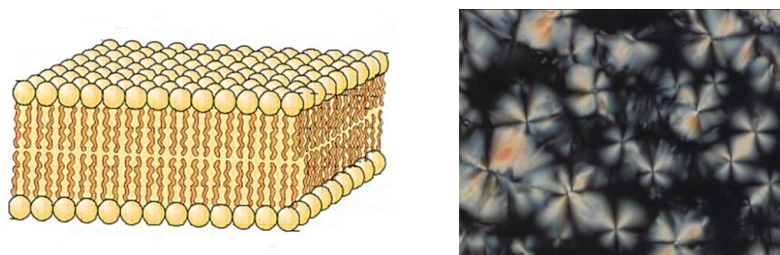


Figure 1.3: Schematic representation of a lamellar phase (left) and its typical “maltese crosses” in the polarizing microscope (right).

The L_β phase differs from the L_α phase by the state of the carbonic chains. In fact, in the L_α phase the hydrophobic chains are molten, while in the L_β phase they possess a partial crystallinity which induces long-range ordering between lamellae. The L_c phase has the chains of each surfactant molecule “frozen” into specific lattice sites and is the most ordered of the three lamellar phases.

Like all anisotropic phases, lamellar mesophases exhibit distinct optical textures, when confined in thin slabs between crossed polarizers and viewed through an optical microscope with polarized light. Typically the texture is mosaic-like, often accompanied by “Maltese crosses” (see fig. 1.3).

HEXAGONAL PHASES. The standard picture of a hexagonal mesophase consists of a dense packing of cylindrical micelles, arranged on a 2D hexagonal lattice (see fig. 1.4 a).

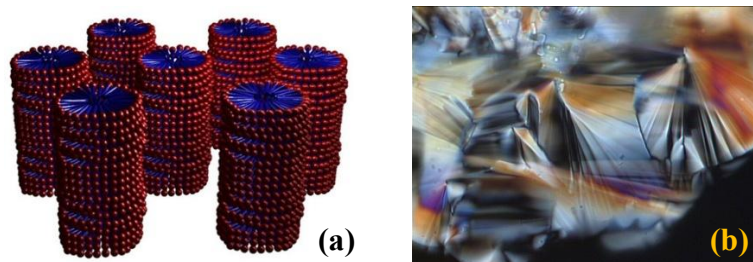


Figure 1.4: Schematic representation of a direct hexagonal phase (a) and their typical pattern in the polarizing microscope (b).

In normal topology the hydrocarbon chains are contained within the cylindrical aggregates such that the polar-apolar interface has a direct mean curvature. Inverse topology hexagonal phases have water within the cylindrical aggregates and the hydrocarbon chains fill the voids between the hexagonally packed cylinders. Normal topology hexagonal phases are denoted by H_I while inverse topology hexagonal phases are denoted by H_{II} . When viewed under a polarized light microscope hexagonal phases exhibit birefringence, giving rise to characteristic optical textures. Typically these textures are smoke-like, fan-like or mosaic in appearance (see fig. 1.4 b). Generally the hexagonal phases are highly viscous.

CUBIC PHASES. Cubic phases are structures which possess three-dimensional periodicity. There are two types of molecular aggregates, micellar and bicontinuous structures: in the cubic micellar phase, micelles are packed on a cubic (face-centered or body-centered) lattice, while bicontinuous cubic structures consist of a curved bilayer lying on an Infinite Periodic Minimal Surface (IPMS). Infinite Periodic Minimal Surface (IPMS) are surfaces entirely composed of saddle points, showing zero mean curvature. These minimal surfaces are generally located at the lipid bilayer midplane (reversed phases) or in the middle of the water layer (normal phases).

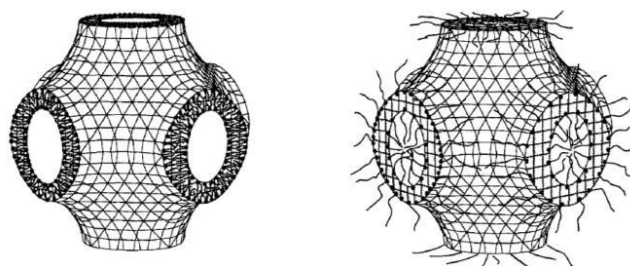


Figure 1.5: Schematic picture of one possible bicontinuous cubic phase of symmetry $Im3m$. (Left) A reversed and (right) a direct cubic phase.

Three types of bicontinuous cubic mesophases have been identified in lyotropic lipid mixtures, belonging to space groups $Pn3m$, $Im3m$, and $Ia3d$, as sketched in figure 1.6.

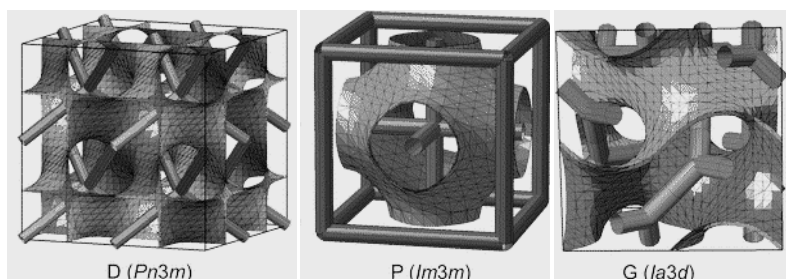


Figure 1.6: The three minimal surfaces, D, P, and G, which sit at the bilayer mid-plane and underlie the bicontinuous cubic phases $Pn3m$, $Im3m$, and $Ia3d$.

SPONGE PHASE (L_3). It consists of a spatially disordered hyperbolic amphiphilic bilayer in water, and can be viewed as a lamellar phase break-up, in which channels connect only locally ordered bilayers (see fig. 1.7). Sponge mesophases are characterized by flow birefringence (giving anisotropic optical textures) while they are isotropic at rest. Sponge phases can also be considered to be a melt of bicontinuous cubic phase.



Figure 1.7: Schematic of the L_3 phase (sponge) structure.

INTERMEDIATE PHASES. There are experimental evidences of the existence of lyotropic phases with lower symmetries, which are sometimes called “intermediate phases”. Usually, they are observed in mixtures with long chain amphiphiles or amphiphiles with restricted flexibility. Examples are the rhombohedral phase and the “mesh” phase in which the lamellae present pores or holes filled up with the solvent (see fig. 1.8). These holes may or may not be correlated from one layer to the other.

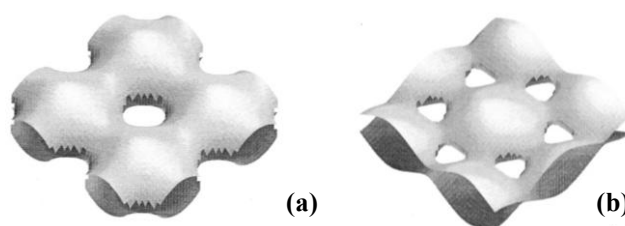


Figure 1.8: (a) sketch of one layer of the centered tetragonal mesh structure and (b) sketch of one layer of the rhombohedral mesh structure.

1.2 Liquid Crystalline nanoparticles

Liquid crystalline nanoparticles are receiving much attention because of their potential applications in various areas, including the formulation of functional food and drug nanocarriers.⁸⁻¹¹ The category of nanoparticulate carriers includes liposomes, cubosomes (aqueous dispersions of inverted-type bicontinuous cubic phases) hexosomes (aqueous dispersions of inverted-type hexagonal phase) and dispersed sponge phases. Cryo-TEM images of liposomes, cubosomes, hexosomes and dispersed sponge phase are reported in figure 1.9. Lipid liquid crystalline nanoparticles are commonly prepared using either a bottom-up or a top-down approach. In general, a hydrophilic polymeric stabilizer is used to efficiently cover the outer surface of the dispersed particles and to retain the internal nanostructures. The bottom-up approach is mainly accomplished by diluting and then homogenizing a liquid mixture of the emulsifier and lipid in water (nanoparticles form by nucleation in the aqueous solution), while the top-down approach implies the fragmentation of a massive LC phase in an aqueous solution of the emulsifier.

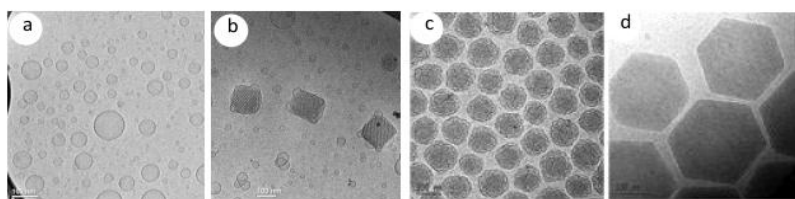


Figure 1.9: Cryo-TEM images of liposomes, cubosomes, a dispersed sponge phase and hexosomes.

The latter method allows, in principle, for the entrapment of hydrophilic drugs (oligonucleotides, peptides, and proteins) that, on the contrary, cannot be easily introduced when preparing the dispersions directly from the components.

1.2.1 Liposomes.

Liposomes (from the greek words lipo (fat) and soma (body)) are small spherical vesicles in which one or more aqueous compartments are completely enclosed by a bilayer of amphiphilic molecules, such as phospholipids and cholesterol. They have been identified by Alec Bangham and his group, at Babraham Institute of Animal Physiology in the '60, studying phospholipid dispersions as a model for a cell membrane. The first formal reference to "liposomes" appears in a 1968 paper entitled "Phospholipid spherules (liposomes) as a model for biological membranes" authored by Dr. Weissmann and his post-doctoral colleague Grazia Sessa.¹²

Liposomes were first considered as safe delivery vehicles for various bioactive agents for therapeutic as well as diagnostic applications, including drugs, vaccines, cosmetics and nutraceuticals, probably because of their three main characteristics. They are typically small in size and fall in the range of about 25 to 1000 nm and easily disperse in the aqueous medium. Second, their closed bilayer structures are capable to encapsulate water-soluble drug molecules in their aqueous core and oil-soluble ones in the hydrophobic region of the

bilayer even simultaneously, thus providing a synergistic effect. The third characteristic is that they can shield an encapsulated molecule from free radicals, metal ions, pH and enzymes that might otherwise result in degradation of the bioactive compound. Liposomes are also effective in reducing systemic toxicity of encapsulated drugs using a lower dosage formulation.

For many applications, narrow vesicle size distribution as well as high stability during a long storage time period is necessary. Thus, the preparation method of vesicles is very important, since the formation of most vesicles requires input of external energy. There are four general methods employed to produce liposomes that are typically known as:

- Hydration of dry lipid film: this is a multistep process where a lipid thin film is created on the flask walls by evaporation of chloroform and rehydrated using appropriate buffer solution causing vesicular formation.
- Ethanol injection: injection of ethanolic solution of lipids into rapidly stirred aqueous buffer phase usually gives small and meta-stable vesicles.
- Detergent dialysis: this foresees the use of a suitable detergent, such as octyl glucoside, to solubilize the dry lipid in buffer solution followed by dialysis to remove the detergent.
- Sonication or mechanical stirring of aqueous lipid dispersion: vigorous shaking suffices for sample homogenisation.
- Finally, extrusion using membrane filters of a chosen pore size allows the formation of monodisperse and unilamellar vesicles.

Liposomes are generally classified by grouping them based upon their lamellarity, size, surface charge, and functionality. These properties can be tuned substantially changing composition and/or method of preparation. They can be formed of a single bilayer membrane (fig. 1.2c), so called small unilamellar vesicles (SUV having diameter $d \sim 20-100$ nm), large unilamellar vesicles (LUV, $d > 100$ nm), giant unilamellar vesicles (GUV, $d > 1000$ nm) based on their size ranges. If more than one bilayer is present then they are called multilamellar vesicles (MLV) or multivesicular vesicles (MVV) when small vesicles are trapped within the large vesicles, some schematic representation are reported in fig. 1.10. The introduction of positively or negatively charged lipids provides the liposomes a surface charge that can be used for specific application. The presence of positively charged surfactant facilitates binding with anions such as those found in DNA: therefore cationic liposomes (CLs) can be utilized as non-viral vectors in gene therapy. This kind of nucleolipidic complex is referred as lipoplex.¹³ In the past two decades many studies¹⁴ have been carried out giving evidence that CLs are able to selectively deliver active agents efficiently and specifically to certain tissues such as tumor endothelium, lungs and liver: this makes them quite attractive for cancer and other genetic pathologies therapy.

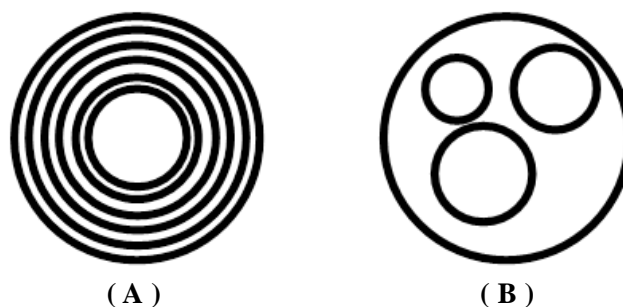


Figure 1.10: Schematic presentation of a MLV (A) and a MVV (B).

Since the stratum corneum, the external layer of the skin, contains a high ratio of negatively charged lipids, cationic liposomes were shown effective for topical and transdermal delivery too. Application of vesicles for skin disease was first shown in '80 by Mezei and Gulasekharam;¹⁵ thereafter, using liposomes in dermal and transdermal drug delivery has been improved constantly. An example is the addition to formulations of penetration enhancers such as ethanol to promote drug permeation (ethosome: liposomes containing ethanol), or so called edge activators, such as sodium cholate or sodium deoxycholate¹⁶⁻¹⁸ that makes liposomes ultradeformable and able to pass the skin barrier squeezing through its pores.^{17,19,20}

Liposome surface can be covered with polymers (an example is reported in fig. 1.11 A) such as polyethylene glycol (PEG) - they are referred as pegylated or stealth liposomes - and exhibit prolonged half-life in blood circulation. These sterically stabilized liposomes are involved in passive targeting of the material they carry. Liposomes can be conjugated to antibodies or ligands to enhance target-specific drug therapy (an example is reported in fig. 1.11 B): they are known as immune-liposomes and use active targeting to release the encapsulated drug on the specific receptor.

Liposomes made from synthetic lipids are also being used. They include nonionic surfactant lipids and polymers, which can be chemically more stable than others and can improve bioavailability of active compounds.

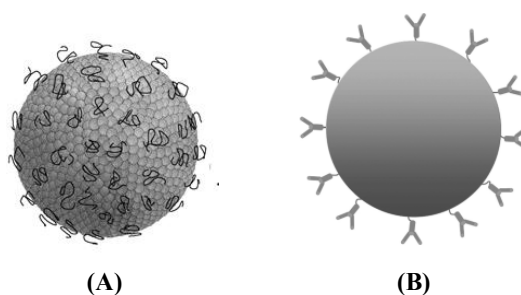


Figure 1.11: liposomes with 2 kind of surface modification. (A) pegylated (B) conjugated with ligands.

1.2.2 Vesicle lipid gels.

Generally speaking gels are soft, solid-like, or semisolid in nature, and consist of at least two components, one of these being a liquid that is present in a substantial quantity. Although the liquid content is high, on a

time scale of seconds, a gel should not flow under the influence of its own weight. Thomas Graham coined the term “gel” in 1864²¹ and it has been in use ever since then. Vesicular lipid gels (VLGs) are highly concentrated lipid dispersions of semisolid consistency and vesicular morphology.^{22–24} Dispersed vesicles yield low-viscosity solutions as long as their effective volume fraction (given by the volume fraction of the bilayer material and the encapsulated solvent) remains well below that of densely packed spheres. Once an effective volume fraction of 0.494 is reached, a hard-sphere crystallization would be expected to begin.²⁵ The formation of a vesicle gel depends on the size and concentration of the vesicles. They are under investigation as potential implantable depots for sustained release of bioactive agents.²⁶ VPGs can be prepared by high-pressure homogenisation of high concentrations of phospholipid molecules. Vesicular phospholipid gels can also be prepared by the heating method²⁷ without using toxic volatile organic solvents or detergents. Upon dilution, VPGs constitute normal diluted liposome dispersions. Then the origin of the rheological properties of vesicle gels result primarily from steric interaction between spherical objects and depend much less on specific molecular interactions, which are often important for other gel structures. A key parameter is the effective volume fraction of the vesicles, since for gel formation of spherical objects dense packing is required. However, the rheological properties of the vesicle system, such as the elastic or shear modulus (as well as the yield stress), not only depend on the dense packing but will also strongly depend on the strength of interaction between the vesicles, e.g. on the electrostatic interactions between the vesicles.²⁸ It appears that vesicular lipid gels could be useful as parenteral depot formulations. Alternatively, by mixing with excess buffer, VLGs may be converted to unconcentrated liposome suspensions with small particle sizes.²⁹ Consequently, VLGs are also useful as intermediates for liposome dispersions, especially those with drugs with high leakage rates and poor storage stabilities. By virtue of the *in vitro* drug release and the entrapment investigations of vesicles gels built up of phospholipids, containing bioactive agents such as 5-fluorouracil³⁰ and chlorhexidine,³¹ good applicability of these carriers is expected as implantable gels or as re-dispersed liposomes.

1.3 Emulsions

An emulsion is a dispersion of drops in another liquid where the two liquids are not miscible in all proportions; it is thus a two phase system. The phases are, for simplicity, called oil and water. In this context “oil” means a hydrophobic liquid, e.g. benzene, hexadecane, or a triglyceride oil; and “water” means an aqueous solution. Nearly all emulsions contain at least another substance, generally referred as “emulsifier”. The emulsifier is needed to form an emulsion, and its properties determine whether the emulsion will be of the oil in water (o/w) or of the water in oil (w/o) type. All emulsifiers are surfactants that adsorb at the oil-water interfaces, lowering the interfacial tension γ . Since the surfactant must be soluble in at least one of the two phases in order to be active during emulsification, the adsorption layer formed will generally be a Gibbs type monolayer.

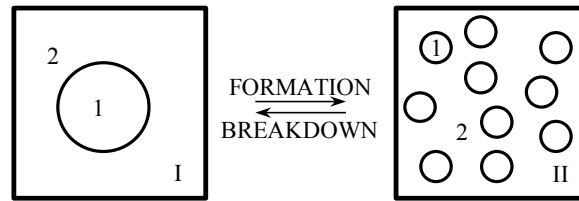


Figure 1.12: Schematic representation of emulsion formation and breakdown.

In order to understand the mechanism of formation and breakdown of an emulsion, consider a system in which an oil is represented by a large drop 1 of surface area A_1 immersed in a liquid 2, which is now subdivided into a large number of smaller droplets with total surface area A_2 (therefore $A_2 \gg A_1$), as shown in fig. 1.12. It can be assumed that the interfacial tension γ_{12} is almost the same for the large and smaller droplets as the latter are generally in the region of 0.1 μm to few microns in size.

The change in free energy in going from state I to state II is given by two contributions: the surface energy term (that is positive) that is equal to $\Delta A\gamma_{12}$ (where $\Delta A = A_2 - A_1$); the entropy of dispersions term which is also positive (since the production of a large number of droplets is accompanied by an increase in the configurational entropy) which is equal to $T\Delta S^{\text{conf}}$. From the second law of thermodynamics:

$$\Delta G^{\text{form}} = \Delta A\gamma_{12} - T\Delta S^{\text{conf}} \quad \text{Eq. 1.5}$$

In most cases, $\Delta A\gamma_{12} \gg T\Delta S^{\text{conf}}$, which means that ΔG^{form} can be positive, which implies that the formation of emulsions is not spontaneous, unless a strong decrease of γ_{12} occurs. When spontaneous emulsification takes place, a microemulsion, that is a thermodynamically stable system, forms. When the surfactant is not efficient enough in decreasing γ_{12} , work must be added to obtain emulsification. In the latter case, emulsions, that are kinetically stable systems only, are formed. Generally the emulsions droplets are in the range of microscopic or colloidal size (typically around 1 μm) for this reason they appear opaque. Emulsions made by the mechanical shaking of the pure immiscible liquids are very unstable and break rapidly towards the

separated bulk phases. They may be stabilized by the addition of surfactants which protect the newly formed droplets from coalescence.³²

In the absence of a strong stabilization mechanism, the emulsion will break by sedimentation, creaming, flocculation, coalescence, Ostwald ripening, or a combination of all these processes. This situation is illustrated graphically in fig. 1.13 where different paths for emulsion breakdown processes are represented. In the presence of a stabilizer (surfactant), an energy barrier is created between the droplets and therefore the reversal from state II to state I is slowed down as a result of the presence of these energy barriers (Fig.1.12).

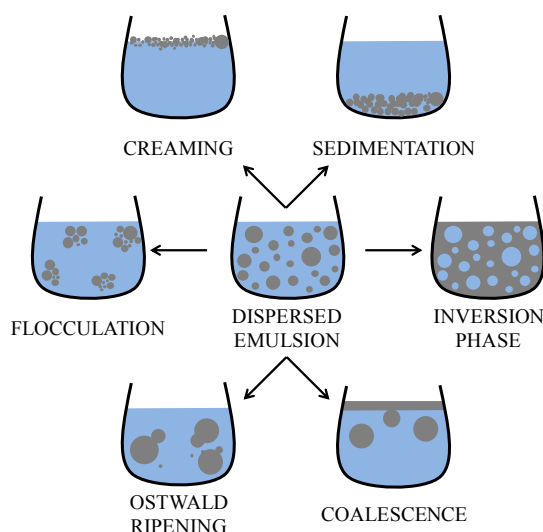


Figure 1.13: Schematic representation of the various breakdown processes in emulsions.

Thus, in the presence of the energy barriers, the system becomes kinetically stable. The physical phenomena involved in each breakdown process are not simple, and requires an analysis of the various surface forces involved. In addition, these processes may take place simultaneously rather than consecutively, which in turn complicates the analysis.³³ A summary of each of the breakdown processes is provided in the following sections, together with details of each process.

1.3.1 *Creaming and Sedimentation*

Creaming is the process by which buoyant droplets emulsion tend to rise to the top of a container. It is the same process as sedimentation, but in the opposite direction.³⁴ Taking into account that emulsions with monodisperse droplets, cannot be easily produced, polydispersity of the dispersed phase along with the low viscosity of the medium and significant differences in the density between the dispersed phase and the medium are always factors that tend to reduce the kinetic stability. Thus creaming or sedimentation occur as a result of external forces, usually gravitational or centrifugal. When such forces exceed the thermal motion of the droplets (Brownian motion), a concentration gradient builds up in the system such that the larger droplets move more rapidly either to the top (if their density is less than that of the medium) or to the bottom (if their density is greater than that of the medium) of the container. In the limiting cases, the droplets may

form a close-packed (random or ordered) array at the top or bottom of the system, with the remainder of the volume occupied by the continuous liquid phase.

1.3.2 Flocculation

This process refers to aggregation of the droplets (initially without any change in primary droplet size) into larger units. It is the result of the van der Waals attractions which are universal with all disperse systems. Flocculation occurs when there is not sufficient repulsion to keep the droplets apart at distances where the van der Waals attraction becomes very weak. Flocculation may be either strong or weak, depending on the magnitude of the attractive energy involved.

1.3.3 Ostwald Ripening

If the droplets in an emulsion are polydisperse, a possible breakdown mechanism is the Ostwald ripening: the smaller drops are gradually incorporated in the larger ones as a result of different solubility. The driving force is the difference in the chemical potential, and hence in solubility, of the material between small and large droplets. The material is transported by diffusion: the mass transfer process can be called isothermal distillation; and the result is disproportionation (more specifically coarsening) of the droplet size distribution. Ostwald ripening generally proceeds with the cube of the average radius varying linearly with time. Initially the process reduces the polydispersity, but the progress of the process brings to exceeds the optimal curvature of the emulsifier and phase separation occurs.³⁵

1.3.4 Coalescence

This refers to the process of thinning and disruption of the liquid film between the droplets, with the result that fusion of two or more droplets occurs to form larger droplets. The limiting case for coalescence is the complete separation of the emulsion into two distinct liquid phases. The driving force for coalescence is the surface or film fluctuations; this results in a close approach of the droplets whereby the van der Waals forces are strong and prevent their separation.

1.3.5 Phase Inversion

Phase-inversion can occur as a result of temperature modifications near the phase-inversion temperature (p.i.t.) of a non ionic surfactant when it is used to stabilize an emulsion. Incidentally, it is often possible to reach volume fractions up to about 0.98 without phase-inversion occurring, provided that the Laplace pressure of the droplets is rather small.^{36,37}

1.3.6 Liquid crystals and emulsions

The description about various liquid crystals has been given in section 1.1.3. The stabilization of emulsions by lamellar liquid crystals has been reported by Friberg et al.³⁷ In order to further stabilize emulsions, crystallization of lamellar liquid crystalline phases located at the water/oil interface resulting in the formation

of a so-called gel phase has been reported.^{38–40} It has been demonstrated by Engels et al. that changes in the type and concentration of the co-emulsifier caused the formation of a lamellar gel phase surrounding the oil droplets inside an oil-in-water (o/w) emulsion which increased the stability of the emulsion from 5 days to more than 1 month.⁴⁰ It was found that the physico-chemical properties of the system remained unaffected by the change of the co-surfactant. The viscous lamellar film surrounding the emulsion droplets may be several layers thick and reduces the attraction potential between the droplets. As a result, the lamellar layer acts as a barrier against coalescence.³⁷ Emulsions containing a third phase or multimolecular layers of lyotropic liquid crystals are often found in cosmetic products and are therefore widely used by the cosmetics industry to adjust or optimize specific properties of the product such as viscosity or consistency, storage stability or application convenience.⁴¹ Recently, it has been reported that long-term stable w/o emulsions can be obtained by dispersing water in the lamellar and reverse hexagonal phases formed by monoolein-based systems.^{42,43} Skin permeation experiments demonstrated that emulsions containing liquid crystalline phases compared to an emulsion without liquid crystals, showed enhanced skin penetration of the hydroquinone and octadecenedioic acid. The increase in skin penetration was attributed to an increased partitioning of the drugs into the skin. In the case of salicylic acid, no effect on skin penetration of liquid crystalline phases in emulsion was observed. This effect was suggested to be due to different interaction of drug and surfactants forming liquid crystalline phases in the emulsions.⁴⁴

1.4 The monoolein (MO) - water system

Monoolein (MO), or glycerol monooleate, is a well known polar, nonionic lipid commonly used as an emulsifying agent and as a food additive since the 1950s.⁴⁵

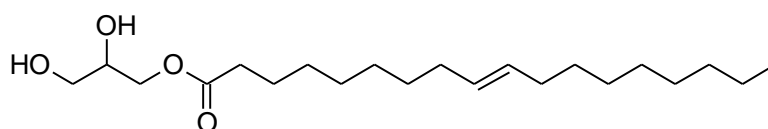


Figure 1.14: Monoolein structure.

MO swells in water, giving rise to several lyotropic liquid crystalline structures,^{38,46–49} as shown in its phase diagram in figure 1.15.

Upon increasing the water content the MO/W binary system shows a small region of reverse micellar (L_2) phase followed by a lamellar ($L\alpha$) phase, and by a C_G (Ia3d space group) and a C_D (Pn3m space group) bicontinuous cubic phase. The C_G phase evolves towards a reverse hexagonal (H_{II}) phase above 80 °C, whereas the C_D phase can coexist with water excess.

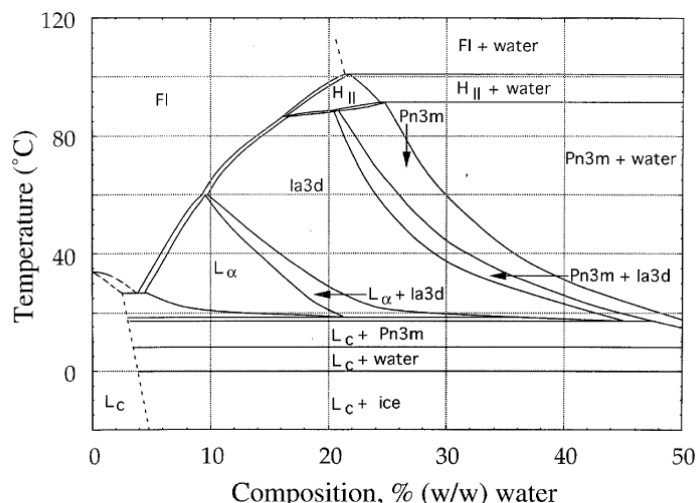


Figure 1.15: Phase diagram of the MO/W system at ambient pressure. The concentration is expressed as weight of water per weight of the mixture. Phases are labeled as given in the text. FI stands for fluid isotropic phase.

From a pharmaceutical viewpoint, MO shows a number of interesting properties. MO is nontoxic, biodegradable, and biocompatible material classified as GRAS (generally recognized as safe), and is included in the FDA Inactive Ingredients Guide and in nonparental medicines licensed in the UK. Its biodegradability comes from the fact that monoolein can undergo the lipolysis due to diverse kinds of esterase activity in different tissues. The use of MO-based systems, in particular bicontinuous cubic and hexagonal LC phases, in the drug delivery field is reported in several works.^{38,46-49} These LC phases have the potential for control over release rates, low toxicity, and versatility in application across a range of administration regimes, including oral,⁵⁰ transdermal,^{51,52} and parenteral delivery.^{7,53,54}

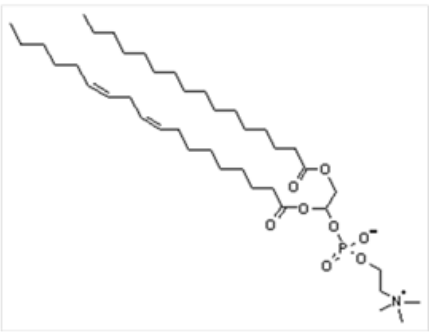
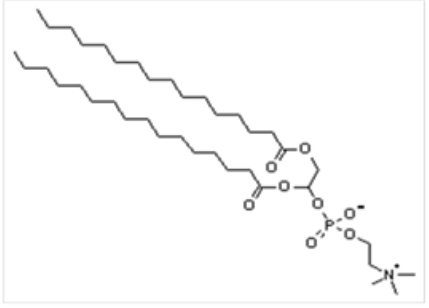
1.5 The Lecithin (LCT) - water system

Lecithin is usually used as synonym for phosphatidylcholine (PC), which is the major component of a phosphatide fraction which is frequently isolated from either egg yolk, or soya beans and is commercially available in high purity. PC is a mixture of differently substituted sn-glycerol-3-phosphatidylcholine backbones. As can be seen from Table 1.2, the structure of PC is variable and dependent on fatty acid substitution. In the sn-1-position, saturated acyl-groups, and in sn-2-position, unsaturated species are more common.⁵⁵ Fatty acids of mainly 16-20 C in chain length dominate in egg PC. The sn-1-chain typically shows an average of 16 C, whereas the sn-2-chain shows an average of 18 C. Naturally occurring unsaturated fatty acids are almost entirely of all-cis-conformation.⁵⁶

The complete binary phase diagram of lecithin-water is presented in figure 1.16.⁵⁷ Dry egg lecithin is present in at least partially crystalline form until about 40 °C. Above this temperature it forms a “wax-like” phase up to about 88 °C. From 88 to 109 °C it forms a viscous isotropic phase which gives face-centered cubic

spacings. Above 110 °C its texture is “neat” and the structure is assumed to be lamellar until its final melting point at 231 °C.

Table 1.2: Different species of PC and their natural occurrence in egg yolk lecithin (mol/mol) (values after Kuksis).⁵⁵


<p>Palmitoyl/Linoleoyl [16:0/18:2] - PC (PLPC) 21.8% in Egg PC</p>

<p>Di-Palmitoyl [16:0/16:0]- - PC (DPPC) 0.72% in Egg PC</p>

Hydrated lecithin forms (except for a small zone of cubic phase at low water concentrations and high temperature) a lamellar liquid crystalline phase. Soya lecithins contain more Phosphatidic Acid (PA) and Phosphatidylinositol (PI) than egg lecithin, and are also reported to show excellent emulsifying properties,⁵⁸ which led to development of various parenteral emulsions.

This phase contains up to 45% water at 20 °C. Mixtures containing more water separate into two phases, the lamellar liquid crystalline phase and water. In the melting curve of hydrated lecithin a eutectic is noted at about 16% water and the cubic phase seen when less water is present disappears at this composition of the mixture.

The surface area per molecule at 21°C has been determined as 59.3 Å². With increasing water content, molecular area increases to about 71.7 Å², and lamellar structures (L_α) become predominant.

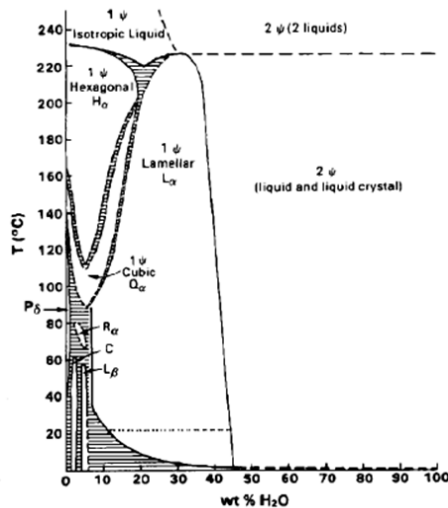


Figure 1.16: Influence of temperature and water content on phases of lecithin (modified after Small). C = Crystalline / H₂ = Hexagonal liquid crystalline / L_α = Lamellar liquid crystalline / L_β = Lamellar gel / Q_α = Cubic disordered / R_α = Rhombohedral disordered.

1.6 Skin delivery

Skin is the largest organ in the human body and functions as a protective barrier. The large surface area (1.8 m²) and easy accessibility of skin make it one of the attractive routes for drug delivery. Skin route can be used in the treatment of dermatological and systemic diseases. Drug application on the skin is simple, controlled and non-invasive. However, the outermost layer of the skin, stratum corneum (SC), limits drug absorption through the skin.⁵⁹ As showed in Figure 1.17 SC can be described as a “brickwall”, in which the dead protein containing corneocyte remnants are embedded in the intercellular lipid matrix (mortar).

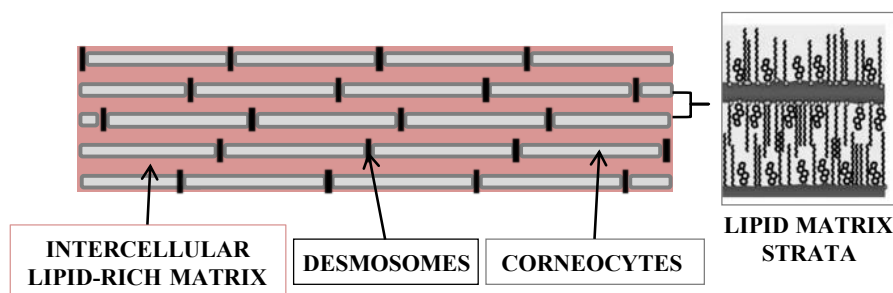


Figure 1.17: Diagram of the brick and mortar model of the stratum corneum with a simplified lamellar organization of intercellular domains showing the major stratum corneum lipids.

Drugs can permeate either across the stratum corneum, or via hair follicles or sweat glands. Penetration pathways are sketched in figure 1.18. Permeation through stratum corneum takes place through the lipid matrix that is critically important barrier structure in the skin.⁶⁰ Permeation through hair follicles and sweat glands avoids the SC, but the surface area of these routes constitutes only less than 0.01% of the total skin area, which diminishes the importance of this route in dermal and transdermal drug delivery.

Drugs are delivered to and through the skin using various types of formulations/delivery systems such as powders, solutions, sprays, suspensions, emulsions, ointments, creams, pastes, gels, and patches. For dermatological applications, formulations are targeted to different layers of the skin to protect (e.g., sunscreens), enhance the appearance (e.g., cosmetics), or deliver medicaments (e.g., for acne, psoriasis) to the skin (Table 1.3).

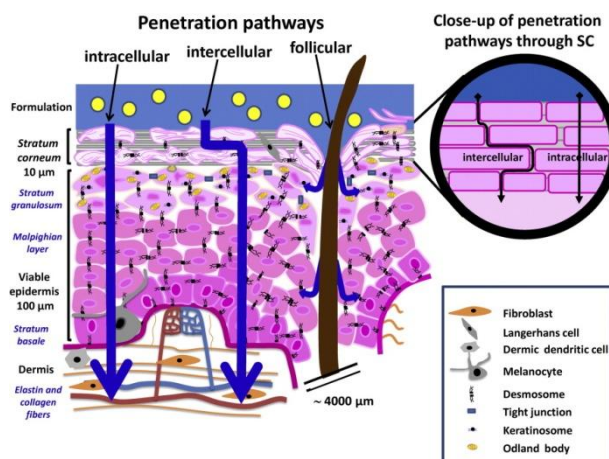


Figure 1.18: Sketch of the three penetration pathways: intracellular, intercellular and follicular. The upper right inset is a close-up of the stratum corneum showing the intracellular pathway and the tortuous intercellular pathway.⁶¹

Basic agreement exists about the mechanism of colloid-dependent modulation of drug permeation through the skin. For example, drug interactions with a colloid on the skin more often than not diminish drug partitioning into the barrier and thus lower transdermal drug transport. Some epicutaneously applied aggregate colloids may also reduce the skin barrier height. This typically involves a deterioration of intercorneocyte lipid seals by aggregate components or (partial) organ occlusion. Both these phenomena potentially increase drug partitioning and/or diffusivity in the stratum corneum and thus enhance transdermal drug diffusion.⁶²

Liposomes have been used both for improved localized drug deposition into the skin, and for improved transdermal delivery.⁶³ Different mechanisms have been proposed for penetration enhancement, including liposome fusion with the SC, intact liposome penetration in the SC, and transappendageal penetration.⁶⁴ Permeation of intact liposomes in the skin is unlikely, and the delivery properties of liposomes are improved if fusogenic lipids are used in the formulation.^{65,66} Such lipids (e.g. lysolipids, cationic lipids, unsaturated lipids with small head groups) act as permeation enhancers in the stratum corneum. Liposomes have also been utilized as vectors in non-invasive gene therapy and topical vaccination.^{67,68} In a gel formulation the contact time on skin or mucosa is typically much longer than that of an aqueous solution owing to the more favorable adhesive and/or rheological properties. An extended contact time at the site of administration might increase the absorption of the drug substance, opening up the possibility of: giving a lower dose of the administered drug, using longer dosing intervals, or both. A dosage form with favorable properties might render high patient compliance.

Table 1.3: Target sites for topical and transdermal drug delivery

Skin layer	Cosmetics/drugs
Stratum corneum	Cosmetics Sunscreens Antimicrobials Skin protectants
Viable epidermis	Anti-inflammatory agents Antiproliferative agents Antihistamines Vaccines Gene therapy
Hair follicles	Antiacne agents Antimicrobials Depilatories Vaccines, gene therapy

1.7 Franz cell

In vitro percutaneous absorption studies have become an important tool in the evaluation of potential drug candidates and prototype topical formulations for drug release and cutaneous delivery. Selection of the appropriate diffusion cell system, proper study design, and skin source and quality are all critical components for success.

One of the most widely used in vitro technique for studying permeation is the Franz diffusion cell.⁶⁹ The Franz Cell apparatus (showed in Figure 1.19) consists of two primary chambers separated by a membrane. Although animal or synthetic skin can be used as the membrane, human skin is preferred. The test product is applied to the membrane via the top chamber. The bottom chamber contains fluid from which samples are taken at regular intervals for analysis. This testing determines the amount of active that has permeated the membrane at each time point. The chamber is maintained at a constant temperature of 37 °C. Depending on the vehicle, the rate of permeation for a given drug as determined via Franz cell analysis can vary significantly (perhaps from 10 to 50 fold).

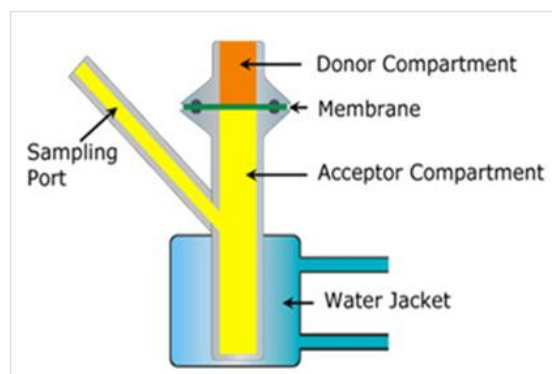


Figure 1.19: Sketch of Franz Cell apparatus.

In a typical *in vitro* percutaneous absorption study, a clinically relevant dose of each prototype formulation is applied to excised skin mounted in Franz diffusion cells. Skin should be exposed to the formulation no longer than 24 hours because of deterioration of skin integrity with time. Receptor fluid samples are collected at regular intervals. At the end of the exposure period, residual formulation can be removed from the skin surface by washing, wiping, tape-stripping, or combinations thereof. After removal of the residual formulation from the skin surface, the epidermis is separated from the dermis by blunt dissection. The epidermis, dermis, and receptor fluid samples are then analyzed for drug content by use of sensitive analytical methods like LC/MS, HPLC etc., and the profile of drug delivery is assessed. Apart from skin, the Franz diffusion cell is used with synthetic membranes, either for skin simulation or as a quality control assessment of topical product application, mainly because synthetic membranes, unlike skin, are inert and do not introduce biological variations. Synthetic membranes for skin simulation, such as the silicone-based membranes polydimethylsiloxane and Carbosil are generally hydrophobic and rate limiting, imitating the stratum corneum. In contrast, synthetic membranes for quality control (such as release performance of formulation), such as cellulose esters (used in experiments of section 4) and polysulfone, are required to act as a support rather than a barrier. These synthetic membranes also often contain pores; hence, they are called porous membranes. The barrier potential of porous membranes is dictated by the probability of a molecule entering and diffusing through the pores, and the factors governing selectivity to diffusion would be the relative molecular size, molecular shape and its electrostatic interactions with the membrane.⁷⁰ Conversely, aporous media appear to offer some rate-limiting factor to permeation and may, therefore, more closely simulate diffusion through biological tissue. The barrier properties here generally relate to the solubility of the diffusing molecule in the polymer matrix (partition coefficient between donor vehicle and membrane) and the ease of diffusant passage through the polymer.

1.8 *Micrococcus lysodeikticus* assay

Lysozyme activity after release, was measured by a method reported in literature.⁷¹ *Micrococcus lysodeikticus* (Sigma) bacterial cell suspension was used to quantitatively determine the bioactivity of the enzyme. Lysozyme is known to digest the cell wall of bacteria. The bacterial cells were dispersed in potassium phosphate buffer (66 mM, pH 6.24) in the concentration of 0.015 % w/v. It was further diluted with the same buffer so that initial absorbance was approximately 1.50 at 450 nm. An appropriately diluted lysozyme solution (0.1 ml) was added into 2.5 ml of bacterial suspension and the absorbance at 450 nm was recorded every 15 s during a total incubation period of 5 min at 25 °C. The bioactive lysozyme concentration was determined by the following equation:

$$\text{units/mL lysozyme} = [(\Delta E_{450 \text{ nm}} / \text{min}_{\text{Test}} - \Delta E_{450 \text{ nm}} / \text{min}_{\text{Blank}})(df)] / [(0.001)(0.1)] \text{ Eq:1.6}$$

where $\Delta E_{450 \text{ nm}} / \text{min}$ is the reduction in the absorbance at 450 nm per minute, df is the dilution factor, 0.001 is the change in absorbance at 450 nm as per the unit definition of lysozyme activity, 0.1 is volume (in ml) of lysozyme used for the assay.

2 Chapter

2.1 Theoretical background

2.1.1 Introduction

This section will briefly describe the techniques, which are essential to understand experimental data, used to obtain the results presented in this thesis.

The liposomal system was characterized with photon correlation spectroscopy (PCS) in terms of mean particle size, surface charge and polydispersity. Basic information are also given for the Cryo-TEM technique used to visualize morphology of nanosystems. Bilayer thickness and thermotropic behaviour were determined by small angle X-ray scattering (SAXS). Rheological measurements were carry out on both, vesicular lipid gel and liposomal liquid formulation, to study deformation and flow of the system in terms of stress, strain, temperature, and time.

Finally some general information are reported concerning technological characterization: i.e. topical release experiments.

2.2 Dinamic Light Scattering

2.2.1 Introduction

Dynamic Light Scattering (also known as PCS - Photon Correlation Spectroscopy) measures Brownian motion and relates this to the size of the particles. Brownian motion is the random movement of particles suspended in liquids or gases resulting from the impact of molecules with the surrounding medium. Normally DLS is concerned with measurement of particles suspended within a liquid. The larger the particle, the slower the Brownian motion will be. An accurately known temperature is necessary for DLS since viscosity is required, and viscosity of a liquid is related to temperature. The temperature also needs to be stable, otherwise convection currents in the sample will cause non-random movements that will ruin the correct interpretation of size. The velocity of the Brownian motion is defined by a property known as the translational diffusion coefficient (usually given with the symbol, D). The size of a particle is calculated from the translational diffusion coefficient by using the Stokes-Einstein equation 2.1:

$$d(H) = kT/3\pi\eta D \quad \text{Eq.:2.1}$$

here: $d(H)$ = hydrodynamic diameter, D = translational diffusion coefficient, k = Boltzmann's constant, T = absolute temperature, η = viscosity.

Note that the diameter that is measured in DLS is a value that refers to how a particle diffuses within a fluid so it is referred to as a hydrodynamic diameter. The diameter that is obtained by this technique is the

diameter of a sphere that has the same translational diffusion coefficient as the particle. The translational diffusion coefficient will depend not only on the size of the particle “core”, but also on any surface structure, as well as the concentration and type of ions in the medium. The ions in the medium and the total ionic concentration can affect the particle diffusion speed by changing the thickness of the electric double layer referred as Debye length (k^{-1}). Thus a low conductivity medium will produce an extended double layer of ions around the particle, reducing the diffusion speed and resulting in a larger, apparent hydrodynamic diameter. Conversely, higher conductivity media will reduce the electrical double layer thickness and the measured hydrodynamic diameter. Any change at the surface of a particle that affects the diffusion speed will correspondingly change the apparent size of the particle. For example an adsorbed polymer layer extended out into the medium will reduce the diffusion speed more than if the polymer is lying flat on the surface. The nature of the surface and the polymer, as well as the ionic concentration of the medium can affect the polymer conformation, which in turn can change the apparent size by several nanometers. All particle-sizing techniques have an inherent problem in describing the size of non-spherical particles. The sphere is the only object whose size can be unambiguously described by a single figure. Different techniques are sensitive to different properties of the particle, e.g. projected area, density, scattering intensity, and in general will produce different mean sizes and size distributions for any given sample. Even the size in a microscope image will depend on parameters set such as edge contrast etc. It is important to understand that none of these results are inherently “correct”. The hydrodynamic diameter of a non-spherical particle is the diameter of a sphere that has the same translational diffusion speed as the particle. If the shape of a particle changes in a way that affects the diffusion speed, then the hydrodynamic size will change. For example, small changes in the length of a rod-shaped particle will directly affect the size, whereas changes in the rod’s diameter, which will hardly affect the diffusion speed, will be difficult to detect.

2.2.2 Light Scattering Theories

Formal light scattering theory may be categorized in terms of two theoretical frameworks. One is the theory of Rayleigh scattering (after Lord Rayleigh) that is, strictly speaking as originally formulated, applicable to small, dielectric (non-absorbing), spherical particles. If the particles are small compared to the wavelength of the laser used (typically less than $d = \lambda/10$ or around 60 nm for a He-Ne laser), then the scattering from a particle illuminated by a vertically polarized laser will be essentially isotropic, i.e. equal in all directions.

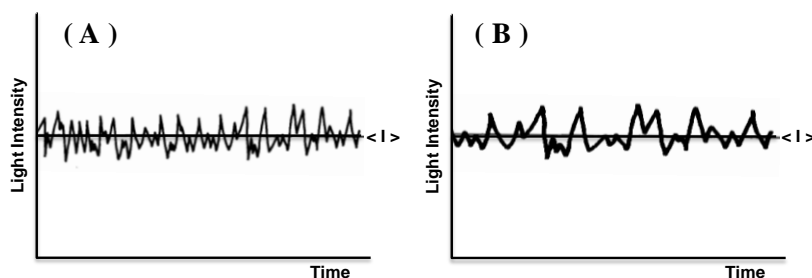


Figure 2.1 A-B: Intensity mean value fluctuations of small (A) and large (B) particles vs time.

The Rayleigh approximation tells us that $I \propto d^6$ and also that $I \propto 1/\lambda^4$, where I = intensity of light scattered, d = particle diameter and λ = laser wavelength. The second is the theory of Mie scattering (after Gustav Mie) that encompasses the general spherical scattering solution (absorbing or non-absorbing) without a particular bound on particle size. Accordingly, Mie scattering theory has no size limitations and converges to the limit of geometric optics for large particles. Mie theory, therefore, may be used for describing most spherical particle scattering systems, including Rayleigh scattering. However, Rayleigh scattering theory is generally preferred if applicable, due to the complexity of the Mie scattering formulation. Rayleigh scattering from many particles in a large volume is essentially constant as a function of time. Scattering from a sufficiently small volume is not constant over time but fluctuates about an average value (ie. for a sufficiently small volume element the local concentration changes as molecules diffuse in and out as a function of time). These fluctuations contain important information as their frequency is dependent upon how fast the solute molecules move, furthermore, the fluctuations of scattering intensity as a function of time are different depending on the size of the particles (see **Figure 2.1 A and B**).

Most common method for analyzing the fluctuation in scattering intensity is the autocorrelation function. A correlation function is a mathematical construct designed to determine how long a given signal stays correlated. It is expressed as the ratio of the product of scattering intensity (I) at time t and time $(t + \tau)$ and average scattering intensity squared, also known as Siegert relationship or second correlation function (Eq.: 2.2):

$$g_2(\tau) = \frac{\langle I(t) \cdot I(t+\tau) \rangle}{\langle I(t) \rangle^2} \quad \text{Eq.: 2.2}$$

Conceptually, we are measuring how similar the scattering intensity (ie. Particle distribution) is at time t and $(t + \tau)$. As the time increment (τ) is increased, $g_2(\tau)$ decays exponentially as the particles have more time to move. When a single component dominates scattering the autocorrelation function decays according to:

$$g_2(q; \tau) = \left(1 + c e^{-2q^2 D_t \tau} \right) \quad \text{Eq.: 2.3}$$

where c is the concentration and $q = 4\pi n \lambda^{-1} \sin(\theta/2)$ is the scattering vector that contains (λ) the laser wavelength, the refractive index of the solution (n) and the scattering angle (θ). Thus, the decay rate is lower (correlation time is longer) at low scattering angles than at high angles. You can also slow the fluctuations by shifting to a longer wavelength. The physical reason is that the molecules must diffuse *farther* to change the speckle pattern at low q . The exponential decay can be linearized by taking the “ln” of each side and D can be calculated from the slope of (Eq: 2.4):

$$\ln[g_2(q; \tau) - 1] = \ln c - 2q^2 D_t \tau \quad \text{Eq: 2.4}$$

In most cases, samples are polydisperse. Thus, the autocorrelation function is a sum of the exponential decays corresponding to each of the species in the population. To extract as much useful information as possible from an autocorrelation function the cumulant method can be used, from which more information can be derived about the variance of the system developing the polynomial series of first correlation function (Eq: 2.5) as follows:

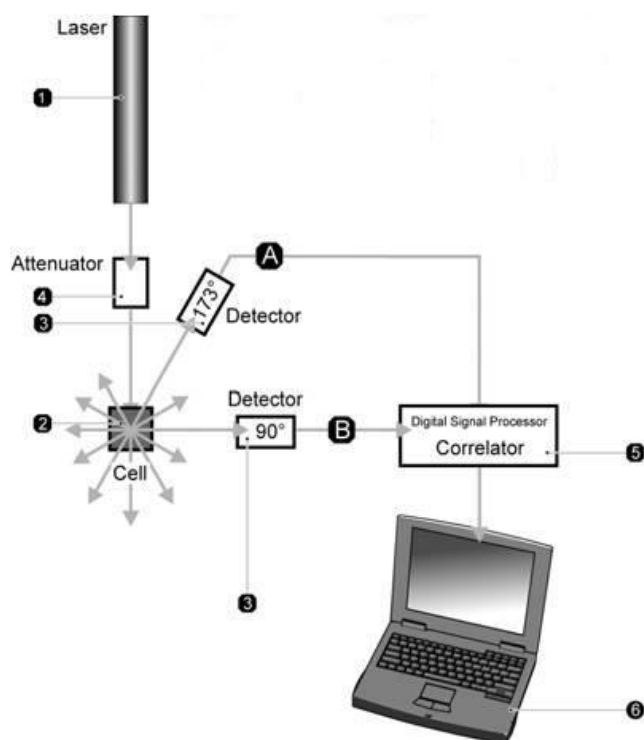
$$g_1(\mathbf{q}; \tau) = \left(e^{-\overline{q^2 D_t} \tau} \right) \left(1 + \frac{\mu_2}{2!} \tau^2 - \frac{\mu_3}{3!} \tau^3 + \dots \right) \quad \text{Eq: 2.5}$$

where $\overline{q^2 D_t}$ is the average decay rate and $\frac{\mu_2}{(\overline{q^2 D_t})^2}$ is the second order polydispersity index (or an indication of the variance). A third-order polydispersity index may also be derived but this is necessary only if the particles of the system are highly polydisperse. The z-averaged translational diffusion coefficient D_z may be derived at a single angle or at a range of angles depending on the wave vector \mathbf{q} .

One must note that the cumulant method is valid for small τ . One should seldom use parameters beyond μ_3 , because over fitting data with many parameters in a power-series expansion will render all the parameters including $\frac{\mu_2}{(\overline{q^2 D_t})^2}$ and μ_2 , less precise. The cumulant method is far less affected by experimental noise than others methods such as CONTIN algorithm or Maximum entropy method for which we refer to specific readings.⁷²⁻⁷⁵

2.2.3 Optical Configuration of a Dynamic Light Scattering Instrument.

A typical DLS system comprises six main components. As reported in figure 2.2: a laser 1 is used to provide a light source to illuminate the sample particles within a cell 2. Most of the laser beam passes straight through the sample, but some is scattered by the particles within the sample. A detector 3 is used to measure the intensity of the scattered light. As a particle scatters light in all directions, it is (in theory), possible to place the detector in any position and it will still detect the scattering. Depending on machine model the detector position will be at either 173° or 90° . The intensity of the scattered light must be within a specific range since the detector can successfully measure it. If too much light is detected then the detector will become overloaded. To overcome this an “attenuator” 4 is used to reduce the intensity of the laser and hence



reduce the intensity of the scattering.

Figure 2.2: Scheme of DLS apparatus.

Attenuator can work in two ways depending on particle size:

- For samples that do not scatter much light, such as very small particles or samples of low concentration, the amount of scattered light must be increased. In this situation, the attenuator will allow more laser light through to the sample.
- For samples that scatter more light, such as large particles or samples of high concentration, the amount of scattered light must be decreased. This is achieved by using the attenuator to reduce the amount of laser light that passes through to the sample.

The appropriate attenuator position is automatically determined by the software machine during the measurement sequence and covers a transmission range of 100% to 0.0003%. The scattering intensity signal

for the detector is passed to a digital signal processing board called a correlator 5. The correlator compares the scattering intensity at successive time intervals to derive the rate at which the intensity is varying. This correlator information is then passed to a computer 6, where a specialist software will analyse the data and derive size information.

2.3 Zeta-potential

Zeta potential measurements help to characterize the surface of colloidal systems, such as liposomes, nanospheres and nanocapsules, and predict their behaviour in different environments.

2.3.1 Introduction

The classical explanation of the stability of colloidal suspensions is based on DLVO (Derjaguin-Landau and Verwey-Overbeek) theory.^{76,77} It looks at the balance between two opposing forces: electrostatic repulsion and dispersion attractive forces, that exist among particles as they approach each other due to the Brownian motion they are undergoing. The total potential (V_T) of the system is given by the Equation 2.6:

$$V_T = V_A + V_R + V_S \quad \text{Eq. 2.6}$$

where V_S is the sterical potential energy, it usually makes an important contribution in presence of adsorbed polymers only. Much more important is the balance between V_A and V_R , these are the attractive and repulsive contributions. The most important contribution to attractive forces is given by London forces (or dispersion forces), the simplest potential for short range interaction between 2 identical spheres in vacuum is:

$$V_A = -aA/(12H) \quad \text{Eq. 2.7}$$

where a is the particle radius, A is the Hamaker constant and H is the interparticle distance.

The electrostatic repulsive potential V_R simplified for small potential, under 25 mV, that permit Debye-Huckel approximation can be expressed through 2 different equations depending on particle geometry. The first used for a plane infinite surface at low potentials, the potential decreases exponentially with distance from the charged surface, is :

$$V_R = \Psi = \Psi^0 \exp(-\kappa H) \quad \text{Eq. 2.8}$$

where, Ψ^0 is the surface potential, $1/\kappa$ is the Debye length. The second is used for spherical interfaces :

$$V_R = \Psi = \Psi^0 a/r \exp[-\kappa(r-a)] \quad \text{Eq. 2.9}$$

where a is the particle radius, $(r-a)$ is the distance from charged surface.

2.3.2 Electric double layer

The double layer model is used to visualize the ionic environment in the vicinity of a charged surface. It is a matter of fact that at the interface between a dispersed particle and the dispersing medium it can be recognized a region of space having different properties from bulk. In figure 2.3 is reported the scheme for the electric double layer model.

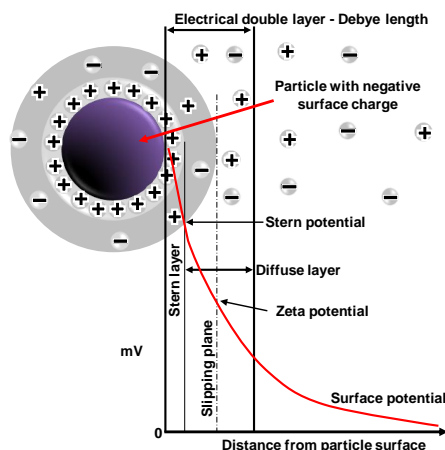


Figure 2.3: Zeta potential and schematic of liquid layers surrounding the particle.

The charged particle surface affects the distribution of ions in the surrounding interfacial region, resulting in an increased concentration of counter ions (ions of opposite charge to that of the particle) close to the surface. Thus an electrical double layer exists around each particle.

The liquid layer surrounding the particle exists as two parts; an inner region, called the Stern layer, where the ions are strongly bound and an outer, diffuse, region (Guy Chapman layer) where they are less firmly attached. Within the diffuse layer there is a notional boundary inside which the ions and particles form a stable entity. When a particle moves, ions within the boundary move with it, but any ions beyond the boundary do not travel with the particle. This boundary is called the surface of hydrodynamic shear or slipping plane and defines the electrokinetic unit. The potential that exists at this boundary is known as the Zeta potential (or ζ -potential).

The magnitude of the zeta potential gives an indication of the potential stability of the colloidal system. Currently, in the field of drug delivery systems, Zeta potential is used to characterize the type of interaction between the colloidal particle used as a carrier and the active substance; i.e. whether the drug is encapsulated within the body of the particle or simply adsorbed on the surface. This is important because adsorbed drug may not be protected from enzymatic degradation, or may be released very rapidly after administration.

If all particles in suspension have a large negative or positive ζ -potential then they will tend to repel each other and there is no tendency to flocculate. However, if the particles have low zeta potential values then there is no force to prevent the particles coming together and flocculating. The general dividing line between stable and unstable suspensions is generally taken at either +30 mV or -30 mV. Particles with zeta potentials more positive than +30 mV or more negative than -30 mV are normally considered very stable.

2.3.3 Measuring ζ -potential

When an electric field is applied across an electrolyte, charged particles suspended in the electrolyte are attracted towards the electrode of opposite charge. Viscous forces acting on the particles tend to oppose this movement. When equilibrium is reached between these two opposing forces, the particles move with constant velocity.

The velocity of the particle is dependent on the following factors :

1. Strength of electric field or voltage gradient.
2. The Dielectric constant of the medium.
3. The Viscosity of the medium.
4. The ζ - potential.

The velocity of a particle in an electric field is commonly referred to as its Electrophoretic mobility. With this knowledge it is possible to obtain the ζ -potential of the particle by application of the Henry equation. The Henry equation is :

$$U_E = [\varepsilon \zeta f(\kappa a)] / 1.5\eta \quad \text{Eq. 2.10}$$

Where: U_E is the electrophoretic mobility, ε is the dielectric constant, ζ is the Zeta-potential, $f(\kappa a)$ is the Henry's function, and η is viscosity. Two values are generally used as approximations for the $f(\kappa a)$ determination: either 1.0 or 1.5. For curved surface the shape of the double layer can be described in terms of dimensionless quantity " κa ", which is the ratio of radius of curvature to double-layer thickness. When a spherical particle can be treated as a point charge in an unperturbed electric field, but the particle is large enough for Stokes' law to apply, κa is small, $f(\kappa a) = 1$ and it is referred to as Huckel approximation. When the double layer is effectively flat, κa is large, $f(\kappa a) = 1.5$ and is referred to as the Smoluchowski approximation.

2.4 Small angle X-Ray Scattering (SAXS)

Small-angle X-ray (SAXS) diffraction technique gives essential information on the local ordering and structure of colloidal systems on a scale from 1 to 100 nm.

X-rays are electromagnetic waves with wavelengths of typically few Ångstroms, that can be generated by accelerating electrons towards a metal target (anode) where the kinetic energy possessed by the electrons are converted to quanta of radiation. When reaching certain critical energies an electron in the metal K-shell is excited. This causes electrons from the outer shells to jump and fill the void. This results in high intensity spikes of radiation with well defined wavelengths. The Copper-K α ($\lambda = 1.542 \text{ \AA}$) is one of the more common wavelength used.

The basic principle of X-ray diffraction techniques is that an electron present in the path of a X-ray will start to oscillate with the same frequency and amplitude as the original beam. The electron is said to scatter radiation. Periodical electron density fluctuations within the sample may thus give rise to constructive interferences in certain discrete angles that appears on the detector as a scattered X-ray beam and thereby giving a diffraction pattern.

In a typical SAXS experiment a monochromatic beam of incident wave vector k_i is selected and falls on the sample. The scattered intensity is collected as a function of the so-called scattering angle 2θ . Elastic interactions are characterized by zero energy transfers, such that the final wave vector k_f is equal in modulus to k_i . The relevant parameter to analyze the interaction is the momentum transfer or scattering vector $q = k_f - k_i$, defined by $q = (4\pi / \lambda) \sin\theta$, and θ is half the scattering angle. The standard unit for q is \AA^{-1} .

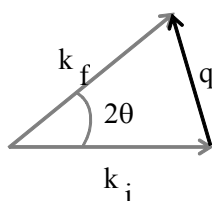


Figure 2.4 :Schematic representation of the scattering vector.

If the scattering object has an ordered structure constructive interference of the out-coming X-rays may occur, giving rise to peaks in the scattering profile as described by Bragg's Law:

$$n\lambda = 2d \sin\theta \quad \text{Eq. 2.11}$$

where n is an integer, λ is the wavelength of the incoming X-rays, d is the lattice spacing and θ is the angle between the incoming X-rays and the scattering planes.

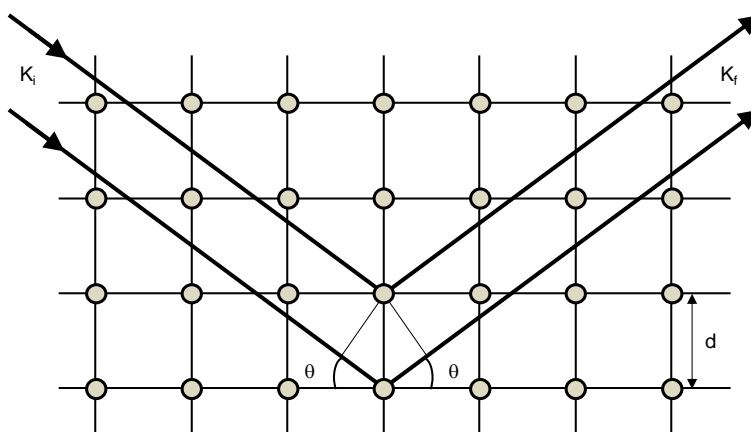


Figure 2.5 Bragg's description of diffraction.

Small angle X-ray scattering (SAXS) is the most recognized method to study the structural features of liquid crystalline mesophases, both in their bulk or dispersed form. There are two regions of the diffraction pattern that are used to identify the phase structure. The small angle region identifies the symmetry and long range organization of the phase, whereas the wide angle region gives information on the molecular packing. Peaks can arise also from non crystalline structures, such as microemulsions, vesicles dispersion and micellar systems, but in this case, broad peaks are commonly observed.

Particularly unilamellar vesicles exhibit diffraction patterns with no quasi-Bragg peaks, only purely diffuse scattering. There exist sophisticated and generally applicable data analysis techniques⁷⁸⁻⁸³ which can be successfully used for the analysis of this kind of data.

The scattered intensity of a stack of layers, averaged over all orientations in three-dimensional space, is given by:

$$I(q) = S(q) |F(q)|^2 / q^2 \quad \text{Eq. 2.12}$$

where $F(q)$ is the bilayer form factor and $S(q)$ is the intraparticle structure factor. However, the lipid dispersion may well contain, to a certain extent, positionally uncorrelated bilayers, such as unilamellar vesicles (ULVs). This is especially true for weakly bound multibilayer systems, so such kind of system need an additional term for the global intensity,⁸⁴ which relates to the diffuse scattering by these uncorrelated objects. Then equation 2.12 becomes:

$$I(q) = |F(q)|^2 S(q) / q^2 + N_u |F(q)|^2 / q^2 \quad \text{Eq. 2.13}$$

where N_u is a scaling constant for the additional diffuse scattering term. A global model to describe the scattered intensity of uncorrelated lipid bilayers, e.g. ULVs, can be written setting the first term of Equation 2.13 equal to zero and $N_u = 1$, to obtain:

$$I(q) = |F(q)|^2 / q^2 \quad \text{Eq. 2.14}$$

This equation describes the global scattered intensity of a polydisperse liposomal dispersion.

Structure determination of lipid bilayers is complicated by disorder within the bilayer due to the high lateral and vertical mobility of the lipid molecules and a diversity of fast motions and vibrations of lipid atoms or quasimolecular fragments.⁸⁵ The consequence is that the obtainable electron density profiles in the direction normal to the plane of the bilayers are intrinsically of low resolution. A lipid bilayer can equally well be represented in reciprocal space by many different real-space models, such as strip models, “distorted” crystalline models, Gaussian models and hybrid Gaussian strip models. However, the various models are not equally useful and realistic in real space. A very realistic model appears to be the hybrid type, where the electron-dense headgroup is represented by two Gaussians and the electron-sparse region at the methyl terminus of the hydrocarbon chains by another Gaussian with negative amplitude (Fig. 2.6). This model also

accounts for the difference in electron density $\Delta\rho$ of the interbilayer water and hydrocarbon chains. However, additional information on the lipid specific volume and methylene electron density is required to evaluate this model.⁸⁶

A Gaussian description of the bilayer electron density proposed by Pabst et al. 2000 appears to be the simplest of the realistic bilayer models, requiring the adjustment of only four parameters (Fig. 2.6). Here:

$$\rho(z) = \exp[-(z - z_H)^2 / 2\sigma_H^2] + \exp[-(z + z_H)^2 / 2\sigma_H^2] - \rho_r \exp(-z^2 / 2\sigma_c^2) \quad \text{Eq. 2.15}$$

is given by two Gaussians of width σ_H centred at $\pm z_H$ representing the headgroup, and a further Gaussian of width σ_C at the centre of the bilayer accounting for the hydrocarbon chains $\rho_r = (\rho_C - \rho_a) / (\rho_H - \rho_a)$ is the ratio of the methyl-terminus electron density amplitude to that of the headgroup, where ρ_a is the electron density of the interbilayer aqueous solution (water), which is set to zero.

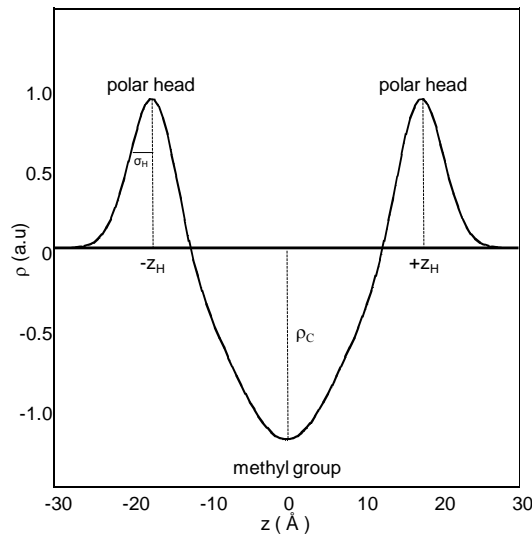


Figure 2.6. One-dimensional electron density profile model. The Gaussians centered at $\pm z_H$ characterize the position of the head group and $2\sigma_H$ is its width.

Fourier transformation of equation 2.15 gives:

$$F(q) = (2\pi)^{1/2} [2\sigma_H \exp(-\sigma_H^2 q^2 / 2) \cos(qz_H) - \sigma_C \rho_r \exp(-\sigma_C^2 q^2 / 2)] \quad \text{Eq. 2.16}$$

The electron density profile permit to determine bilayer thickness (d_B) through the following equation:

$$d_B = 2(z_H + 2\sigma_H) \quad \text{Eq. 2.17}$$

The full-q-range models to fit low-resolution X-ray diffraction data from pattern exhibiting only weak quasi-Bragg peak scattering can be applied to multibilayers vesicles too, but is not considered here, for specific information see Pabst et al. 2003⁸⁷ and references herein.

2.5 Transmission Electron Microscopy (TEM)

Transmission Electron Microscopy (TEM) is a well known technique for imaging solid materials at atomic resolution. Structural information can be acquired both by (high resolution) imaging as well as by electron diffraction.

The design of a transmission electron microscope (TEM) is analogous to that of an optical microscope. In a TEM high-energy (>100 kV) electrons instead of photons and electromagnetic lenses instead of glass lenses are used. The electron beam passes an electron-transparent sample and a magnified image is formed using a set of lenses. This image is projected onto a fluorescent screen or a CCD camera.

2.5.1 Cryo-TEM

The application of TEM to direct visualization of self-assembled colloidal nanostructures in water requires rapid vitrification of the samples, and so the technique is referred to as cryogenic TEM or Cryo-TEM. Cryo-TEM is frequently used to study morphology, size and size distribution of dispersed self-assembly structures. Nowadays, fast Fourier transforms (FFTs) of Cryo-TEM images are often used to get a precise determination of interplanar distances and angles between crystallographic planes.

For the Cryo-TEM, specimens are prepared without chemical treatment such as fixation, dehydration and resin embedding which can potentially cause artifacts. Samples are immersed quickly into liquid ethane at its freezing point, then stored in liquid nitrogen are transferred to a special TEM device. Due to the fast cooling rates occurring during this process the water in the sample is vitrified. Through the vitrification, supramolecular structures such as cubosomes and liposomes are better preserved since the rearrangement of water molecules during formation of ice crystals is mostly prevented.

2.6 Rheology

Rheology is the study of the flow and deformation of matter. Rheological properties of many different substances including paint, plastics, rubber, and lubricants are important to their applications. Typically, the rheological properties of non Newtonian materials are studied to develop models to understand the behavior of such solutions. Most drag reducing surfactant solutions are non-Newtonian even at low concentrations. These types of solutions have unusual rheological behavior because of the presence of the micelles. For example, surfactant solutions undergo structural changes when they self repair themselves upon removal from high shear. Several rheological properties are important to study in order to develop a better

understanding of a solution's behavior. These properties include shear viscosity, shear-induced structure, first normal stress difference, and shear stress.⁸⁸

2.6.1 Shear Viscosity

Viscosity is a property of a fluid which is a measure of its resistance to flow. Viscosities can be measured using a viscometer, which has the ability to determine changes in viscosity with time or with shear rate or shear stress. Viscometers can also detect if a solution undergoes shear thinning or thickening with time. Shear thinning is when a solution's viscosity decreases with increasing shear while shear thickening is the opposite, where a solution's viscosity increases with increasing shear. A particular solution's composition can have a dramatic effect on its viscosity. For example, at high shear rates dilute surfactant solutions with micelles will exhibit viscosity close to that of water while the viscosity of the pure surfactant is much greater than that of water. Also, the addition of salts to surfactant solutions may increase or decrease the viscosity of the solution depending on the concentrations of both the surfactant and salt.

2.6.2 Shear Induced Structure (SIS)

Shear induced structure (SIS) is a phenomenon that occurs when a shear thinning solution undergoes a sudden increase in viscosity as the shear rate applied to the solution increases. According to Yunying Qi this coincides with a change in the structure of the micelles at a critical shear rate causing formation of a "shear induced structure". The sizes of these structures may be orders of magnitude larger than the rod-like micelles resulting in a large increase in viscosity. This increase forms a peak in the viscosity because the structures are not stable and as the shear rate increases further, shear thinning will occur again. The critical shear rate at which SIS occurs is a function of the concentrations of all components in a solution as well as the temperature and geometry used in a rheometer. Although this is the typical explanation for SIS behavior, no detailed understanding of this phenomenon has been reached.

2.6.3 Theory

Fundamental relationship linking force and material deformation are called constitutive equations.⁸⁹ For an elastic solid, the constitutive equation is Hooke's law, which states that the applied shear stress (σ) is proportional to the produced shear strain (γ) or alternately:

$$\sigma = G\gamma \qquad \text{Eq. 2.18}$$

Here σ is the shear force per unit area, and γ is defined as the relative change in length. The proportionality constant G , is called the shear modulus and is an intrinsic property of an elastic solid. For Hookean solids when the stress is removed, the strain becomes zero and the material regains its original shape and structure. A similar constitutive equation exists for a viscous or Newtonian liquid. Newton's law of viscosity states that the shear stress is proportional to the rate of strain, or shear rate ($\dot{\gamma}$):

$$\sigma = \eta \dot{\gamma} \quad \text{Eq. 2.19}$$

The proportionality constant η is defined as the viscosity of the material. Thus, a Newtonian liquid will undergo a constant rate of deformation under an applied stress, and when the stress is removed it will remain in the shape and structure it has adopted. The viscosity of a material is a measure of its internal resistance to flow and reflects the rate at which energy is dissipated in the material. Many small-molecule liquid solutions, such as water, honey and various oils, obey Newton's law.

Viscosity, which describes the physical property of a liquid to resist shear-induced flow, may depend on 6 independent parameters:

$$\eta = f(S, T, p, \dot{\gamma}, t, E) \quad \text{Eq. 2.20}$$

Where:

- "S" is the parameter that denotes the physical-chemical nature of a substance being the primary influence on viscosity, i.e. whether the liquid is water, oil, honey, or a polymer melt etc.
- "T" is the parameter linked to the temperature of the substance. Experience shows that viscosity is heavily influenced by changes of temperature. As an example: The viscosity of some mineral oils drops by 10% for a temperature increase of only 1°C.
- "p" is the parameter "pressure", it is not experienced as often as the previous ones. Pressure compresses fluids and thus increases intermolecular resistance. Liquids are compressible under the influence of very high pressure-- similar to gases but to a lesser extent. Increases of pressure tend to increase the viscosity. As an example: Raising the pressure for drilling mud from ambient to 1000 bar increases its viscosity by some 30%.
- " $\dot{\gamma}$ " is the parameter "shear rate" is a decisive factor influencing the viscosity of very many liquids. Increasing shear rates may decrease or increase the viscosity.

"t" is the parameter "time". It denotes the phenomenon that the viscosity of some substances, usually dispersions, depends on the previous shear history, i.e. on the length of time the substance was subjected to continuous shear or was allowed to rest before being tested.

"E" is the parameter "electrical field". It is related to a family of suspensions characterized by the phenomenon that their flow behavior is strongly influenced by the magnitude of electrical fields acting upon them. These suspensions are called either "electro-viscous fluids" (EVF) or "electro-rheological fluids" (ERF). They contain finely dispersed dielectric particles such as aluminum silicates in electro-conductive liquids such as water which may be polarized in an electrical field. They may have their viscosity changed instantaneously and reversibly from a low to a high viscosity level, to a dough-like material or even to a solid state as a function of electrical field changes, caused by voltage changes.

There are several materials that obey these constitutive equations. They can be completely characterized by measuring the respective parameter G or η . But in reality many systems, such as colloids, polymers and gels, do not obey these simple constitutive relation. Instead these materials have properties between those of a Hookean solid and a Newtonian liquid and can be classified as non-Newtonian or viscoelastic. For these materials, the viscosity is a function of shear-rate and hence, not constant, and the shear modulus has two components signifying elastic and viscous character respectively.

A plot of the shear-stress vs. shear-rate is called the flow curve of the material. The simplest type of a flow curve is shown in Figure 2.7, for a Newtonian liquid. The viscosity in equation 2.19 is assumed to be constant and independent of $\dot{\gamma}$.

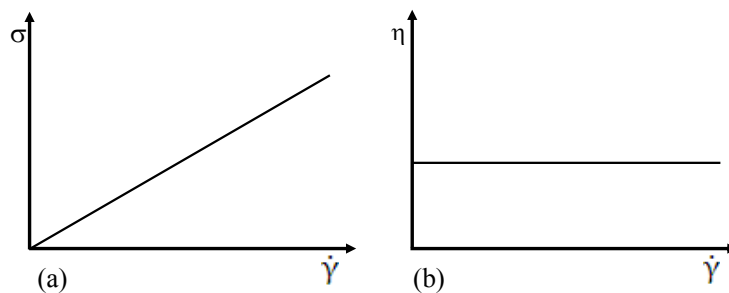
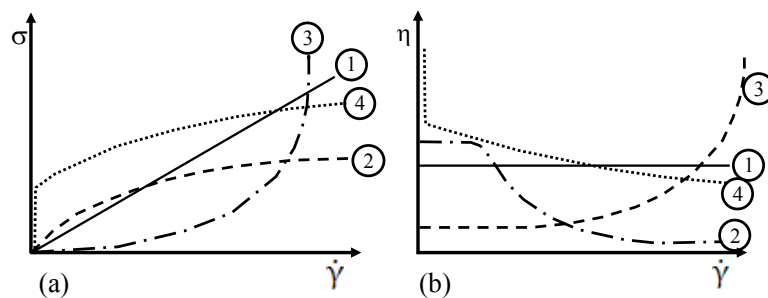


Figure 2.7: (a) flow curve of a Newtonian liquid. (b) viscosity curve of a Newtonian liquid.

Another diagram is very common: η is plotted versus $\dot{\gamma}$. The diagram shown in Figure 2.7 (b) is called the “Viscosity Curve”. Viscosity measurements always first results in the flow curve.

These results can then be rearranged mathematically to allow the plotting of the corresponding viscosity curve. The different types of flow curves have their counterparts in types of viscosity curves as reported in the following Figures 2.8 a and b.

Liquids which show pseudo-plastic flow behavior under certain conditions of stress and shear rates are often just called “pseudo-plastic liquids”. These liquids show drastic viscosity decreases when the shear rate is increased from low to high levels. Technically this can mean that for a given force or pressure more mass can be made to flow or the energy can be reduced to sustain a given flow rate. Fluids which become thinner as the shear rate increases are called “pseudo-plastic”.



Figures 2.8: (a) Flow and (b) viscosity curves plot for various types of common flow behavior: ①Newtonian liquid. Non-Newtonian liquid: ②Pseudoplastic liquid; ③Dilatant liquid; ④Pseudoplastic liquid with yield point = plastic liquid.

Very many substances such as emulsions, suspensions, or dispersions of technical and commercial importance belong to this group. Many liquid products that seem to be homogeneous are in fact composed of several ingredients: particles of irregular shape or droplets of one liquid are dispersed in another liquid or polymer solutions with long entangled and looping molecular chains. At rest, all of these materials will maintain an irregular internal order and correspondingly they are characterized by a sizable internal resistance against flow, i.e. a high viscosity. With increasing shear rates, matchstick-like particles suspended in the liquid will be turned lengthwise in the direction of the flow. Chain-type molecules in a melt or in a solution can disentangle, stretch and orient themselves parallel to the driving force.⁸⁸ Particle or molecular alignments allow particles and molecules to slip past each other more easily. Shear can also induce irregular lumps of aggregated primary filler particles to break up and this can help a material with broken-up filler aggregates to flow faster at a given shear stress.

For most liquid materials the shear-thinning effect is reversible - often with some time lag - i.e. the liquids regain their original high viscosity when the shearing is slowed down or terminated: the chain-type molecules return to their natural state of non-orientation. At very low shear rates pseudo-plastic liquids behave similarly to Newtonian liquids having a defined viscosity η_0 independent of shear rate - often called the “zero shear viscosity”. A new phenomenon takes place when the shear rate increases to such an extent that the shear induced molecular or particle orientation by far exceeds the randomizing effect of the Brownian motion: the viscosity drops drastically. Reaching extremely high shear rates the viscosity will approach asymptotically a finite constant level: η_1 . Going to even higher shear rates cannot cause further shear-thinning: The optimum of perfect orientation has been reached.

There is one other type of material characterized by a shear rate dependent viscosity: “dilatant” substances - or liquids which under certain conditions of stress or shear rate show increasing viscosity whenever shear rates increase. This flow behavior most likely complicates production conditions, it is often wise to reformulate the recipe in order to reduce dilatancy. Plasticity describes pseudo-plastic liquids which additionally feature a yield point. They are mostly dispersions which at rest can build up an intermolecular/interparticle network of binding forces (polar forces, van der Waals forces, etc.). These forces restrict positional change of volume elements and give the substance a solid character with an infinitely high viscosity. Forces acting from outside, if smaller than those forming the network, will deform the shape of this solid substance elastically. Only when the outside forces are strong enough to overcome the network forces - surpass the threshold shear stress called the “yield point” - does the network collapse. Volume elements can now change position irreversibly: the solid turns into a flowing liquid. Typical substances showing yield points include oil well drilling muds, greases, lipstick masses, toothpastes and natural rubber polymers.

Plastic liquids have flow curves which intercept the ordinate not at the origin, but at the yield point level of σ_0 . For pseudo-plastic liquids, thinning under the influence of increasing shear depends mainly on the particle/molecular orientation or alignment in the direction of flow surpassing the randomizing effect of the

Brownian movement of molecules. This orientation is again lost just as fast as orientation came about in the first place. Plotting a flow curve of a non-Newtonian liquid not possessing a yield value with a uniformly increasing shear rate - the “up-curve”-, one will find that the “down-curve” plotted with uniformly decreasing shear rates will just be superimposed on the “up-curve”: they are just on top of each other or one sees one curve only. It is typical for many dispersions that they not only show this potential for orientation but additionally for a time-related particle/molecule-interaction.

This will lead to bonds creating a three-dimensional network structure which is often called a “gel”. In comparison to the forces within particles or molecules, these bonds - they are often hydrogen or ionic bonds - are relatively weak: they rupture easily, when the dispersion is subjected to shear over an extended period of time. When the network is disrupted the viscosity drops with shear time until it asymptotically reaches the lowest possible level for a given constant shear rate. This minimum viscosity level describes the “sol”-status of the dispersion. A thixotropic liquid is defined by its potential to have its gel structure reformed, whenever the substance is allowed to rest for an extended period of time. The change of a gel to a sol and of a sol to a gel is reproducible any number of times.

The Figure 2.9 describes thixotropy in graphical form. In the flow curve, the “up-curve” is no longer directly underneath the “down-curve”. The hysteresis now encountered between these two curves surrounds an area that defines the magnitude of this property called thixotropy. This area has the dimension of “energy” related to the volume of the sample sheared which indicates that energy is required to break down the thixotropic structure.

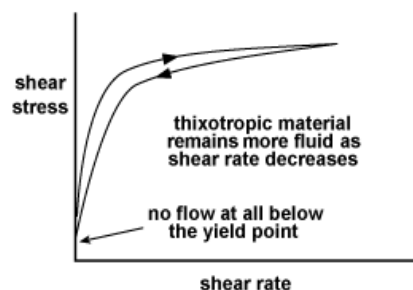


Figure 2.9: Flow curve for thixotropic material.

Rheopective liquids are characterized by a viscosity increase related to the duration of shear. When these liquids are allowed to rest they will recover the original - i.e. the low - viscosity level. Rheopective liquids can cycle infinitely between the shear-time related viscosity increase and the rest-time related decrease of viscosity. Rheopexy and thixotropy are opposite flow properties.

2.6.4 The rheometer

Rheological measurements provide important information on soft materials, specifically on the relation between microstructure and macroscopic properties. These measurements are typically performed on a rheometer under steady or dynamic oscillatory shear.

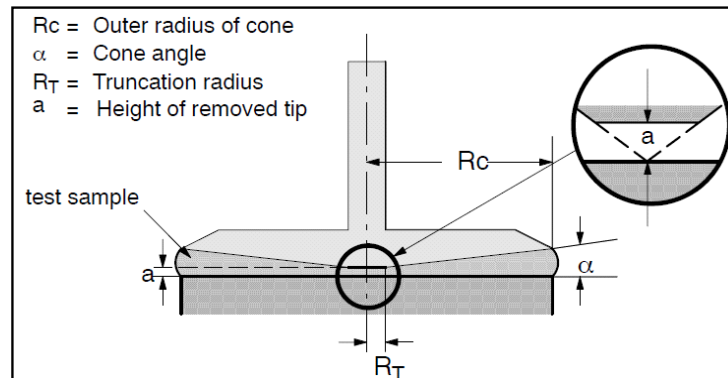


Figure 2.10: Cone-and-plate sensor system rheometer with truncated cone.

Typical geometries used in rheometers are the cone-and-plate (used in our study and schematically reported in Figure 2.10), the parallel plate, and the concentric cylinder or Couette. Figure 2.11 shows the instrument used for experiments.

In rotational rheometer as the one reported in Figure 2.10 sample flows between a cone-and-plate sensor, where one of the two is stationary and the other rotates. This model resembles twisting a roll of coins causing coins to be displaced by a small angle with respect to adjacent coins. In *steady shear rheology*, the sample is subjected to a constant shear-rate ($\dot{\gamma}$) (e.g. by applying a continuous rotation at a fixed rate on a rotational instrument), and the response is measured as a shear-stress σ . The ratio of shear-stress σ to shear-rate $\dot{\gamma}$ is the (apparent) viscosity η .



Figure 2.11: Rheometer MARS III Thermo Haake Scientific equipped with a cone-plate geometry and cone-plate angle 1°.

In *dynamic or oscillatory rheology*, a sinusoidal strain $\gamma = \gamma_0 \sin(\omega t)$ is imposed on the sample. Here, γ is the strain-amplitude (i.e. the maximum applied deformation) and ω is the frequency of the oscillations. The sample response will be in the form of a sinusoidal stress $\sigma = \sigma \sin(\omega t + \delta)$ which will be shifted by a phase angle δ with respect to the strain waveform. Using trigonometric identities, this stress waveform can be decomposed into two components, one in-phase with the strain and the other out-of-phase by 90° :

$$\sigma = G' \gamma \sin(\omega t) + G'' \gamma \cos(\omega t) \quad \text{Eq. 2.21}$$

where G' = Elastic or Storage Modulus

and G'' = Viscous or Loss Modulus

The elastic modulus G' is the in-phase component and provides information about the elastic nature of the material. Since elastic behavior implies the storage of deformational energy, this parameter is also called the storage modulus. The viscous modulus G'' , on the other hand, is the out-of-phase component and characterizes the viscous nature of the material. Since viscous deformation results in the dissipation of energy, G'' is also called the loss modulus. For these properties to be meaningful, the dynamic rheological measurements must be made in the “*linear viscoelastic*” (LVE) regime of the sample. This means that the stress must be linearly proportional to the imposed strain (i.e., moduli independent of strain amplitude). In that case, the elastic and viscous moduli are only functions of the frequency of oscillations ω and are true material functions. A log-log plot of the moduli vs. frequency, i.e. $G'(\omega)$ and $G''(\omega)$, is called the frequency spectrum or *dynamic mechanical spectrum* of the material. Such a plot represents a signature of the material microstructure. The important advantage of dynamic shear is that it allows us to characterize microstructures without disrupting them in the process. The net deformation imposed on the sample is minimal because the experiments are restricted to small strain amplitudes within the LVE regime of the sample. As a result, the linear viscoelastic moduli reflect the microstructures present in the sample at rest. This is to be contrasted with steady shear, where the material functions are always obtained under flow conditions corresponding to relatively drastic deformations. We can therefore correlate dynamic rheological parameters to static microstructures, and parameters under steady shear to flow-induced changes in microstructure.

2.7 Optical Microscopy

Liquid crystals are found to be birefringent, due to their anisotropic nature. That is, they demonstrate double refraction (having two indices of refraction). Light polarized parallel to the director has a different index of refraction (that is to say it travels at a different velocity) than light polarized perpendicular to the director. When light enters a birefringent material, the process is modelled in terms of the light being broken up into the fast (called the ordinary ray) and slow (called the extraordinary ray) components.

Because the two components travel at different velocities, the waves get out of phase. When the rays are recombined as they exit the birefringent material, the polarization state has changed because of this phase difference. For monochromatic light (single frequency), the magnitude of the phase difference is determined by the length and the birefringence of the material. If the sample is very thin, the ordinary and extraordinary components do not get very far out of phase. Likewise, if the sample is thick, the phase difference can be large. If the phase difference equals 360° , the wave returns to its original polarization state and is blocked by the second polarizer. The size of the phase shift determines the intensity of the transmitted light. In a typical liquid crystal, the birefringence and length are not constant over the entire sample. This means that some areas appear light and others appear dark, taken between crossed polarizers. The light and dark areas that denote regions of differing director orientation, birefringence, and length. Due to their different microscopic arrangements, every lyotropic liquid crystalline phase possesses a typical pattern under polarized light visible with the help of an optical microscope. Lamellar and hexagonal phases are birefringent, while cubic and micellar phases are optically isotropic. Lamellar phases show a typical mosaic-like texture often accompanied by “Maltese crosses” (see fig. 1.3), whereas hexagonal phases display a fan-like pattern (see fig. 1.4).

2.8 Nuclear Magnetic Resonance (NMR)

2.8.1 ^2H NMR Quadrupolar Splittings in Anisotropic LC

Nuclei with a spin quantum number $I \geq 1$, such as ^2H , have an electric quadrupolar moment that can interact with nonzero net electric field gradients giving multiple resonance of $2I$ peaks.⁹⁰ If we consider the static ^2H NMR spectrum of an anisotropic liquid crystalline sample prepared in heavy water these peaks would be separated by the splitting:

$$\Delta\nu_q = \frac{3}{m} P_b \chi S_b \quad \text{Eq 2.18}$$

where $m = 4$ and 8 for the lamellar and hexagonal phase, respectively. P_b is the fraction of the observed nucleus in the bound state, χ is the quadrupolar coupling constant, and $S_b = 1/2(3 \cos^2 \theta_D - 1)$ is the order parameter related to the average time orientation (θ_D) of the nucleus with respect to the surfactant chain axis. For water molecules, P_b is linearly dependent on the surfactant/water (S/W) molar ratio, and on the number of bound water molecules per polar head n_b . Then eq 2.18 can be rewritten as:⁹⁰

$$\Delta\nu_q = \frac{3}{m} n_b \frac{S}{W} \chi S_b \quad \text{Eq 2.19}$$

Lamellar and hexagonal phases are uniaxial phases with a symmetry axis (usually called the director) that lie along the cylinder-axis in H_{II} phases while it is perpendicular to the bilayer planes in L_α phases. It is possible to demonstrate that the $\theta_D = 90^\circ$ orientation of the director axis with respect to the main magnetic field would

have a splitting of one-half that obtained at the $\theta_D = 0^\circ$ orientation. Furthermore, the intensity of the $\theta_D = 90^\circ$ peak would decline steadily to the $\theta_D = 0^\circ$ peak which would have the least intensity. Conversely, if a phase is isotropic (cubic or micellar), on the relevant NMR timescale, static quadrupolar interactions are averaged to zero by molecular motion ($S_b = 0$) and the spectrum, from equation 2.19, would have a single resonance. However, it should be possible to distinguish between diverse phases taking into account their different rheological properties. Indeed, L_2 phases possess a low viscosity, while cubic phases are characterized by a high stiffness. Finally, it is worth noticing that the observation of different quadrupolar splittings or the superimposition of an isotropic and an anisotropic signal leads to identify multiphase systems.

3 Chapter

3.1 MO-based formulations

3.1.1 Introduction

During the past decades advancement in bottom up/top down strategies have improved the ability in matter manipulation, thus favouring the proliferation of sophisticated nanocarriers able to deploy pharmaceutical cargos to specific tissue. Nowadays, along with traditional colloidal dispersions (i.e., micelles, microemulsions, liposomes, etc.),^{91,92} the drug delivery systems arsenal also embraces polymer gel,^{93,94} polyelectrolyte multilayer capsules,⁹⁵ as well as inorganic nanoparticles^{96,97} and composite nanomaterials.⁹⁸

In this context, lipid based self-assembled nanostructures always represent a powerful choice in virtue of their features and performances.^{42,99–103} Moreover, given their intrinsic resemblance to biomembranes, they are greatly appreciated when studying drug/nanocarrier-cell interactions.^{104–106} Liposomes and, in a wider perspective, lipid based vesicles represent an emblematic example of this category. They are a class of self-assembled nanostructures that possess a vast range of applications. Depending on the chemical composition, vesicles may or may not be a true equilibrium state. In the latter case they must be considered as metastable (thermodynamically unstable) nanostructures endowed of high kinetic stability.¹⁰⁷ In spite of the number of articles devoted to this subject, so far, the issue of the thermodynamic or kinetic origin of the vesicles' stability is still a matter of debate.¹⁰⁸

When the volume fraction of the dispersed phase reaches the critical value of 0.494 (the limit before hard sphere crystallization),¹⁰⁹ these bilayered nanostructures may originate viscous systems basically composed of densely packed vesicles, commonly termed vesicle gels. Prepared by high-pressure homogenization and mainly composed of small uni-lamellar vesicles, gels based on phospholipids (Vesicular Phospholipid Gels, VPGs), are known since the early nineties.^{110,111} It was shown that they can serve as sustained release systems for various low molecular weight drugs, especially in the field of anticancer treatments.^{30,112} Importantly, it was recently demonstrated that VPGs may effectively work as a protein depot system, allowing for a prolonged release of erythropoietin.¹¹³

The VPG formulations are often proposed for topical drug delivery¹¹⁴ and depot applications since they overcome the major disadvantage of using vesicles for localized applications, which is the liquid nature of the preparation. Indeed, desirable viscosity of vesicle dispersions is sometimes achieved by vesicles incorporation into polymeric gels^{115,116} or using thickening agents such as cellulose derivatives.¹¹⁷ Nevertheless, in these cases structural modification of the self-assembled nanostructure may arise because of polymer-amphiphile interactions. Moreover, vesicle gels represent a suitable storage form of vesicles because conventional vesicles can be easily obtained upon dilution with water.

Liposomes have been proposed since the early eighties as skin drug delivery systems.¹⁵ Indeed, skin represents an appealing gateway for the delivery of drugs, especially when enteral administration cannot be pursued, or to achieve a better patient compliance.

Every system designed for the skin delivery should be able to favour the permeation of drugs to the deeper skin layers (the viable epidermis and eventually the vascularised derma). However, as in most cases traditional liposomes remain confined to the upper layer of the *stratum corneum* (SC), they were found inadequate for drug delivery through the skin.^{118,119} Therefore, the original liposome nanostructures have been implemented by engineering new liposome nanocarriers variously termed Transferosomes[®], ethosomes, or niosomes, depending on their peculiar features. Transferosomes[®] are liposomes that express high deformability because of the addition of an edge activator, a surfactant having a high radius of curvature that destabilizes the lipid bilayer.^{16,120} Thanks to their elasticity they can squeeze between the corneocytes more easily, entering the deep skin layers. Ethosomes exploit the interdigitation effect of ethanol (which is part of their nanostructure) on lipid bilayers to enhance permeation.^{121,122} Niosomes are vesicles composed of nonionic surfactants and having functions similar to liposomes.^{123,124} It deserves noticing that, despite the huge number of papers published on this topic, the exact mechanisms that drive the penetration process still remain a matter of speculation.^{64,125} However, from an empirical point of view, all these innovative nanocarriers have been found to increase both the dermal and the transdermal release, often without being particularly selective in one sense or the other.¹²⁶

Indeed, when delivering a drug through the skin, it is worth distinguishing between two possible, both desirable, results: the drug local accumulation into the skin (dermal release), or the permeation through the skin (transdermal release).¹²⁷ Plainly, the target of the drug will decide which of the two effects (accumulation or permeation) will be unwanted. For instance, a carrier developed for skin diseases such as autoimmune disorders (e.g., psoriasis), tumors, herpes, or erythema, should effectively cross the SC, and reach the deep skin layers, but, at the same time, should not be released into blood circulation, to avoid either waste of the drug (with the concomitant reduction of the therapeutic response) or side effects associated with systemic delivery (definitely, one of the main reason that underpins the dermal delivery strategy).¹²⁸ However, when targeting the drug delivery to the blood circulatory system high transdermal flux and low accumulation into the skin are required.

In this section are described a novel cationic liposome nanocarrier, composed of monoolein and lauroylcholine chloride, as well as the vesicle lipid gel (VLG) obtained from the same system by increasing the dispersed phase concentration. Furthermore, the performances in topical drug delivery of the cationic liposome nanocarrier were tested.

The investigation reported in paragraph 3.3 is devoted to the evaluation of a novel liposome nanostructure proposed as a platform for the development of nanocarriers able to protect, transport, and release sensitive therapeutic agents.¹²⁹ Such a nanostructure is formulated by combining two penetration enhancers, namely

monoolein and lauroylcholine chloride, combined to rapidly formulate (15 min) a cationic liposome nanostructure endowed of excellent stability (> 6 months) and skin penetration ability, along with low short-term cytotoxicity, as evaluated via the MTT test, while diclofenac was added as a model hydrophobic drug. The physicochemical features, investigated through SAXS, DLS, and cryo-TEM techniques, reveal that the nanostructure is retained after loading with diclofenac in its acid (hydrophobic) form. The drug release performances are studied using intact newborn pig skin.

Bearing in mind the good performances shown by this liposomal system and its possible relevance in the field of topical drug delivery, the 3.4 paragraph is devoted to the exploration of the morphological and the viscoelastic properties of a gel system prepared by simply increasing the vesicles' dispersed phase of the monoolein/lauroylcholine-based formulations. A number of vesicular formulations were prepared, in the range of 4-14 wt% of the dispersed phase, to investigate the system evolution from dilute uni-lamellar vesicles dispersion to a vesicle lipid gel. Morphology, thermal stability up to 55 °C, and viscoelastic properties, along with the effect of acid diclofenac inclusion within the formulation, were evaluated by cryo-TEM, SAXS, and rheological measurements. Moreover, the nanostructure of the vesicle dispersion obtained upon gel dilution in water was assessed by cryo-TEM and SAXS, while DLS was used to monitor the formulation stability (size and ζ -potential).

3.2 Materials and methods

3.2.1 Materials

Monoolein (MO, 1-monooleoylglycerol, RYLO MG 90-glycerol monooleate; 98.1 wt% monoglyceride) was kindly provided by Danisco Ingredients, Brabrand, Denmark. Lauroylcholine chloride (LCh) was from TCI Europe. Distilled water, passed through a Milli-Q water purification system (Millipore), was used to prepare the samples. Diclofenac free acid (DCFH) was obtained by acidic precipitation from a solution of sodium diclofenac purchased from Sigma–Aldrich (Milan, Italy). All substances were used without further purification. All concentrations are given in % (wt/wt).

3.2.2 Formulations preparation

Liposomes and VLG, empty or loaded with DCFH (about 1 mg mL⁻¹), are obtained by dispersing weighed amount of MO in aqueous solutions containing LCh using an Ultra-Turrax T10 (IKA) device, equipped with a S10N-5G dispersing tool working at 30000 rpm for 10 minutes.

Concerning liposomes characterization, it was performed as a function of cationic surfactant content, the total dispersed phase (MO + LCh) was between 3.5-3.8 wt%.

While VLG characterization was performed as a function of dispersed phase (MO + LCh, indicated as DP in the section 3.4) content between 4-14 wt%.

The sample volume was usually 3 mL. To obtain drug-loaded liposomes, DCFH was dissolved in the melted monoolein before Ultra-Turrax dispersion. All the samples were analyzed at least 48 h after their preparation. Liposomes loaded with drug were analyzed after separation of non encapsulated drug.

Biological assays and ex vivo release test have been performed on liposomal formulation only, while rheological experiments concerns VLG formulation.

3.2.3 Dynamic Light Scattering (DLS) and Zeta (ζ)-Potential Experiments

Particle size and ζ -potential determinations of the vesicles were performed with a ZetaSizer nano ZS (Malvern Instruments, Malvern, UK) at a temperature of 25 ± 0.1 °C. Samples were backscattered by a 4 mW He–Ne laser (operating at a wavelength of 633 nm) at an angle of 173°. At least 2 independent samples were taken, each of which was measured 3 up to 5 times.

3.2.4 Small-Angle X-ray Scattering (SAXS) Experiments

Small-angle X-ray scattering was recorded with a S3-MICRO SWAXS camera system (HECUS X-ray Systems, Graz, Austria). Cu K α radiation of wavelength 1.542 Å was provided by a GeniX X-ray generator, operating at 50 kV and 1 mA. A 1D-PSD-50 M system (HECUS X-ray Systems, Graz, Austria) containing 1024 channels of width 54.0 μ m was used for detection of scattered X-rays in the small-angle region. The working q -range (Å^{-1}) was $0.003 \leq q \leq 0.6$, where $q = 4\pi \sin(\theta)\lambda^{-1}$ is the modulus of the scattering wave vector. Thin-walled 2 mm glass capillaries were filled with the liposomal dispersions for the scattering

experiments. The diffraction patterns were recorded for at least 3600 s. The solvent background scattering was subtracted from the intensity, and the resulting quantity was normalized and denoted as $I(q)$. The distance between the sample and detector was 265 mm. To minimize scattering from air, the camera volume was kept under vacuum during the measurements. Silver behenate ($\text{CH}_3\text{-(CH}_2\text{)}_{20}\text{-COOAg}$) with a d spacing value of 58.38 Å was used as a standard to calibrate the angular scale of the measured intensity. SAXS patterns were analyzed in terms of a global model using the program GAP (Global Analysis Program)^{84,87,130} previously described in Chp. 2.

3.2.5 *Biological assay*

3.2.5.1 *CELL CULTURES AND TREATMENTS*

Mouse 3T3 fibroblasts (ATCC collection) were grown at 37 °C in phenol red-free Dulbecco's modified Eagle's medium (DMEM, Invitrogen, USA) with high glucose, supplemented with 10% (v/v) fetal bovine serum, penicillin (100 U mL^{-1}), and streptomycin ($100 \mu\text{g mL}^{-1}$) (Invitrogen) in 5% CO_2 incubator at 37 °C. Cells were grown in 35 mm dishes, and experiments were carried out two days after seeding, when cells had reached 80 - 90% confluence. Liposome formulations and LCh solutions were added to the cells at a concentration of 1:200 (10 μL of sample in 2 mL of medium), and incubated at 37 °C for 2, 4, 24, and 48 h. Oleic acid and monoolein were dissolved in DMSO at a concentration of 100 and 430 mM respectively. These concentrated solutions were added to the culture medium at a dilution 1:1000. For live cell imaging, after replacing the sample suspension with fresh serum-free medium, cells were loaded with fluorescent probes, that after incubation time were washed out before imaging session. Cells were supravivally stained with the following probes (ex, em = fluorescence excitation and emission): 300 nM Nile Red (9-diethylamino-5H-benzo[α]phenoxazine-5-one) for 15 min (ex 470 ± 20 , em 535 ± 40 for neutral lipids; ex 546 ± 6 , em 620 ± 60 for cytoplasmic membrane); 650 nM Hoechst 33258 for 15 min (ex 360 ± 20 , em 460 ± 25). Vehicles were DMSO for Nile Red and water for Hoechst. Stock solutions were 1000-fold concentrated not to exceed the 0.1% concentration of vehicle in the medium. Nile Red was from Fluka (Buchs, SG, Switzerland), Hoechst from Sigma-Aldrich (St Louis, MO, USA). The Nile Red is an ideal probe for the detection of lipids, as it exhibits high affinity, specificity and sensitivity to the degree of hydrophobicity of lipids. The latter feature results in a shift in the fluorescence emission, from red to green, correlating with the level of hydrophobicity of lipids.¹³¹ Accordingly, cytoplasmic membranes mostly composed of phospholipids are generally stained in red, whereas neutral lipids encased in the lipid droplets are stained in green. Hoechst is a blue dye used for counterstaining the nucleus and to evaluate cell proliferation or chromatin condensation.

3.2.5.2 *FLUORESCENCE MICROSCOPY AND IMAGE ANALYSIS*

Light microscopy observations were made using a Zeiss (Axioskop) upright fluorescence microscope (Zeiss, Oberkochen, Germany) equipped with 20 \times and 40 \times /0.75 NA water immersion objectives and a HBO 50 W

L-2 mercury lamp (Osram, Berlin, Germany). Twelve-bit-deep images were acquired with a monochrome cooled CCD camera (QICAM, Qimaging, Canada) with variable exposure. The adopted filters allowed a virtually complete separation of the emissions and the simultaneous observation of the Nile Red and Hoechst probes. In general, microscope operations (filter exchanges, exposure time settings and focus adjustments) required an interval of 30 - 60 s between images of different fluorochromes. This resulted in a slight displacement of structures, because of live cell movements. Image analysis and quantification of lipid droplets were performed with Image Pro Plus software (Media Cybernetics, Silver Springs, MD).

3.2.5.3 MTT ASSAY FOR CELL VIABILITY

Cell viability was analyzed by the MTT (3(4,5-dimethylthiazolyl-2)-2, 5-diphenyltetrazolium bromide, Sigma) colorimetric assay. 3T3 fibroblasts were seeded in 24-well plates (3×10^4 cell/well) and cultured overnight in serum-containing media. Then cells were incubated in the presence of the different liposome formulations (1:200, 2.5 μ L of liposome formulation in 500 μ L of medium), monoolein (430 μ M in DMSO) and LCh solutions (47, and 202 μ M) for 2, 4, 24 and 48 h at 37 °C. MO and LCh solutions are equimolar with the lipid and surfactant present in the liposome formulations. Treated cells were incubated with MTT (0.5 mg mL⁻¹) for 2 h at 37 °C. Then, media were removed, and cells were lysed with DMSO. Absorbance was measured at 570 nm using a microplate reader (Synergy 4, Synergy™ Multi-Detection Microplate Reader, BioTek Instruments). All measurements were performed in triplicate and repeated at least three times. Results are shown as percent of cell viability in comparison with non-treated control cells.

3.2.5.4 STATISTICS

Statistical analysis was carried out with Excel (Microsoft Co., Redmond, WA). Results were expressed as a mean \pm standard deviation (SD). Statistically significant difference was evaluated by two sample t test with $p < 0.001$ as a minimal level of significance.

3.2.6 In vitro Release

3.2.6.1 GEL PREPARATION

Hydroxypropylmethyl cellulose (HPMC) gel (2%) was prepared by carefully hydrating and slowly stirring the polymer at room temperature for 24 h to ensure uniform mixing while avoiding bubble production. After gel formation acid diclofenac was incorporated, at the same concentration of the liposomal formulation, under constant stirring.

3.2.6.2 DRUG LOADING EFFICIENCY (E%)

Liposome dispersions loaded with DCFH (LDH) were separated from the untrapped material by gel chromatography on Sephadex G75. Sephadex was allowed to swell in water for two hours, and then in a 50-cm column fitted with the polymer dispersion. 1 mL of formulation was loaded on Sephadex, and then eluted samples were assayed for drug content. Drug loading efficiency, expressed as the percentage of the

amount of drug initially used, was determined by high performance liquid chromatography (HPLC) after disruption of vesicles with 0.025% non-ionic Triton X-100. Diclofenac content was quantified at 227 nm using a chromatograph Alliance 2690 (Waters, Italy). The column was a Symmetry C18 (3.5 μ , 4.6 \times 100 mm, Waters). The mobile phase was a mixture of 30% water and 70% acetonitrile (v/v), delivered at a flow rate of 0.5 mL min⁻¹. A standard calibration curve (peak area of diclofenac versus known drug concentration) was built up by using working, standard solutions (1.0 - 0.01 mg/mL). Calibration graphs were plotted according to the linear regression analysis, which gave a correlation coefficient value (R²) of 0.998. The DCFH retention time was 1.5 minutes, and the minimum detectable amount was 2 ng/mL.

3.2.6.3 DEFORMABILITY MEASUREMENTS

Liposome dispersion was extruded at constant pressure through 19-mm polycarbonate filters of definite pore size (50 nm), using an extrusion device Liposofast[®] (Avestin, Canada).

3.2.6.4 EX VIVO SKIN PENETRATION AND PERMEATION STUDIES

Experiments were performed non-occlusively by means of Franz diffusion vertical cells with an effective diffusion area of 0.785 cm², using newborn pig skin. One-day-old Goland–Pietrain hybrid pigs (about 1.2 kg) were provided by a local slaughterhouse. The skin, stored at -80 °C, was pre-equilibrated in physiological solution at 25 °C, two hours before the experiments. Skin specimens (n = 6 per formulation) were sandwiched securely between donor and receptor compartments of the Franz cells, with the *stratum corneum* (SC) side facing the donor compartment. The receptor compartment was filled with 5.5 mL of physiological solution, which was continuously stirred with a small magnetic bar, and thermostated at 37 \pm 1 °C throughout the experiments to reach the physiological skin temperature (i.e., 32 \pm 1 °C). 100 μ L of the formulation to be tested (0.1% DCFH loaded liposome or gel formulation) was placed onto the skin surface (6 cells for each formulation). At regular intervals of 2 h, up to 24 h, the receiving solution was withdrawn and analyzed by HPLC for drug content. After 24 h, the skin surface of specimens was washed and the SC was removed by stripping with adhesive tape Tesa[®] AG (Hamburg, Germany). Each piece of the adhesive tape was firmly pressed on the skin surface and rapidly pulled off with one fluent stroke. The epidermis was separated from the dermis with a surgical sterile scalpel. Tape strips, epidermis, and dermis were placed each in methanol, sonicated to extract the drug and then assayed for drug content by HPLC.

3.2.7 Rheology

Rheological analyses were performed in triplicate using a stress control rheometer (MARS III Thermo Haake Scientific) equipped with a cone-plate geometry and cone-plate angle 1° (gap 53 μ m with diameter 20 mm and 60 mm, respectively, depending on the sample viscosity) operating both in steady and oscillation mode. The selected temperatures of 25 and 32 °C were controlled by the Peltier device with an accuracy of \pm 0.1°C. To prevent evaporation of water, the cone-plate cell was covered by a solvent trap. Steady state stress sweep experiments were carried out both in control stress and control rate mode to investigate the flow curves for

several samples in the range DP 4-14 wt%. For each flow curve, zero-shear viscosity was checked at low shear rates to determine the correspondent Newtonian plateau region.

For the dynamic oscillatory rheology investigation the samples were exposed to increasing stress (0.01-100 Pa) at a constant frequency ($f = 0.1$ or 1 Hz) to determine the linear viscoelastic range of the samples. Then, selected stress values in the linear region (usually 1-10 Pa) were used in the other oscillation tests.

In oscillatory frequency sweep experiments the samples were exposed to a stepwise of increasing frequency ($f = 0.01$ -100 Hz range) at a constant stress in the field of linear viscoelasticity. The frequency range (expressed in terms of angular frequency $\omega = 2\pi f$), the shear storage (elastic) G' and loss (viscous) G'' moduli both in Pa were plotted in logarithmic-linear scale. Graphical data were reported as the mean of the three curves obtained from the repetitions.

For full theory about methods employed in these works see Chp. 2.

3.3 Physicochemical, Cytotoxic, and Dermal Release Features of a Novel Cationic Liposome Nanocarrier.

3.3.1 Characterization of the Nanocarrier

A series of liposome samples with total monoolein (MO) concentration corresponding to around 4 wt% and increasing amount of lauroylcholine (LCh) were prepared by simply dispersing the components (MO and LCh) in water using an Ultra Turrax device as described in the Experimental section. Samples compositions are reported in Table 3.3.1.

Table 3.3.1. Liposome composition (wt %), mean diameter (nm \pm SD), polydispersity index (PI), and zeta (ζ -potential (mV \pm SD)).^a

Sample	MO/LCh/W	Mean diameter	PI	ζ -potential
LPS0.3	3.3/0.3/96.4	82 \pm 23	0.325	57.3 \pm 4.6
LPS0.4	3.2/0.4/96.4	82 \pm 9	0.275	65.7 \pm 1.1
LPS0.7	3.0/0.7/96.3	77 \pm 26	0.292	71.0 \pm 2.4
LPS1.3	2.5/1.3/96.2	87 \pm 35	0.354	82.8 \pm 0.5
LDH	3.3/0.3/96.4	202 \pm 1	0.121	36.0 \pm 0.8

[a] LDH indicates the acid diclofenac loaded liposomes.

The liposomes morphology was evaluated via transmission electron microscopy at cryogenic temperature (cryo-TEM). In Figure 3.3.1A,B we show micrographs representative of the discussed samples. As can be seen, though some larger bilamellar liposomes were also observed, these systems mainly consist of homogeneously dispersed small unilamellar vesicles (SUVs). Interestingly, some of the double walled liposomes show a defect (indicated by a white arrow), which is very common for this kind of nanostructure, the so-called interlamellar attachment (ILA).

Such semi-toroidal bilayer attachments between flat bilayer sheets represent intermediates during the process of membrane fusion (as in this case) or phase transitions.¹³² Results from dynamic light scattering (DLS, see Table 3.3.1) analysis confirm those previously discussed and collected via cryo-TEM. Accordingly, samples are composed by liposome having a mean diameter of about 80 nm and characterized by a relatively narrow size distribution, with a polydispersity index (PI) around 0.3.

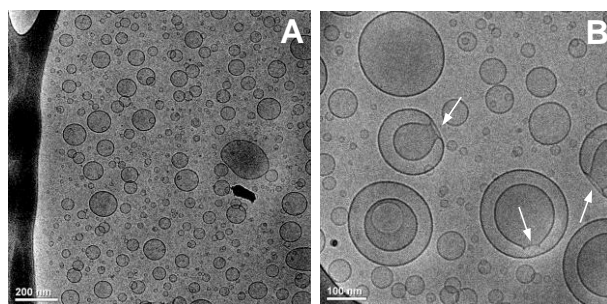


Figure 3.3.1. Cryo-TEM images of the sample LPS0.3 showing (A) unilamellar and (B) bilamellar liposomes. White arrows in B indicate interlamellar attachments (see the text).

The formation of MO-based SUVs is conditioned to LCh addition. This short-chain surfactant intercalates between the MO palisade, decreasing the MO effective packing parameter (P_{eff} , defined as the ratio v/a_0l , where v is the volume of the surfactant tail, a is the cross-sectional area of the surfactant polar head, and l is the fully stretched length of the surfactant hydrophobic tail), and disturbing the regular arrangement of both the lipid tails and the polar heads. This allows for the bilayer folding toward the liposomal nanostructure. Consequently, the absence of correlation observed between the amount of LCh used for sample preparation and the size of the liposomes is quite surprising. This fact deserves some comments. The mechanisms that determine the stability, size and shape of the vesicles are complex and have been widely discussed.¹³³ Briefly, the bending of the lipid bilayer to form a vesicle imposes a strain on a symmetric bilayer, as the inner monolayer has a negative curvature, while the outer has a positive curvature. In many cases the magnitude of this curvature energy is thought to be significant enough to make the vesicles inherently unstable, and energy has to be added to allow bilayer folding. It follows that the liposome formation is favoured by soft bilayers, since less energy is required for the bending of the bilayer. Thus, it can be inferred that in these liposome formulations the inner structure of the dispersions is basically dictated by the energy input supplied through the Ultra Turrax device, rather than by the composition of the formulation. On the contrary, as reported in Table 3.3.1, liposomes exhibit a positive ζ -potential that, as expected, increases with LCh concentration. Collected values are in the range 57.3 - 82.8 mV. Since the ζ -potential reflects the net charge on the surface of the liposome, these values indicate the increased amount of the cationic surfactant entrapped within the MO palisade, while varying samples composition and, at the same time, the good stability against aggregation and fusion of these colloidal suspensions.^{134,135} Sample stability was checked by visual (naked eye) inspection and measuring size distribution, polydispersity index, and ζ -potential during some months. Formulations have good long-term stability (when stored at room temperature), and appreciable variation of these parameters could not be detected even after six months.

Variable temperature SAXS experiments were also performed in the range of 25 - 55 °C to evaluate thickness and stability of the lipid bilayer. Within the temperature range investigated, the bilayer thickness calculated with the Global Analysis Program (GAP, see the Experimental section) was found equal to 47 ± 1 Å. This value does not change significantly upon increasing the temperature and/or the LCh amount, thus

highlighting once again the high stability of these formulations. It should be remarked that these fully hydrated bilayers are thicker with respect to that measured in the lamellar phases of the MO/water binary system (water content around 15%) for which a structure parameter of 42 Å was assessed.¹³⁶

3.3.2 Cytotoxicity Assays

Given the potential application of these liposome formulations as drug carriers, their toxicity against mouse 3T3 fibroblasts was evaluated in vitro at different incubation time (2, 4, 24, 48 h) according to the MTT assay (which measures levels of metabolically active mitochondrial dehydrogenase enzymes). As shown in figure 3.3.2, compared to untreated control cells sample LPS0.3 did not show a significant cytotoxic activity in the first 4 h of incubation time. Differently, a statistically significant cytotoxic effect could be observed with LPS1.3. In this case the treatment caused more than 50% of cell death. At long-term exposure (24, 48 h), both liposome formulations induced massive cell death (more than 80% cell killing).

Cytotoxicity experiments were supported by fluorescence microscopy observations of 3T3 cells that had been previously treated with the liposomes under the same conditions and, after liposome wash-out, were co-loaded with Nile Red and Hoechst probes to identify lipid droplets and nuclear morphology, respectively. Lipid droplets are dynamic organelles mainly involved in fat storage (essentially neutral lipids as triacylglycerols and cholesteryl esters) used for lipid metabolism and the synthesis of membrane lipids.

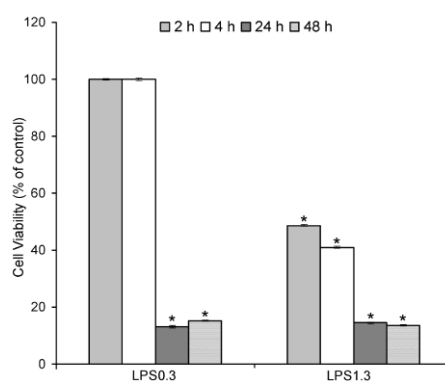


Figure 3.3.2. Results of MTT assay of the 3T3 cells exposed to the liposome formulations (1:200, 2.5 µL of liposome formulation in 500 µL of medium). 3T3 fibroblasts were incubated with liposomes formulation for 2, 4, 24, 48 h. Cell viability was determined by using the MTT reagent. The percent of treated cells was normalized to the untreated control cells. Error bars indicate the standard deviation of three different experiments with three duplicates per experiments. Statistically significant differences are indicated by * $p < 0.001$ vs. untreated cells by *t*-test.

Upon short time exposure (2, 4 h) to LPS0.3 liposomes, cells did not show any changes either in the morphology or in the intracellular membrane compartments, while chromatin condensation was not detected. Conversely, enhanced lipid droplet formation was observed, suggesting that cells were able to produce and accumulate triacylglycerols from MO-based liposomes (Figure 3.3.3B).

In contrast, treatment of 3T3 cells with LPS1.3 formulation led to the appearance of proapoptotic cells with condensed cell nuclei, and altered intracellular lipid distribution. The red fluorescence of polar lipids in the cytoplasmic membranes appeared very strong, and the green fluorescence of lipid droplets was less visible and intense compared to control cells (Figure 3.3.3C). At long exposures (24, 48 h) both liposome formulations induced massive cell death as shown by detection of rare apoptotic cells with chromatin condensation (Figure 3.3.3E, F).

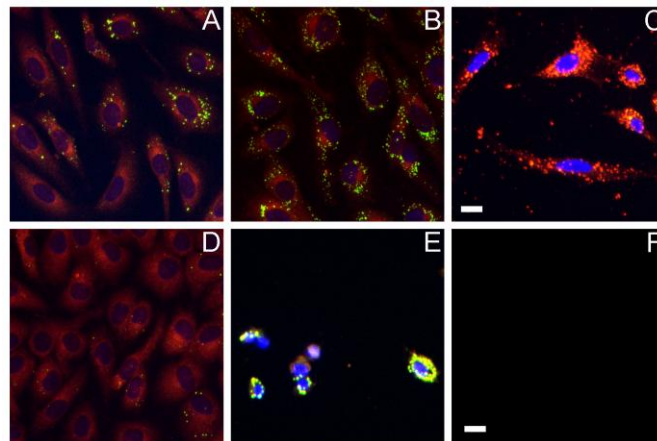


Figure 3.3.3. Representative composite color images of the 3T3 cells exposed to the liposome formulations. Membranes (red) and lipid droplets (green) were stained with Nile Red (colocalization in yellow), nuclei (blue) with Hoechst 33258. A, B, C: short-time treatments (2, 4 h). (A) control cells, (B) cells treated with LPS0.3 liposomes, (C) cells treated with LPS1.3 liposomes. D, E, F: long-time treatments (24, 48 h). (D) control cells, (E) cells treated with LPS0.3 liposomes, (F) cells treated with LPS1.3 liposomes. Scale bars = 20 μ m.

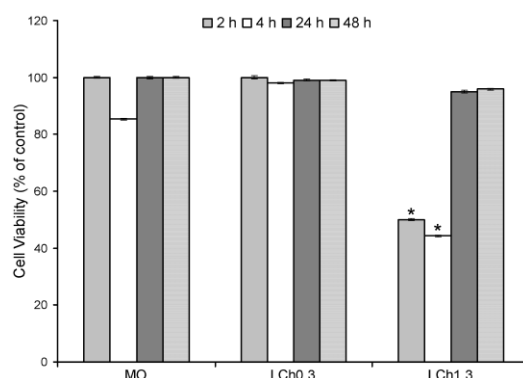


Figure 3.3.4. Results of MTT assay of the 3T3 cells exposed to MO and LCh solutions. 3T3 fibroblasts were incubated with monoolein (430 μ M) and LCh solutions (47 and 202 μ M) for 2, 4, 24, 48 h. Cell viability was determined by using the MTT reagent. The percent of treated cells was normalized to the untreated control cells. Error bars indicate the standard deviation of three different experiments with three duplicates per experiments. Statistically significant differences are indicated by * $p < 0.001$ vs. untreated cells by t -test.

Subsequently, the cytotoxicity of MO and LCh solutions were examined through the MTT assay. When exposed to MO or LCh0.3 alone, either at short or at long incubation time, the treatment did not cause cell death (Figure 3.3.4). On the contrary, more than 50% of cells treated with LCh1.3 formulation showed significant toxicity at short incubation time compared to un-treated control cells, MO and LCh0.3-treated cells. Remarkably, at longer incubation periods cells regained their normal proliferation capacity.

Figure 3.3.5 shows that MO and LCh-treated cells display extensive deposits of lipid droplets, which increase with exposure time. After short treatment with sample LCh1.3, the living cells (50% viability) showed chromatin condensation with intense red fluorescence of the cytoplasmic membranes (see Figure 3.3.5C). However, at longer incubation periods, cells regained their normal proliferation capacity as shown by normal chromatin condensation and cell culture confluence (see Figure 3.3.5F).

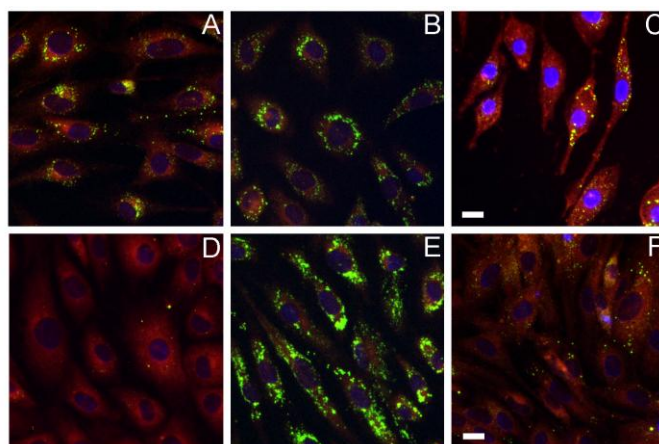


Figure 3.3.5. Representative composite color images of 3T3 cells exposed to the MO and LCh solutions. Membranes (red) and lipid droplets (green) were stained with Nile Red (colocalization in yellow), nuclei (blue) with Hoechst 33258. A, B, C: short-time treatments (2, 4 h). (A) control cells, (B) cells treated with MO, (C) cells treated with LCh1.3 solution. D, E, F: long-time treatments (24, 48 h). (D) control cells, (E) cells treated with MO, (F) cells treated with LCh1.3 solution. Scale bars = 20 μm .

3.3.3 Lipid Droplet Evaluation

Lipid droplet formation is usually induced by long-chain unsaturated fatty acid such as oleic acid.¹³⁷ Administration of exogenous unsaturated fatty acids, especially oleic acid (one of the most frequently used unsaturated fatty acid penetration enhancer), has been reported to increase membrane permeability even if their mechanism of action has not been completely elucidated.¹³⁸ After their internalization, free fatty acids are converted to fatty acyl-CoA, which can be either oxidized in mitochondria, or utilized in the endoplasmic reticulum as substrate for the synthesis of phospholipids, cholesterol esters and triacylglycerols.¹³⁹

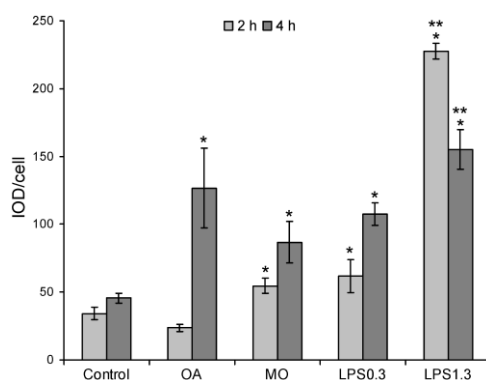


Figure 3.3.6. IOD (Integrated Optical Density) per cell related to lipid droplets formation in 3T3 cells exposed to the oleic acid (OA), monoolein (MO) and liposome (LPS) formulations. Quantification of lipid droplets in 3T3 fibroblasts incubated with OA (100 μM), MO (430 μM) and liposomes was performed with Image Pro Plus. Error bars indicate the standard deviation of at least two independent experiments. Statistically significant differences are indicated by * $p < 0.001$ versus untreated control cells and by ** $p < 0.001$ versus monoolein-treated cells by t-test.

Fluorescence-based detection of lipid droplets is commonly achieved in live cells with the green emission of Nile Red. To examine the possible role of liposome formulations in the lipid droplet formation, treatments were applied to semi-confluent monolayer of 3T3 cells, which contained few lipid droplets. Indeed, lipid droplets of 3T3 fibroblasts are present in high number in proliferating cells, but this number decreases in semi-confluent cells, and strongly diminishes when cells arrive at confluency and stop proliferation due to contact inhibition.¹⁴⁰

After liposome treatment, the lipid droplet formation was examined with green-emission of Nile Red in comparison to untreated cells (as a control), oleic acid-treated cells (as a positive control) and monoolein-treated cells. Experiments were performed only at short-term incubation (2, 4 h, see Figure 3.3.6), because long-term exposure induced massive cell death. Compared to MO-treated cells, statistically significant increased production of lipid droplets was detected with LPS1.3 formulation treatment, whereas no differences were detected with LPS0.3 treatment.

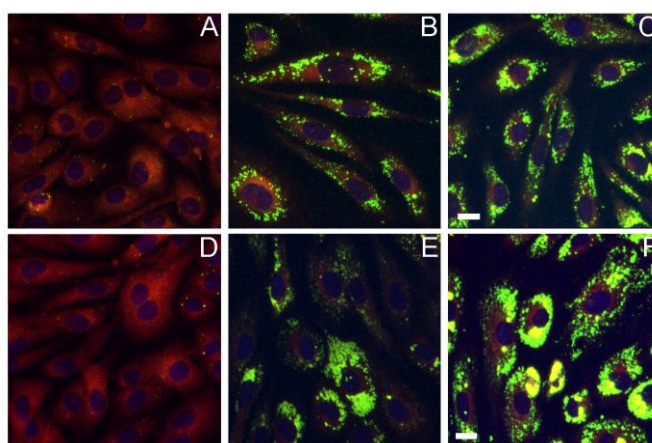


Figure 3.3.7. Representative composite color images of 3T3 cells exposed to the oleic acid and monoolein at 24 and 48 h of incubation time. Membranes (red) and lipid droplets (green) were stained with Nile Red (colocalization in yellow), nuclei (blue) with Hoechst 33258. A, B, C: 24 h treatment. (A) control cells, (B) cells treated with oleic acid, (C) cells treated with monoolein. D, E, F: 48 h treatment. (D) control cells, (E) cells treated with oleic acid, (F) cells treated with monoolein. Scale bars = 20 μm .

This result confirms the strong internalization ability of LCh. OA and MO-treated cells were able to proliferate normally, produce and accumulate neutral lipids in form of lipid droplets also at longer exposition time, where, however, lipid droplets appeared aggregated into large clusters, thus preventing the quantification of the lipid droplet as illustrated in Figure 3.3.7, where long-term experiments are reported.

3.3.4 Characterization of the Drug Loaded Nanocarrier

To check the ability of these innovative formulations in hosting molecules of pharmaceutical interest, diclofenac (DCFH) was added in its acid form (LDH, drug loaded liposome formulation). On the basis of the cytotoxicity tests the formulation with the lowest content of cationic surfactant (LPS0.3) was chosen. This

formulation can nominally host 0.1 wt % of DCFH. Acid diclofenac may interact with the lipid bilayer leading to modifications in the membrane properties.

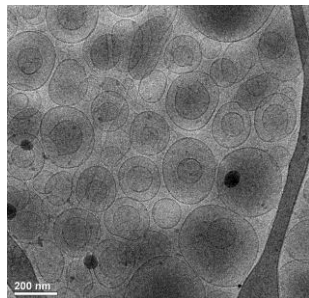


Figure 3.3.8. Cryo-TEM image of the sample LPS0.3 loaded with 0.97 mg/mL of acid diclofenac (LDH formulation).

Therefore, the influence of drug encapsulation on the liposome nanostructure was investigated. Measurements on liposomes loaded with drug were performed after separation of non-encapsulated active molecule.

Before discussing the role of DCFH in the morphological changes of the liposomes, it deserves noticing that diclofenac has a solvophobic behavior that depends on pH. Actually, it was found that this molecule predominantly exists in its acid (hydrophobic) form at pH 3.0, while at pH 7.4 this molecule is almost completely present in its ionized (hydrophilic) form.¹⁴¹ Since in LPS0.3 and LDH formulations pH 4.5 and 3.0 were respectively measured, it can be safely assumed that all the loaded diclofenac is in its hydrophobic form.

The cryo-TEM analysis revealed that the vesicular structure was maintained after the addition of low levels of DCFH, but liposomes increase in size, while the morphology is altered to some extent (see figure 3.3.8). Indeed, along with approximately spherical liposomes some elongated elliptical liposomes are also observed in LDH formulation. DLS measurements confirm the huge increase of liposomes size, with respect to empty liposomes formulations, with a mean diameter varying from about 80 to 200 nm (see Table 1). In addition, bilamellar nanostructures are present in higher numbers, and they appear slightly deformed compared to liposomes without the drug.

Taken as a whole, these results strongly suggest that DCFH, intercalating within the bilayer, modifies the lamellar bending. The effect of the encapsulation of the drug can be interpreted as follows.

Preferred location of DCFH within the bilayer leads to an increment of the hydrophobic tails volume and, in turn, to a greater value of the effective packing parameter. It is worth to recall here that a reduction of MO P_{eff} was called into play to justify the liposome formation (see above). Hence, the DCFH molecule operates against the effect of the LCh surfactant (causing a more rigid bilayer) and partially re-establishes the flatness of the original MO bilayer.

Concerning the measured ζ -potential, it is interesting to point out that the addition of only 0.1 wt% (0.97 mg mL⁻¹) of DCFH decreases the vesicle charge of about 20 mV. Indeed, the ζ -potential shift due to the DCFH loading was expected to a lesser extent because of its inclusion within the lipid palisade.

SAXS analysis through GAP of the drug-loaded system showed an almost unchanged d_B value of the liposomes bilayer in the LDH formulation (46 Å) with respect to that measured in the blank system (47 Å). Figure 3.3.9 shows the SAXS patterns obtained from the LPS0.3 and LDH formulations. Although in the LDH formulation cryo-TEM analysis indicated a strong presence of bilamellar vesicles, the contribution of these structures does not emerge in the SAXS pattern.

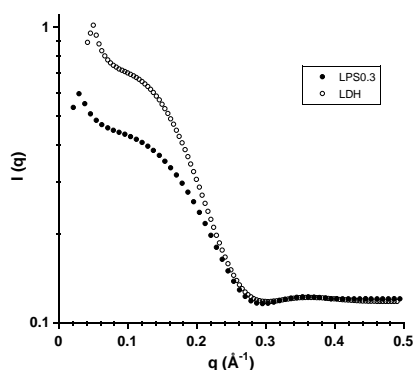


Figure 3.3.9. SAXS patterns of empty (LPS0.3) and drug loaded (LDH) liposomes.

Therefore, it can be properly fitted with pure diffusing scattering model, the same used for unilamellar vesicles (see the Experimental Section). The best fit parameter from the GAP modeling of the SAXS patterns are given in Table 2. For all the formulations examined, such analysis gives for the z_H parameters (which essentially represents the length of the MO hydrocarbon chain, see Scheme 1) a value very close to that reported in literature for MO-based nanostructures (17 Å).

3.3.5 *Ex Vivo Skin Penetration and Permeation Tests*

Liposomes were able to encapsulate large amount of DCFH (E% ~ 51 %). To evaluate the capability of this carrier to enhance the dermal and transdermal delivery of DCFH, a permeation study by using the Franz cell apparatus and newborn pig skin was carried out through the whole skin and in non occlusive condition for 24 h. In Figure 3.3.10 the amount of permeated DCFH per area is plotted against time, and is compared with a gel formulation having the same drug concentration. Examination of the permeation graphs suggests that the systems under consideration reached steady-state conditions, but after different lag times. DCFH showed a shorter lag time (2 h) when incorporated in gel formulation, while in liposomal formulation, because of the very low flux obtained, it was not possible to calculate a lag time value from the curve.

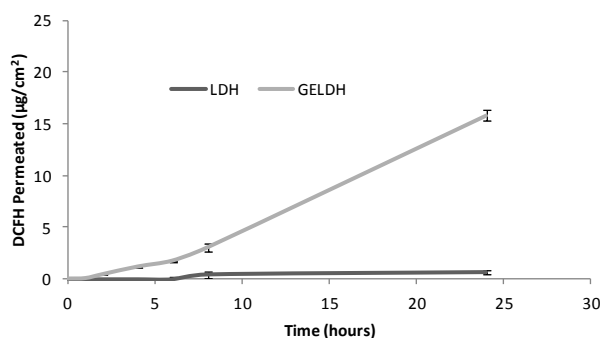


Figure 3.3.10. Ex vivo permeation of DCFH through newborn pig skin from liposomes and gel formulation (control). Each value is the mean \pm standard deviation of six experimental determinations.

The mean amount of the drug permeated after 24 h experiment from the gel was $15.81 \mu\text{g cm}^{-2}$, while $0.72 \mu\text{g cm}^{-2}$ DCFH was delivered by the liposomes. The latter value appears extremely low. It means that after 24 h only 1% of the drug is released through the skin. The Local Accumulation Efficiency (LAC) values, representing the ratio of diclofenac accumulated into the whole skin versus that permeated through the skin, was also calculated. The lowest LAC value was obtained with DCFH loaded gel (0.23), while an anomalously high value (25.31) was found when the DCFH loaded liposome formulation was used. In Figure 3.3.11 the amounts of drug accumulated into the different skin layers are reported. Remarkably, DCFH accumulation was enhanced when the liposomal formulation was used. In particular, the presence of DCFH was predominantly recorded into the viable epidermis, while deposition into the dermis was only 0.02%.

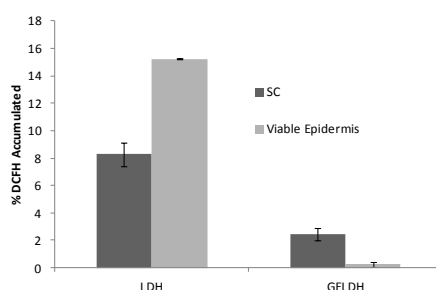


Figure 3.3.11. Cumulative amount of DCFH retained into newborn pig skin layers after 24 h non-occlusive treatment with liposomes and gel formulation (control). Each value is the mean \pm standard deviation of six experimental determinations.

When the gel formulation containing the same amounts of the drug is used, DCFH mainly accumulated into the SC (only 0.04 % of DCFH was found in the dermis). These data prove that LDH formulation was able to induce drug accumulation into the skin strata with a very poor transdermal delivery. Liposome flexibility is often called into play to explain enhanced dermal and transdermal delivery, therefore a measurement of the liposome bilayer deformability was carried out by the extrusion method. Since LDH dispersion was not able to pass through filters of 50 nm pores size, these experiments definitely certify the low deformability of this kind of vesicles.

3.4 Physicochemical and rheological properties of a novel monoolein-based vesicle gel

3.4.1 From vesicles to vesicle gel and back

A series of vesicle-based dispersions were prepared with a MO/LCh fixed ratio and increasing amount of dispersed phase (MO + LCh), indicated as DP, from 4 up to 14 wt%. Samples were prepared by simply dispersing the components (MO and LCh) in water using an Ultra Turrax device as described in the Experimental section. Sample compositions and their macroscopic flow behavior are reported in Table 3.4.1. All samples appeared bluish, while macroscopic viscoelastic behaviour changed from low-viscous liquid to not-flowing gel-like system as a function of DP content. Samples nanostructure was evaluated via SAXS. Some representative SAXS patterns are reported in Fig. 3.4.1. As can be seen, increasing the fraction of DP results in the appearance of quasi-Bragg peaks in the scattering curve. DP4 exhibited a pure diffuse scattering curve, while DP6 and DP12 showed low resolved peaks that can be attributed to an increase in the lamellarity of the system. Finally, DP14 scattering curve is characterized by the presence of three quasi-Bragg peaks.

Table 3.4.1. Sample composition and macroscopic behaviour

Sample	MO/LCh/W (wt %)	Macroscopic behaviour
DP4	3.3/0.3/96.4	Sol
DP6	5.1/0.5/94.4	Sol
DP8	7.0/0.6/92.4	Sol
DP9	7.9/0.7/91.4	Low viscous gel
DP10	8.8/0.8/90.4	Low viscous gel
DP12	10.6/1.0/88.4	High viscous gel
DP13	11.9/1.1/87.0	High viscous gel
DP14	13.2/1.2/85.6	Stiff gel

The SAXS profile clearly indicates the formation of aggregates with oligo- or multi-lamellar structure. The average interbilayer distance between adjacent bilayers (d_{av}), corresponding to 20 ± 3 nm, was calculated by using the Bragg relation $d_{av} = 2\pi h/q$, where q is the position of the various quasi-Bragg peaks, and h is the Miller index.

The morphology of DP14 vesicular gel has been observed by transmission electron microscopy at cryogenic temperature (cryo-TEM).

In agreement with SAXS results, the cryo-TEM image reported in Fig. 3.4.2 showed that the most concentrated formulation (DP14) is composed by closely packed vesicles possessing an oligo-lamellar structure (OLV). In addition, the interbilayer distance (d) obtained by the image analysis was found of 21 ± 4 nm, in conformity with the value (20 ± 3 nm) obtained through SAXS.

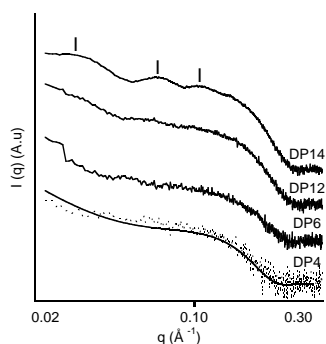


Figure 3.4.1. Log-Log plot of SAXS patterns collected at 25 °C of the samples DP4, DP6, DP12, DP14. Curves are shifted for clarity with multiplication factor 5. Dotted line in DP4 represent experimental curve with superimposed fitting curve (continuous line) obtained with GAP analysis.

It is worth to recall here that the formation of oligo- or multi-lamellar vesicles usually occurs in systems initially constituted by diluted uni-lamellar vesicles when the DP concentration is increased. Indeed, although vesicle shrinking or lamellar phase formation represent alternative morphological evolution pathways, the development of multi-walled vesicles represents the most convenient way in which these kind of systems may arrange the additional interfacial area.

In other words, upon increasing the DP content the number of uni-lamellar vesicles increases until they approach a critical effective volume fraction. Once this threshold is reached, multi-walled vesicles may start to form in order to achieve a more densely packed configuration. Furthermore, nanostructures observed in Fig. 3.4.2 appear as circular or, sometimes, peanuts-like concentric bilayers. Deviations from spherical shape are commonly observed in VLG systems, since also distorted morphologies allows for a better vesicles accommodation.

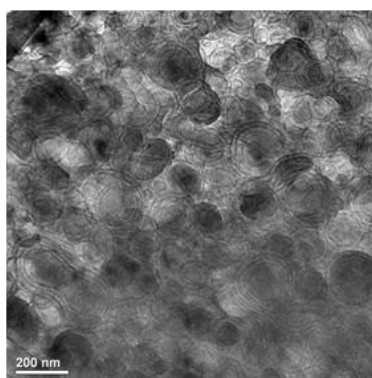


Figure 3.4.2. Cryo-TEM image of the VLG sample DP14 with composition MO/LCh/W = 13.2/1.2/85.6 (wt%) showing oligolamellar close-packed vesicles.

VLG can be regarded as an easy way to store vesicles for a subsequent application, such as systemic use. Indeed, upon a simple VLG dilution, the spontaneous formation of small uni-lamellar vesicles (SUVs) often occurs. Therefore, to test the possibility that upon increasing the water content SUVs form also in the system under investigation, the DP14 VLG was diluted with water while a gentle shaking was applied for a few

minutes. The resulting vesicle dispersions, which contained about 4 wt% of dispersed phase, was re-investigated by SAXS, cryo-TEM and DLS for nanostructure, morphology and long-term stability.

The SAXS profile, reported in Fig. 3.4.3 and superimposed to that of DP4, shows the typical diffuse scattering pattern of single, non-interacting bilayers.

The marked difference in the Guinier part of the two SAXS patterns evidenced that the particle size is dependent of the preparation pathway, showing that this vesicular aggregates are not the equilibrium state for this system. To shed some more light on the colloidal stability of the vesicles investigated in this work, the sample DP4 was newly prepared by mixing MO and LCh in water through a vortex mixer. In a couple of days such a system phase separated.

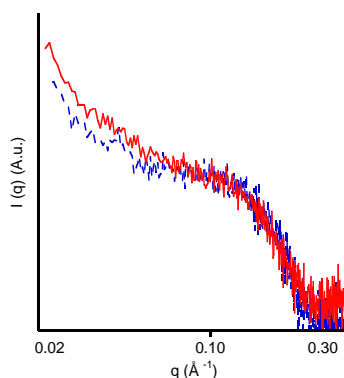


Figure 3.4.3. Log-Log plot of SAXS patterns collected at 25°C of the VLG diluted sample (dashed line) of composition MO/LCh/W = 3.3/0.3/96.4 (wt %) compared with the DP4 sample (solid line) having the same nominal composition.

This simple experiment has profound consequences. Indeed, since the property of being formulated by mixing the components without energy input is a fundamental requisite displayed by thermodynamically stable vesicle systems, the formerly reported experiment definitely proved that the system under investigation, although endowed of a very long shelf-life, is only kinetically stable.

The bilayer thickness d_B calculated with GAP (see the Experimental section) of the diluted VLG was found equal to $47 \pm 1 \text{ \AA}$, in agreement with previously reported data. In Fig. 3.4.4 the micrograph of this sample is reported. Uni-lamellar vesicles dominate the sample, although some tubular vesicles are also present (not shown). From the rheological point of view this sample is identical to the sample DP4. Dilute VLG were monitored by DLS for 6 months to check formulation stability.

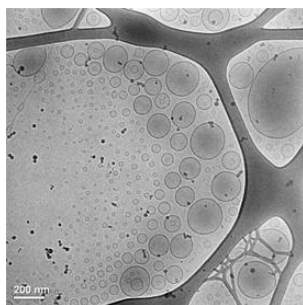


Figure 3.4.4. Cryo-TEM images of the sample MO/LCh/W 3.3/0.3/96.4 (% wt) obtained from dilution of VLG (DP14).

Freshly prepared vesicles are characterized by a particle size distribution having an average diameter (D_{av}) of 79 nm and a polydispersity index (PI) of 0.277. One month old samples did not show any change in both D_{av} and PI, but 6 months after preparation these two parameters increased up to 94 nm and 0.430 respectively. ζ -potential values remained around + 60 mV over the entire period.

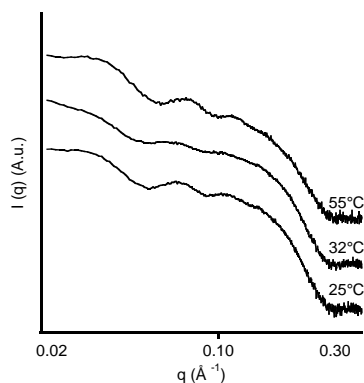


Figure 3.4.5: Log-Log plot of SAXS patterns reported as stack plot of the VLG sample with composition MO/LCh/W = 13.2/1.2/85.6 (wt%) collected at 25, 32, and 55 °C.

The thermal stability of the DP14 formulation was assessed via SAXS measurements performed at 25, 32 and 55 °C. The scattering patterns are shown in Fig. 3.4.5. Particularly, the diffraction pattern at the highest temperature demonstrated the persistence of the nanostructure order and, compared to the system at 25 °C, a slight (1 nm) decrease of d due to thermal fluctuations. Given the potential application of this VLG system as a drug carrier, the ability in hosting molecules of pharmaceutical interest was tested by entrapping 1 mg/g of diclofenac in its acid, hydrophobic form (DCFH). Compared to the formulation not carrying the drug, the latter showed an almost identical SAXS pattern (see Fig. 3.4.6). It can be therefore concluded that the vesicles hydrophobic compartment can suitably accommodate the DCFH drug without losing the original nanostructure.

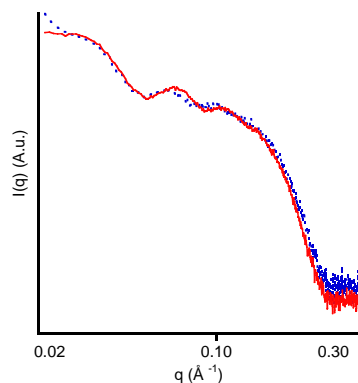


Figure 3.4.6: Log-Log plot of SAXS patterns of the VLG sample empty (red solid line) and loaded with 1 mg/g of HDCF (blue dotted line) collected at 25 °C.

3.4.2 Rheological characterization of VLG

The rheological behavior of a dispersion of vesicles depends on the interaction between vesicles and the vesicle deformability. In vesicles based systems, because of the great amount of solvent vesicles encapsulate into their interior, the effective volume fraction ϕ_v is much larger than the nominal surfactant ϕ_s contained in vesicles bilayers. As a result, even at extremely low DP, in such systems vesicles are densely packed and a highly viscous behavior and (possibly) a yield stress are observed, indicating a gel-like behavior.

To understand the effect of the deformation of the VLG induced by the shear forces, steady state flow curves in terms of dynamic viscosity η vs shear rate $\dot{\gamma}$, were performed as a function of the total DP, in the range 4-14 wt%. Rheograms were also obtained for the model drug delivery system formulated with DCFH. Differently from the sample at the lowest DP content (4 wt%), which is characterized by a constant value of viscosity ($\eta = 9.7 \pm 0.4$ mPa·s) over a wide range of shear rate (Newtonian liquid), formulations prepared at the higher DP content showed a non-linear behavior typical of non-Newtonian pseudoplastic fluids. Indeed, above certain threshold shear rate, η decreases as $\dot{\gamma}$ increases.

Table 3.4.2. Best non-linear fits of the Cross equation

DP (wt %)	η_0 (Pa·s)	K (s)	m
4	$0.0097 (\pm 4 \cdot 10^{-4})$	$0.0027 (\pm 5 \cdot 10^{-4})$	$0.31 (\pm 0.04)$
6	$0.049 (\pm 1 \cdot 10^{-3})$	$0.14 (\pm 0.02)$	$0.35 (\pm 0.05)$
8	$2.28 (\pm 0.02)$	$1.75 (\pm 0.09)$	$0.65 (\pm 0.08)$
9	$150 (\pm 2)$	$52 (\pm 6)$	$0.8 (\pm 0.1)$
10	$5300 (\pm 300)$	$850 (\pm 84)$	$1.10 (\pm 0.05)$
12	$8500 (\pm 350)$	$3360 (\pm 320)$	$1.06 (\pm 0.04)$
14	$37 \cdot 10^3 (\pm 2 \cdot 10^3)$	$396 (\pm 77)$	$1.3 (\pm 0.2)$
DCFH	$36 \cdot 10^3 (\pm 1 \cdot 10^3)$	$2025 (\pm 200)$	$1.0 (\pm 0.1)$

This phenomenon, the so-called shear-thinning, is rather common in oligo- and multilamellar vesicle systems.¹⁴² A widely accepted concept is that at low ϕ_v vesicles relax the external stress through simple Brownian motion by changing particle position distribution. However, cryo-TEM images of more concentrated samples show oligo-lamellar organization for densely packed vesicles (see Fig. 3.4.2).

A possible physical reason of the shear thinning observed in the steady-state shear viscosity experiments at higher DP is that while increasing the shear rate outer shells of oligo-lamellar vesicles may be stripped off thereby leading to smaller vesicles that do not contribute much to the systems viscosity. Other reasonable explanations can be invoked. Particularly, vesicular structure can be deformed during shearing and/or randomly distributed vesicles can come in alignment during shearing. Thus, though dilute vesicle solutions can be treated as hard-sphere dispersions, at moderate to high concentrations the response to mechanical stress can assume the properties of viscoelastic gels near $\phi_v^* = 0.74$ (the maximum packing fraction for spheres). However, at very low shear rate, a region may exist where viscosity remains constant even for non-Newtonian systems, usually defined as zero-shear viscosity η_0 .⁸⁸ At very high shear rate, viscosity may become constant again, giving rise to a behavior known as limiting viscosity at infinite shear η_∞ . Among the various models useful to describe the shear-thinning behavior of most of complex systems, the Cross equation¹⁴³ can be invoked to interpret the flow curves observed in the system under investigation:

$$\frac{\eta_0 - \eta}{\eta - \eta_\infty} = (K\dot{\gamma})^m \quad \text{Eq.: 3.4.1}$$

The dimensionless parameter m is known as the (Cross) rate constant, which is a measure of the degree of dependence of viscosity on shear rate in the shear-thinning region. A value of zero for m indicates Newtonian behaviour with $m \rightarrow 1$ for increasingly shear thinning behaviour. K is known as the (Cross) time constant (or, sometimes, as the Consistency) and has the dimension of time. The reciprocal, $1/K$, gives a critical shear rate, a useful indicator of the onset shear rate for shear thinning.

In the limit $\eta \gg \eta_\infty$ eq. 3.4.1 can be reduced to the following expression:

$$\eta(\dot{\gamma}) = \frac{\eta_0}{1 + (K\dot{\gamma})^m} \quad \text{Eq.: 3.4.2}$$

Figure 3.4.7 shows the log-log plot of the flow curves for several DP values together with the best non-linear fits of eq. 3.4.2, while in Table 3.4.2 the fitting parameters are summarized for the explored compositions. As can be noticed from the listed parameters, the vesicle gel loaded with DCFH starts flowing at lower shear rates ($1/2025 \text{ s} = 5 \cdot 10^{-4} \text{ s}^{-1}$) than the correspondent empty system DP14 ($1/396 \text{ s} = 2.5 \cdot 10^{-3} \text{ s}^{-1}$), implying that the former gel is more prone to flow than the latter.

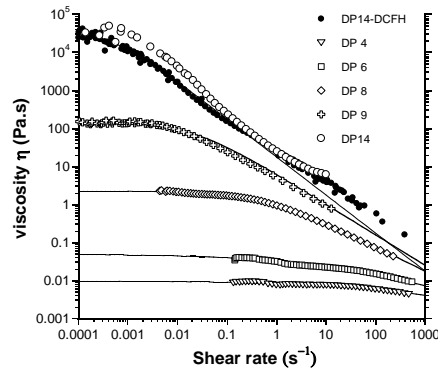


Figure 3.4.7. Log-log plot of shear viscosity vs shear rate measured in steady state experiments as a function of DP. Solid lines are best fits with eq. 3.4.2.

This is in accord with a decrease of storage modulus G' observed for DP14 loaded with DCFH compared to DP14 (see figures. 3.4.9 and 3.4.10) and to the presence of less deformable (hence, worse packed) vesicular aggregates. On the other hand, considering the statistical errors associated to the fitted parameters, both the systems share the same m values, while equal values for η_0 indicate that the material properties are roughly the same in the regime of shear tending to zero, i.e., in regimes of no deformations. The zero-shear viscosity dependence on the vesicle composition can be appreciated by plotting η_0 vs DP as in Fig. 3.4.8.

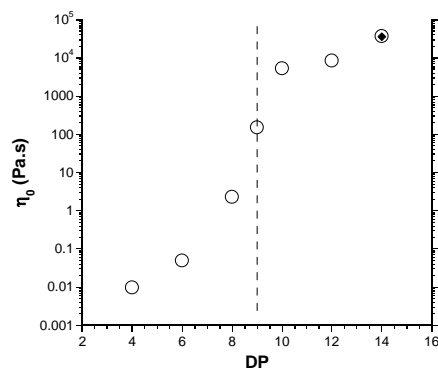


Figure 3.4.8. Semi-log plot of zero-shear viscosity η_0 as a function of DP. Closed rhombus corresponds to the sample DP14 formulated with DCFH. Vertical dashed line indicates a rough transition between sol- and gel-vesicle systems.

The presence of gel-like structures, such as particle gels or colloidal glasses, are basically found under conditions where either repulsive or attractive interactions dominate. For example, concerning ideal hard-sphere particles, the transition from a liquid to a disordered solid phase - a glass - can be observed at volume fractions of about $\phi_v \approx 0.58$.¹⁴⁴

Most of the sol-gel transitions occur through the formation of an interconnected fractal-like network of colloidal particles, which results in a soft viscoelastic solid, known as a gel state.¹⁴⁵ From the rheological data shown, the onset of vesicle gelation can be identified in correspondence of the onset of shear-thinning behavior, when m approaches to unity. This represents the hallmark of densely packed system of vesicles. Above this threshold concentration a dynamical arrest (jamming or gelation) is frequently encountered in

colloidal suspensions.^{134,135} In the system under investigation such a situation is met near DP 9 wt % (see Fig. 3.4.8), when vesicles' mobility is hindered owing to repulsive forces coming from the close presences of neighboring particles. When the surfactant content exceeds DP 9 wt%, oligo- lamellar structures form, as revealed by SAXS (Figure 3.4.1) and Cryo-TEM (Figure 3.4.2).

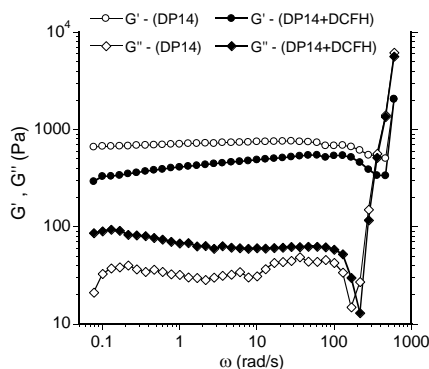


Figure 3.4.9. Linear viscoelastic experiments at 25°C for DP14 sample (open symbols) and DP14 sample loaded with diclofenac DCFH (closed symbols). Circles: storage modulus G' ; diamonds: loss modulus G'' .

Once these samples undergo shear flow, the oligo-lamellar vesicles may strip off and a shear-thinning behaviour can be observed. On the contrary, below DP ca. 9 wt% (uni-lamellar) vesicles can relax the imposed stress through Brownian motions, which is the typical response of Newtonian liquids. Of course, the sol-gel transition is not really sharp and a continuous transition from Newtonian (Cross parameter $m < 1$) to pseudo-plastic behavior ($m \approx 1$) can be observed.

Linear viscoelastic measurements in oscillatory mode showed a near-Maxwell behaviour at low DP, characterized, in the low frequency range, by higher viscous G'' than elastic G' modulus (data not shown).

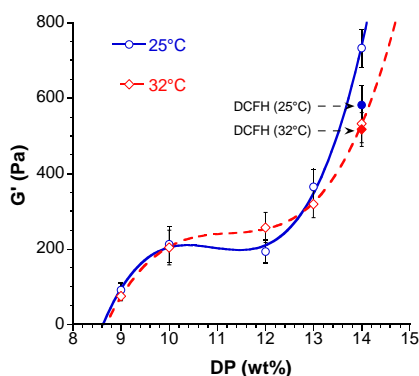


Figure 3.4.10. Storage modulus G' as a function of DP compositions at two different temperatures. $T = 25^\circ\text{C}$: open circles with solid line as guide for eyes; the closed circle corresponds to DP14 gel vesicles encapsulating DCFH. $T = 32^\circ\text{C}$: open diamonds with dashed line as guide for eyes; closed diamond corresponds to DP14 gel vesicles encapsulating DCFH.

The opposite holds in the high frequency regime. Increasing the DP content the viscoelastic properties of the more densely packed OLV showed $G' > G''$. (Fig. 3.4.9, open symbols), both the moduli being almost

frequency independent in the entire frequency range (at least below 200 rad/s). The effect of dispersing DCFH into vesicle bilayers is reflected in a significant decrease of G' and a concomitantly increase of G'' (Fig. 3.4.9, closed symbols). In addition, the G' dependence on DP is more marked at higher DP values.

This means that approaching the maximum packing fraction, vesicle interaction and deformability can give an important contribution to the storage modulus G' .¹⁴⁶ Differently, the complex viscosity is strongly frequency dependent and decreases as the frequency increases with a slope equal to -1 (data not shown). Table 3.4.3 reports, at 25 and 32 °C, the measured G' and G'' moduli at 10 Hz as a function of DP. G' data are also displayed in Fig. 3.4.10, which illustrates a non-linear dependence of the storage modulus vs DP.

In vesicle systems G' is inversely proportional to the cubic power of the vesicle radius. Consequently, the highest G' value observed in Fig. 3.4.10 somehow reflects the vesicles packing compatible with the vesicle sizes and deformability at DP = 14 wt%.

Table 3.4.3. Storage (G') and loss (G'') moduli (in Pa) at 10 Hz obtained at 25 and 32 °C as a function of the dispersed phase DP.

DP (wt%)	25 °C		32 °C	
	G' (Pa)	G'' (Pa)	G' (Pa)	G'' (Pa)
9	91 (\pm 18)	25.7 (\pm 0.8)	75 (\pm 12)	23.0 (\pm 1.5)
10	213 (\pm 47)	19.8 (\pm 3.5)	204 (\pm 46)	23.6 (\pm 3.9)
12	193 (\pm 30)	36.1 (\pm 9.5)	257 (\pm 40)	32.5 (\pm 4.8)
13	365 (\pm 47)	63.4 (\pm 9.2)	319 (\pm 36)	62.5 (\pm 8.9)
14	733 (\pm 50)	69.0 (\pm 9)	532 (\pm 50)	58.0 (\pm 5)
DCFH	582 (\pm 53)	76 (\pm 18)	517 (\pm 45)	90 (\pm 10)

Therefore, the drop of G' observed in the presence of DCFH at $T = 25$ °C (see Fig. 3.4.10) may indicate that drug encapsulation originates larger and less deformable (hence, worse packed) vesicular aggregates. In turn, this suggests that entrapment of DCFH within the bilayer provokes an increase of the elastic bending modulus k_c of the lipid membrane, giving rise to more rigid films akin to the well known effect observed for cholesterol.¹⁴⁷ Such hypothesis is supported by the huge increase in the vesicles' size (from about 80 to 200 nm) previously reported (see paragraph 3.3.4) when a formulation of composition identical to DP4 was loaded with DCFH.¹⁴⁸

The previous arguments are consistent with the dependence of G' on temperature. Indeed, owing to the expected result that k_c decreases as temperature increases,¹⁴⁹ the slight increment of T (from 25 to 32 °C, see Fig. 3.4.10) has a greater effect on the more flexible bilayers of empty vesicles compared to the analogous system loaded with DCFH, leading to $G' \approx G'_{DCFH}$ at DP 14 wt%.

Finally, it deserves here noticing that the drop of G' observed in the DP14 sample loaded with DCFH should result in a strong variation of the quasi-Bragg peaks width. Nevertheless, because of the diffuse scattering superimposed to the SAXS patterns, the Caillé analysis¹⁵⁰ was not practicable (see Fig. 3.4.6).

3.5 Conclusions

We tested two novel cationic nanocarriers both based on monoolein, lauroylcholine and water system, namely a fluid and a gel formulation.

The first one is a liposomal formulation characterized for its physicochemical, cytotoxicity, and drug release features. In spite of the very fast method of preparation (about 15 min) and the absence of any method for the improvement of particle size, Cryo-TEM, SAXS, and DLS experiments highlighted that monoolein and lauroylcholine self-aggregate to form a fairly low polydispersed, robust liposome nanostructure.

Microscopy investigation of living cells and cell viability assays demonstrated that, at short exposure time and low LCh content, liposomes are not toxic. Differently, at long exposure time and/or for high LCh content, they cause extensive cells death. Lipid droplets accumulation also shown that LCh favors internalization. In addition, it was found that at high concentrations and for a short-term treatment, LCh provoked a statistically significant toxic effect that cells were able to repair at longer incubation time, while MO did not affect cells viability at all. On the ground of these results, it can be inferred that the synergistic effects of MO and LCh, regarded as membrane penetration enhancers, is accountable for the observed cytotoxicity of liposome formulations. Another aspect that should be considered is the local concentration of the two penetration components that, with respect to the MO or LCh solutions, is much higher when the cells are exposed to the liposomes formulations, thus provoking greater damages to the cell plasma membrane and intercellular membranes.

The efficacy of a skin penetration enhancer depends on composite physicochemical factors, as well as whether the enhancer is used alone or in combination.¹⁵¹ And the strength of penetration is usually directly proportional to skin irritation (i.e., cytotoxicity).¹⁵² Indeed, the action of an effective penetration enhancer cannot be limited to the skin superficial layers. Rather, diffusing through the SC it reaches the viable epidermis (exactly the scope to which the nanocarrier is designed for). There, the same factors that improve the drug penetration may alter the keratinocyte membranes, thus provoking cytotoxicity. Therefore, the development of an effective drug delivery system able to enhance skin penetration without altering the normal cell viability can be regarded as a real challenge.

The skin penetration mechanism is highly debated, and different hypothesis have been proposed to explain the superior liposome efficiency in dermal and transdermal drug release. These include intact vesicles skin penetration (ultraflexible liposome), vesicle adsorption to and/or fusion with the SC (increased partitioning of the drug into the skin), and structural loosening of the intercellular lipid matrix due to the penetration enhancing action of the vesicle components.⁶⁴ Deformability test and release data ruled out that the cationic liposomes discussed here may cross the skin intact. Definitely, given their low flexibility, it is difficult to

believe they can pass through the (one order of magnitude smaller) skin intercellular path. In addition, this fact may explain the negligible amount of drug found in the receptor compartment of the Franz cell. Once out of the liposome nanostructure the hydrophobic DCFH remains embedded into the skin rather than diffuse into the physiological solution. Conversely, taking into account the particular composition of the proposed nanocarrier, it is very likely that both MO and LCh alter the intercellular lipid matrix, facilitating drug penetration through the SC and accumulation into the viable epidermis. On such basis, this novel formulation can be regarded as an useful nanocarrier for topical drug release, when the systemic delivery ought to be kept to the minimum.

The second nanocarrier concerns a vesicle gel formulation endowed of very long kinetic stability. Its morphological and viscoelastic features have been discussed. Starting from liposomal formulation previously described, and increasing the dispersed phase (DP) content at constant monoolein/lauroylcholine chloride ratio, a vesicular lipid gel can be obtained. Above a dispersed phase content of 13 % wt, a transition from sol- to gel-vesicle system was ascertained through linear viscoelastic experiments. SAXS and cryo-TEM results showed that the most concentrated formulation (DP14) is composed by closely packed vesicles possessing an oligo-lamellar structure (OLV), both the techniques yielding similar interbilayer distance ($d = 21$ nm and 20 nm, from cryo-TEM and SAXS, respectively). The thermal stability of the highest concentrated formulation was assessed via SAXS measurements performed at 25, 32 and 55 °C. Upon water dilution of concentrated vesicle dispersions the nanostructure of the resulting aggregates, containing about 4 wt% of DP, were re-investigated by SAXS, cryo-TEM and DLS to check morphology and long-term stability. All these techniques confirmed that the vesicle solution obtained by dilution is very similar to that prepared by simply dispersing monoolein and lauroylcholine chloride in water at the same concentration. Rheological results showed a typical shear-thinning behavior observed in the majority of vesicle dispersions. In particular, the analysis of the dynamic elastic modulus suggested that the inclusion of hydrophobic acid diclofenac into the lipid bilayer can lead to an increased film rigidity. Within the panorama of vesicular gels, it should be highlighted that the preparation of the gel system here described is easy and very fast, and does not require high-pressure homogenization or organic solvents. These are a number of important points in view of a possible scale-up. Moreover, the elastic rheological response of densely packed vesicles (vesicle gels), also combined to the shear-thinning effect, may rapidly result in a commercially available product valuable in the pharmaceutical and cosmetic field.

The main aim of my Ph'D project was to prepare and to characterize lipid based formulations for drug delivery. At the present state of the art, these two lipid based formulations constitute a powerful and stimulating nanostructured biomaterials that can be easily modulated to tune drug delivery structural properties and controlled drug release performance.

4 Chapter

4.1 Emulsions stabilized by liquid crystals

4.1.1 Introduction

Previous works demonstrated that thermodynamically stable LC phases, preferentially with lamellar or hexagonal nanostructure, can be used as dispersing medium to obtain very stable formulations that may effectively host different types of bioactive molecules. Particularly Mele et al.^{42,43} studied several ternary and pseudo-ternary systems involving glycerol monooleate (MO), water and other components, such as glycerol trioleate (GTO) diglycerol monooleate (DMO) etc. The investigated MO based phase diagrams were shown to share some peculiar features, namely a narrow microemulsion region along with a large area where H_2 and L_α LC phases coexist and, finally, an emulsion region stabilized by H_2 and L_α LC phases.

With the aim of preparing new, cheap, stable, and biocompatible formulations, a preliminary characterization, focused on emulsion region of the ternary system lecithin (LCT), GTO and water, was performed and tested as topical drug delivery system using the model protein Lysozyme (LSZ).

The LCT/GTO/W partial phase diagram was investigated by visual inspection and optical microscopy in polarized light (PLM), small angle X-ray scattering (SAXS) and 2H NMR spectroscopy to determine type, number of phases present and structural parameters. The choice of LCT/GTO mixtures, having a 85/15 (Line A) and 90/10 (Line B) mass ratio corresponds to the emulsion region previously studied in the MO-based systems. LCT is known to favour microstructures having an average zero curvature. The choice of material characterized by technical purity was dictated by the fact that these formulations are of applied interest. Generally, very pure materials are not used for industrial purposes, due to economical balance requirements. Before introducing the ternary systems, we recall relevant data on the surfactant/water systems. In the LCT/W system, at low water content, a variety of temperature-dependent phases are observable (Figure 4.1). At 25 °C and water content above 10 % a lamellar structure (L_α) becomes predominant. At 21 °C and 40-44 wt % water content, the excess of water brings about the formation of a second phase constituted by a dispersion of L_α liquid crystalline particles. Temperature increase causes melting of the L_α phase with the formation of an isotropic liquid at about 220 °C.⁵⁷

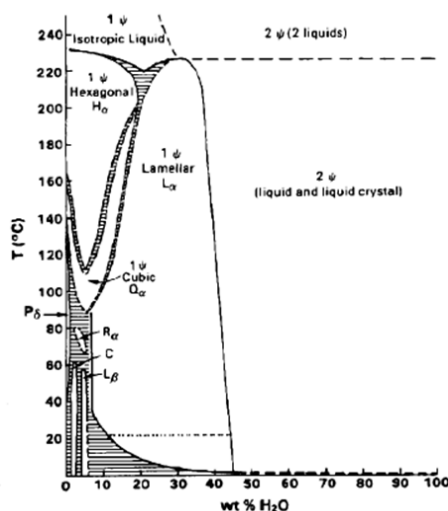


Figure 4.1: The phase diagram for the binary system of lecithin/water. Main phases: LC- L_α L_β : liquid crystalline phases with lamellar structure; LC-Q: liquid crystalline viscous isotropic phase with cubic structure; LC- H_{II} : liquid crystalline with reversed hexagonal structure.

4.1.2 Experimental section

Samples were prepared by weighing the components into glass tubes (diameter, 5 mm), were homogenized by repeated cycles of heating, centrifuged at 2000 rpm, and stored at 25 °C for 1 week before any measurement was taken. The observation of macroscopic properties of the samples (phase number, physical state, homogeneity, and birefringence) at 25 °C allowed a preliminary phase diagram characterization. Emulsion samples for optical microscopy analysis were prepared by addition of water to the other components up to the desired composition into sample tubes. Emulsions samples loaded with bioactive molecule have been prepared replacing a stock solution of the drug (10 mg/mL) dissolved in Phosphate Buffer Saline solution (PBS pH=7.4, 10 mM) to water.

The tubes were stored in a thermostatic oven at 25 °C, observed daily, and centrifuged prior to optical microscopy analysis. All samples appear as yellow viscous semi-fluid formulations which exhibit no macroscopic phase separation.

The partial phase diagrams, at 25 °C, of the ternary LCT/GTO/W is reported in Figure 4.2. Figure 4.3 a-c reports some optical micrographs, at 25 °C, in polarized light of 1-week-old samples, which clearly identify the main anisotropic LC phases observed in the system.

Along the two water dilution Line A and Line B the investigated samples display a phase behavior similar to that reported by Mele et al., with some differences in the proximity of the surfactant corner of the phase diagrams. Indeed, the two-phase region (L_α and H_{II}) disappears, the effect of 10-15 wt % of GTO added to LCT leads to a small region of reverse hexagonal (H_{II}) LC phase that persists up to 5 wt % of water content only. It can be argued that the presence of the hydrophobic molecule GTO allows for the formation of a reverse LC hexagonal phase, which is not observed in the binary LCT/W system at room temperature. Moreover, GTO confers to the mixture the fluidity needed to produce a suitably dispersing medium for water

droplets, as previously reported. The H_{II} LC phase was confirmed either through optical microscopy or SAXS.

With increasing water content a two-phase region was found for the sample of Line B having 10 wt% of water. For a water content higher than 10 wt%, similarly to the MO/GTO/W system,^{42,43} a stable emulsion region forms where the emulsion is stabilized by a mixture of both H_{II} and L_{α} LC phases. In the case of LCT/GTO/W system only the lamellar phase was clearly identified within the emulsion region. This emulsion is stable for several months if stored at 4 °C. However, when left at room temperature, it develops moulds after a few weeks, since no preservatives were added in the formulations at this early stage of the investigation.

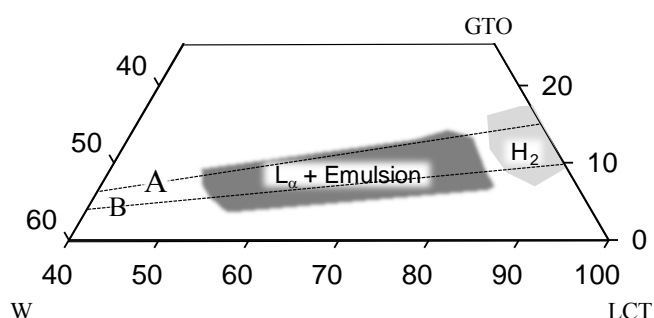


Figure 4.2: Schematic and partial diagram of the ternary system lecithin/glycerol trioleate/water (LCT/GTO/W) at 25 °C. Line A and B represent lecithin/ glycerol trioleate dilution line having a 85/15 and 90/10 mass ratio respectively.

The optical micrographs reported in Figure 4.3a and b show two samples of the Line B, which contain 5 and 25 wt % of water respectively: a birefringent texture typical of the hexagonal and lamellar phase respectively can be seen. Figure 4.3c shows the optical micrograph obtained for a sample in the emulsion region having LCT/GTO/W = 58/11/31. Here, besides a dominant lamellar texture, several water polydisperse droplets can be identified.



Figure 4.3: Optical microscopy: (a) Typical sample, containing 5 wt % of W, in the LC H_2 region of the LCT/GTO 90/10 mass ratio line. (b) Sample containing 25 wt % of W in the emulsion region for the LCT/GTO 90/10 mass ratio. (c) Sample containing 20 wt % of W in the emulsion region for the LCT/GTO 85/15 mass ratio.

The lamellar nanostructure of the matrix was confirmed by SAXS patterns. Figure 4.4 shows the clear L_α patterns of the samples containing 30% of water for both the dilution lines A and B.

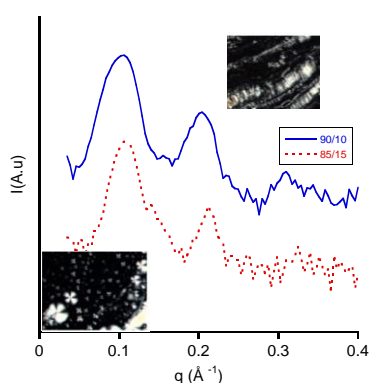


Figure 4.4: SAXS patterns and PLM images (20X magnification) of representative samples: LCT/GTO (85/15)/W 30 % and LCT/GTO (90/10)/W 30 % at 25 °C.

The analysis of the SAXS patterns provide crucial information about the phase behavior and the typical parameters of nanostructure composing the system. Table 4.1 reports the parameters obtained for the whole system, including binary samples for both water dilution lines, at 25 °C. For the LCT/GTO binary system and up to 5 wt % (Line B) and 10 wt % (Line A) of water content, SAXS data show the typical hexagonal diffraction pattern, which do not appear in the binary system as mentioned above. Increasing the amount of water, diffraction patterns are those typical for lamellar LC phase whose interbilayer distance increases with increasing water content as expected.

Table 4.1. SAXS parameters obtained at 25 °C, for samples LCT/GTO equal to 90/10 and 85/15 mass ratio while increasing the amount of water. (a) Sample composition, (b) lipid volume fraction, (c) spatial group, (d) spacing parameter \pm SD, (e) bilayer thickness.

LCT/GTO/W ^a	Φ_{lip} ^b	Spatial group ^c	a (Å) ^d	d _B ^e
90.0/10.0	1.000	H _{II}	54.8 \pm 0.4	-
85.6/9.4/5.0	0.944	H _{II}	55.7 \pm 0.1	-
81.0/8.7/10.3	0.902	H _{II} L _{α}	60.1 \pm 0.9 63.4 \pm 14.9	55.5
76.5/8.5/15.0	0.852	L _{α}	52.5 \pm 0.2	44.7
72.2/8.0/19.8	0.802	L _{α}	55.3 \pm 1.1	44.1
63.2/7.0/29.8	0,704	L _{α}	60,9 \pm 0,6	42,8
58.6/6.4/34.9	0.654	L _{α}	67.2 \pm 0.5	43.9
54.1/6.0/39.9	0.605	L _{α}	67.6 \pm 0.0	40.8
85.0/15.0	1.000	H _{II}	53.2 \pm 0.7	-
80.4/14.2/5.4	0.950	H _{II}	56.8 \pm 0.1	-
76.5/13.5/10.0	0.899	H _{II}	58.2 \pm 0.1	-
72.3/12.7/15.0	0.851	L _{α}	52.8 \pm 0.0	45.0
68.0/12.0/20.0	0.803	L _{α}	55.6 \pm 0.0	44.6
63.7/11.3/25.0	0.759	L _{α}	59.7 \pm 0.1	44.9
59.5/10.5/30.0	0.704	L _{α}	58.4 \pm 0.6	41.1
55.3/9.7/35.0	0.653	L _{α}	70.0 \pm 0.3	45.8
51.1/8.9/40.0	0.605	L _{α}	79.3 \pm 1.1	47.9

Lamellar spacing in binary LCT/W system is around 63 Å,⁵⁷ and similar values are measured in the presence of GTO. Clearly, the insertion of the hydrophobic GTO oil within the LCT bilayers leaves the nanostructures almost unchanged, but at the same time confers the right softness to produce an emulsion that could not be obtained using the lamellar phase of the LCT/W system alone. The coexistence of the emulsion with the LC phase was investigated and confirmed via ²H NMR quadrupolar splittings. The analysis was performed replacing deuterated water (D₂O) to simple water to prepare the samples. The ²H nucleus has a spin quantum number I = 1, and therefore, it possesses an electric quadrupole moment. In anisotropic liquid-crystalline phases (e.g., hexagonal and lamellar phases), the interaction of the quadrupole moment with nearby electric field gradients gives rise to a ²H splitting. In isotropic phases (solutions and cubic phases), the interaction is averaged to zero by the rapid isotropic molecular motions, and thus, a single signal results. In multiphase

samples, due to slow deuteron exchange between the phases, the resultant ^2H spectrum is a superposition of the spectra of the individual phases. The ^2H NMR spectra of samples prepared with D_2O are reported in Figure 4.5. It can be noticed that, although a quadrupolar splitting can clearly be identified, the isotropic signal pertaining to the isotropic phase (i.e. the water droplets dispersed in the L_α LC phase), is predominant in all samples. Figure 4.5-a and b show the results obtained for samples of Line A and Line B respectively. Although the isotropic signal, due to non-structured water, is always predominant in all spectra, some considerations can be done about the shapes of the ^2H NMR signal. Particularly samples having 10 wt % of water, which are identified as hexagonal phase from SAXS pattern, show a ^2H quadrupolar splitting $\Delta\nu_q \sim 1700\text{-}1900$ Hz. Sample containing 30 wt % of water, which are identified as lamellar phases from SAXS pattern, show $\Delta\nu$ around 4000 Hz.

For samples containing 30 wt% of water the quadrupolar splitting can only be seen upon increasing the vertical scale as reported in the inset of Figure 4.5-a. It should be also remarked that the amplitude of the quadrupolar splittings observed for samples having 30 wt % of water is almost double of the hexagonal sample as expected from eq. 2.18.

This is a further confirmation of the occurrence of a lamellar LC phase which coexists with isotropic water droplets in the emulsion region. The occurrence of L_α LC phase in sample with 40 % of water, detectable by SAXS, has not clearly been evidenced by ^2H NMR.

This demonstrates the invariability of the amount of water involved in the thermodynamically stable lamellar LC phases. It can be concluded that the isotropic ^2H NMR signal belongs mainly to the water inside the droplets. Indeed, there is not fast exchange on the NMR chemical shift time scale.

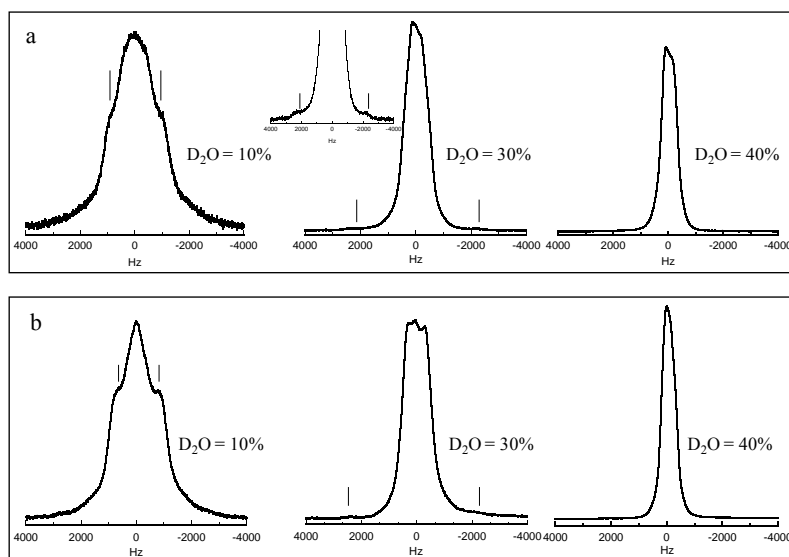


Figure 4.5 ^2H NMR spectra. **a)** LCT/GTO 85/15 with increasing amount of deuterated water. **b)** LCT/GTO 90/10 with increasing amount of deuterated water.

In this work, the LCT/GTO/W system has been partially investigated. The ternary phase diagram is characterized by a narrow H_{II} region along with a large area where L_{α} LC phase coexists with an emulsion region.

The stability toward phase separation is rather high also in the systems characterized by a high polydispersity of the water droplets. This is due to the presence of the LC phases as dispersing medium. The use of thermodynamically stable LC phases, preferentially with lamellar or hexagonal microstructure, allows for the dispersion of many types of liquids. In addition, the typical degradation processes such as creaming, flocculation, and Ostwald ripening are strongly slowed down.

4.2 Drug delivery system based on liquid crystals stabilized emulsion .

Only a limited number of emulsifiers is commonly regarded as safe to use for drug delivery, among them the most important are Pluronic F68[®] (Poloxamer 188), Tween 80[®] (Polysorbate 80) and lecithin. Compared with its synthetic alternatives, lecithin can be totally biodegraded and metabolized, since it is an integral part of biological membranes, making it virtually non-toxic. It is widely used in the food industry and in cosmetics. Due to its affinity for biological membranes, whose is a natural constituent, it promotes the absorption of different types of molecules. It belongs to the category of GRAS (Generally Recognized as Safe) chemicals and has no maximum daily dose (ADI).

For these reasons the LCT based liquid crystals stabilized emulsions (LCSE) were chosen to encapsulate the model protein lysozyme (LSZ). The structural effects of the encapsulation were characterized by SAXS, whereas a release test has been performed to investigate the performance of LCT-based emulsions as drug delivery systems for topical applications.

Major challenges in developing protein-encapsulated systems are (i) instability of encapsulated proteins, (ii) their incomplete release, and (iii) initial burst release. It is widely known that the chemical and mechanical stresses produced during the encapsulation process and the release period may exert damaging effects on the conformational and biological integrity (in terms of biological activity) of the protein.^{153–155} The sample with composition LCT/GTO/W 58/11/31 (w/w %) proved to be quite suitable for protein encapsulation. Empty and LSZ loaded (3 mg/g of lysozyme) samples were prepared in phosphate buffered saline (PBS) solution at physiological pH = 7.4. Samples were stored in a thermostatic oven at 4 °C for one week before any physico-chemical characterization. LCSEs prepared with buffer, and with buffer and LSZ, have the same macroscopic appearance of the corresponding formulation characterized in water, namely a yellow very viscous cream. The effect of PBS on the lamellar nanostructure is evidenced by SAXS lattice parameter (reported in table 5.2) which increases from 58 Å measured in water up to 66 Å in the presence of buffer saline solution at 25 °C. This effect can be explained as follow: despite being electrically neutral, phospholipid membranes attract each other as a result of mutually induced charge fluctuations.¹⁵⁶

Table 5.2: SAXS lamellar lattice parameters ($a \pm SD$) obtained increasing temperatures, for sample LCT/GTO/PBS = 58/11/31 empty or loaded with lysozyme.

Temperature °C	a (Å) Empty LCSE-PBS	a (Å) LSZ loaded LCSE-PBS
4	71.9 ± 0.2	65.0 ± 0.2
25	65.7 ± 0.7	62.6 ± 0.4
37	63.6 ± 0.0	61.2 ± 0.3
55	61.6 ± 0.5	59.5 ± 0.4

Because of different dielectric properties of membranes and the intervening solvent, transient spontaneous electromagnetic fields in one membrane induce correlated fields in the neighboring membrane and vice

versa, thus resulting in an attractive force. This “charge fluctuation” (van der Waals) force is responsible for the spontaneous formation of stable multilamellar structures. When the attractive van der Waals force is exactly balanced by repulsive forces, equilibrium spacing between lamellae is established.^{156,157} Typically, as measured by small-angle X-ray scattering, the interlamellar spacing of neutral membranes in water is around the order of the membrane thickness itself. However, membrane spacing depends sensibly on the nature of the solvent. Therefore, any alteration of the repeat spacing with solvent composition is an indication of a shift in the balance of attractive and repulsive forces between membranes. The swelling of phospholipid bilayers by salt is driven mainly by the weakening of van der Waals attractive forces through screening of charge fluctuations.¹⁵⁸ Therefore, the main reason for the swelling of lamellar arrays with added salt is swelling of the water space between the bilayers, since salt has negligible effects on the thickness of phospholipid bilayers as reported by Petrache et al. 2006.¹⁵⁹ Protein addition produces an opposing effect, LSZ removes ions surrounding the bilayer consequently the screening of charges is weakened and the lattice parameter slightly decreases. Variable temperature SAXS experiments were performed to evaluate thickness and stability of lipid bilayer in the range 4 - 55 °C.

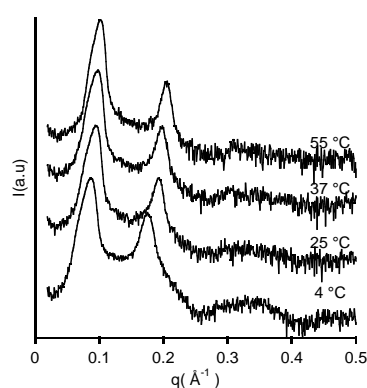


Figure 4.6: SAXS patterns reported as stack plot of the LCSE empty sample with composition LCT/GTO/PBS 58/11/31 (wt %) collected at 4-25-37 and 55 °C.

Lattice constant (a) of the L_{α} phase falls steadily and quite dramatically with increasing temperature due to the increase of hydrocarbon chains fluidity as a result of thermal vibrations. Figure 4.6 shows SAXS patterns for the empty sample LCT/GTO/PBS 58/11/31 in the range of the investigated temperatures. The lamellar order persists even at the lowest and the highest temperatures, thus suggesting a very high stability of this formulation.

4.2.1 *In-vitro* release experiments

The lysozyme loaded emulsion was used to investigate the release at a topical level using the Franz diffusion vertical cells apparatus in non-occlusive way, with an effective diffusion area of 1 cm². The Franz Cell apparatus is an in vitro skin permeation assay frequently used in formulation development. It does allow formulators to determine whether a particular formulation delivers an active agent through the skin-like membrane. It consists of two primary chambers separated by a cellulose acetate membrane. Membranes were

allowed to equilibrate with the receptor phase for 2h before charging each donor compartment with the formulations. The tested formulation is applied to the membrane via the top chamber. The bottom chamber contains a solution of PBS 12 mM, pH = 7.4 as receptor liquid which is maintained at a constant temperature of 37 °C to simulate physiological conditions. One gram of LCSE loaded with 3 mg/g of LSZ protein was put in contact with the membrane and aliquots of samples are withdrawn at regular intervals, during 24 hours, from the bottom chamber for analysis. The release experiment was performed 3 times for each formulation.

The amount of permeated LSZ was determined through UV-Vis spectrophotometer at 280 nm wavelength. Two other systems were used as control formulations: an agar gel and a LCT lamellar phase containing 35 wt% of PBS solution, both loaded with 3 mg/g of LSZ. Release trends are reported in Figure 4.7.

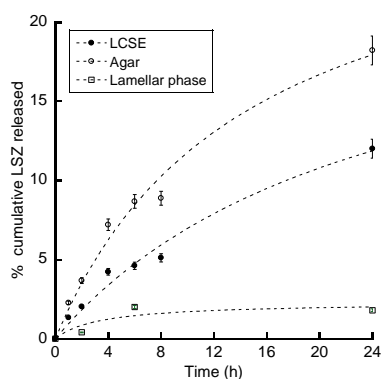


Figure 4.7: In vitro release across cellulose acetate membrane of LSZ after 24 h exposure from LCSE, Agar gel and lamellar phase with composition LCT/PBS 65/35 (% w/w). The cumulated permeated amounts are expressed as % of applied dose (mean \pm SD for n = 3 samples).

The profile of the release obtained for LCSE formulation was almost linear with time, with no detectable time lag. The Agar gel initially releases a greater amount of protein than the LCSE formulation, resulting in a faster release kinetics. The LCSE system is able to release the protein more slowly and for a longer time than the Agar system. The LCT pure lamellar phase system used as control contains the same LCT/PBS mass ratio as the LCSE formulation: they differ only for the absence of GTO in the lamellar LCT/PBS sample. This latter sample shows a very poor release profile. Only 2% of the applied dose was released after 24 h, compared to 10% of released lysozyme from LCSE formulation. Consequently the comparison of the relative release profiles (LCT/PBS vs LCSE) suggests that GTO presence in LCSE improves release performance. The presence of a liquid crystalline phase in the emulsion prevents the “burst release”, usually recognized as unwanted effect in pharmaceutical formulations, as well as poor release showed by pure LC lamellar phase. It should also be remarked that the release profile from LCSE suggests the feasibility of a sustained release. A protein activity assay, based on turbidimetric measurements, was then performed to assess activity preservation of LSZ after the preparation of the formulation and the release experiment. The assay is based

on the lytic ability of lysozyme towards *Micrococcus lysodeikticus*.^{160,161} The results of the analysis of samples withdrawn at different times indicate that about 30% of the LSZ released by LCSE formulation preserves its biological activity. It should be noticed that this last result is quite promising although not particularly good. However it is worth recalling that proteins are very complex molecules to carry and preserve, therefore a simpler release experiment from LCSE formulation was performed using the very stable bioactive molecule caffeine. LCSE system encapsulating 3 mg/g of caffeine was characterized through SAXS, and release performance was tested through Franz cells apparatus using the same conditions described for LSZ. Figure 4.8 shows the SAXS pattern at 25 °C of LCSE sample with composition LCT/GTO/PBS 58/11/31 wt % containing 3 mg/g of caffeine.

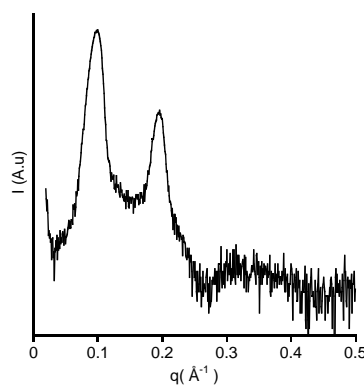


Figure 4.8: SAXS pattern collected at 25 °C for the LCSE sample having composition: LCT/GTO/PBS 58/11/31 (wt %) loaded with 3 mg/g of caffeine.

The first and second order diffraction of lamellar phase are visible at $q_1 = 0.097 \text{ \AA}^{-1}$ and $q_2 = 0.195 \text{ \AA}^{-1}$ respectively, which bring to calculate a lattice repeating distance of $64.6 \pm 0.1 \text{ \AA}$ which is to be compared with 65.7 \AA (see Table 4.2) obtained for the empty LCSE. This result suggests that caffeine, a small, non-ionic, hydrophilic molecule, substantially does not perturb the interlamellar spacing. Concerning topical release measurements, in a previous work Hiwale et al.¹⁶² used a monoolein based emulsion stabilized by LC phases (physical-chemical characterization was performed in 2003 and 2004 by Mele et al.^{42,43} to study the release of caffeine for transdermal/topical application. They found that during in vitro release experiments about 50% of caffeine loaded was released from the emulsion in 24 hours. The amount of permeated caffeine was determined through UV-vis spectrophotometer at 273 nm wavelength. Figure 4.9 shows in vitro release of caffeine from LCSE formulation within 15 hours. The release profile obtained is linear with time and quite rapid, with no detectable time lag. After 2 hours 14 % of caffeine was already released and about 80 % of the loaded caffeine was released from the emulsion after 15 hours.

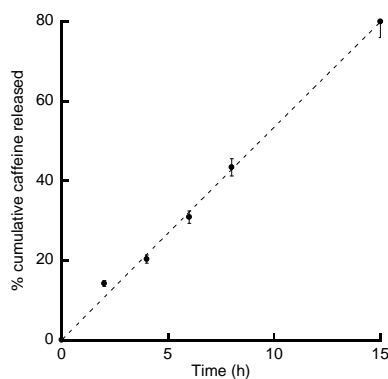


Figure 4.9: In vitro release across cellulose acetate membrane of caffeine after 15 h exposure from LCSE. The cumulated permeated amounts are expressed as % of applied dose (mean \pm SD for $n = 3$ samples).

Clearly the release of caffeine from our LCSE is much faster than that found for LSZ. Indeed macromolecules are expected to release more slowly than a small molecule. Caffeine shows a much faster release also compared to that reported for the analogous Monoolein-based emulsion, very likely due to different interactions with the phospholipid and monoglyceride polar groups. Remarkably, no burst release is observed in any case.

In conclusion the LCSE formulation with composition LCT/GTO/PBS 58/11/31 wt % here investigated was characterized through ^2H NMR and SAXS, whereas its performance as drug carrier was demonstrated using two different molecules, the protein lysozyme and the bioactive molecule caffeine. The full biocompatibility of the formulation ingredients along with the absence of burst release for the investigated cases allow to suggest LCSE as a promising topical drug carrier for sustained release. In fact, this formulation presents other advantages over conventional creams and ointments such as higher storage stability, good production feasibility, higher kinetic stability and in particular the absence of organic solvents in the preparation.

Bibliography

- (1) Schwartz J. W., Bartell, F. E., A M., P. *The Journal of Physical Chemistry* **1949**, 53, 1467.
- (2) Schwartz J. W.; Berch,, A. M. . P. *J. Surface Active Agents and Detergents: 1977, II.*
- (3) Evans H., D. F. . W. *The colloidal domain: where physics, chemistry, and biology meet;*; York, W.-V. N., Ed.; 1994.
- (4) Tanford, C. *The Hydrophobic Effect: Formation of Micelles and Biological Membranes 2d Ed*; J. Wiley., 1980.
- (5) Mitchell B. W., D. J. . N. *J. Chem. Soc. Faraday Trans. II* **1981**, 77, 601.
- (6) Drummond, C. J.; Fong, C. *Current Opinion in Colloid & Interface Science* **1999**, 4, 449–456.
- (7) Landh, T.; Larsson, K. Particles, method of preparing said particles and uses thereof **1996**.
- (8) Barauskas, J.; Johnsson, M.; Tiberg, F. *Nano letters* **2005**, 5, 1615–9.
- (9) Patrick T., S. *Current Opinion in Colloid & Interface Science* **2005**, 10, 274–279.
- (10) Kåre, L. *Current Opinion in Colloid & Interface Science* **2009**, 14, 16–20.
- (11) Yaghmur, A.; Glatter, O. *Advances in Colloid and Interface Science* **2009**, 147-148, 333–342.
- (12) Sessa, G.; Weissmann, G. *Journal of Lipid Research* **1968**, 9, 310–318.
- (13) Dass, C. R.; Choong, P. F. M. *Journal of Controlled Release* **2006**, 113, 155–163.
- (14) Campbell, R. B.; Fukumura, D.; Brown, E. B.; Mazzola, L. M.; Izumi, Y.; Jain, R. K.; Torchilin, V. P.; Munn, L. L. *Cancer Research* **2002**, 62, 6831–6836.
- (15) Mezei, M.; Gulasekharam, V. *Life sciences* **1980**, 26, 1473–1477.
- (16) Cevc, G.; Blume, G. *Biochimica et Biophysica Acta (BBA) - Biomembranes* **1992**, 1104, 226–232.
- (17) Cevc, G. In *Handbook of Biological Physics*; Lipowsky, R.; Sackmann, E., Eds.; North-Holland, 1995; Vol. Volume 1, pp. 465–490.
- (18) Cevc, G. *Critical reviews in therapeutic drug carrier systems* **1996**, 13, 257–388.
- (19) Planas, M. E.; Gonzalez, P.; Rodriguez, L.; Sanchez, S.; Cevc, G. *Anesthesia & Analgesia* **1992**, 75, 615–621.
- (20) Lee, E. H.; Kim, A.; Oh, Y.-K.; Kim, C.-K. *Biomaterials* **2005**, 26, 205–210.
- (21) Graham, T. *Journal of the Chemical Society* **1864**, 17, 318–327.
- (22) Brandl, M.; Gregoriadis, G. *Biochimica et Biophysica Acta (BBA) - Biomembranes* **1994**, 1196, 65–75.
- (23) Tardi, C.; Drechsler, M.; Bauer, K. H.; Brandl, M. *International Journal of Pharmaceutics* **2001**, 217, 161–172.
- (24) Gradzielski, M. *J. Phys.: Condens. Matter* **2003**, 15, R655.
- (25) BJ Alder, T. E. W. *The Journal of Chemical Physics* **1957**, 27, 1208.
- (26) Grohganz, H.; Tho, I.; Brandl, M. *European Journal of Pharmaceutics and Biopharmaceutics* **2005**, 59, 439–448.
- (27) Mozafari, M. R. In *Nanocarrier Technologies*; Mozafari, M. R., Ed.; Springer Netherlands, 2006; pp. 1–16.
- (28) Sein, A.; Engberts, J. B. F. N.; Van der Linden, E.; Van de Pas, J. C. *Langmuir* **1993**, 9, 1714–1720.

- (29) Brandl Drechsler, M., Bachmann, D., Tardi, C., Schmidtgen, M., Bauer, K.H., ., M. *Int.J. Pharm.* **1998**, 187–199.
- (30) Kaiser, N.; Kimpfler, A.; Massing, U.; Burger, A. M.; Fiebig, H. H.; Brandl, M.; Schubert, R. *International Journal of Pharmaceutics* **2003**, 256, 123–131.
- (31) Farkas, E.; Schubert, R.; Zekó, R. *International Journal of Pharmaceutics* **2004**, 278, 63–70.
- (32) B. Binks BP. Binks *The Royal Society of Chemistry: Cambridge, Englan* **1998**.
- (33) T. Tadros *Emulsion Science and Technology* **2009**, 1.
- (34) Robins, M. M. *Curr. Opin. Colloid Interface Sci* **2000**, 265–272.
- (35) Taylor, P. *Colloids Surf A Physicochem Eng Asp* **1995**, 175–185.
- (36) F. Groeneweg P. Jaeger, J.J.M. Janssen, J.A. Wieringa, J.K. Klahn,, W. G. M. A. *Chem Eng Res Des* **1998**, 76 , 55–63.
- (37) Friberg, S. *J Colloid Interface Sci* **1971**, 37, 291–295.
- (38) Larsson, K. Z. *Physik Chem. Neue Folge* **1967**, 56, 173–198.
- (39) K. Shinoda, S. F. *Emulsions and solubilization*; 1986.
- (40) T. Engels W. von Rybinski,, T. F. *Colloids Surf A Physicochem Eng Asp*, **1995**, 99, 141–149.
- (41) T. Engels, W. R. *J Mater Chem* **1998**, 8, 1313–1320.
- (42) S. Mele F. Caboi, M. Monduzzi, S. M. *Langmuir* **2004**, 20, 5241–5246.
- (43) S. Mele M. Monduzzi, S. M. *Colloids Surf A Physicochem Eng Asp* **2003**, 228, 57–63.
- (44) Otto A Kelly CL, Dederen JC, Hadgraft J, du Plessis J:, W. J. W. *Skin Pharmacol Physiol* **2010**, 23, 273–282.
- (45) Strashun, S. I. No Title **1951**.
- (46) Larsson, K. *J. Phys. Chem.* **1989**, 93, 7304–7314.
- (47) Larsson G. J., K. . L. *Disp. Sci. Technol* **1982**, 3, 61.
- (48) Larsson, K. *Nature* **1983**, 304, 664.
- (49) Larsson, K. *Lipids - Molecular Organization, Physical Functions and Technical Applications.*; ; Dundee, T. O. P. L. ., Ed.; 1994.
- (50) Chung J., Um, J. Y., Kwon, I. C., Jeong, S. Y., H., K. *Diabetologia* **2002**, 45, 448–451.
- (51) Chang, C. M. B. *R. Pharm. Res*; 1994; Vol. 11.
- (52) Lopes J. L. C., Oliveira, D. C. R., Thomazini, J. A., Garcia, M. T. J., Fantini, M. C. A., Collett, J. H., Bentley, M., L B., L. *European Journal of Pharmaceutics and Biopharmaceutics* **2006**, 63, 146–155.
- (53) Chang R., C. . B. *J. Controlled Release* **1997**, 46, 215–222.
- (54) Dong, Y.-D.; Larson, I.; Hanley, T.; Boyd, B. J. *Langmuir* **2006**, 22, 9512–9518.
- (55) Myher, J. J.; Kuksis, A.; Breckenridge, W. C.; McGuire, V.; Little, J. A. *Lipids* **1985**, 20, 90–101.
- (56) H Fang, R. J. L. and R. B. G. *The Journal of Biological Chemistry*, 264, 8026-8032. **1989**, 264, 8026–8032.
- (57) Small, D. M. *Journal of Lipid Research* **1967**, 8, 551–557.
- (58) Rydhag, L. *Fette, Seifen, Anstrichmittel* **1979**, 81, 168–173.
- (59) Wildnauer, R. H.; Bothwell, J. W.; Douglass, A. B. *J Investig Dermatol* **1971**, 56, 72–78.
- (60) Sweeney, T. M.; Downing, D. T. *J Investig Dermatol* **1970**, 55, 135–140.

- (61) Bolzinger, M.-A.; Briançon, S.; Pelletier, J.; Chevalier, Y. *Current Opinion in Colloid & Interface Science* **2012**, *17*, 156–165.
- (62) Cevc, G. *Advanced drug delivery reviews* **2004**, *56*, 675–711.
- (63) Maghraby, G. M. M. El; Williams, A. C.; Barry, B. W. *Journal of Pharmacy and Pharmacology* **2006**, *58*, 415–429.
- (64) El Maghraby, G. M.; Barry, B. W.; Williams, A. C. *European Journal of Pharmaceutical Sciences* **2008**, *34*, 203–222.
- (65) Kirjavainen, M.; Urtti, A.; Jääskeläinen, I.; Marjukka Suhonen, T.; Paronen, P.; Valjakka-Koskela, R.; Kiesvaara, J.; Mönkkönen, J. *Biochimica et Biophysica Acta (BBA) - Lipids and Lipid Metabolism* **1996**, *1304*, 179–189.
- (66) Kirjavainen, M.; Urtti, A.; Valjakka-Koskela, R.; Kiesvaara, J.; Mönkkönen, J. *European Journal of Pharmaceutical Sciences* **1999**, *7*, 279–286.
- (67) Shi, Z.; Curiel, D. T.; Tang, D. *Vaccine* **1999**, *17*, 2136–2141.
- (68) *Human Gene Therapy*. November **2000**, *11*, 2253–2259. .
- (69) Franz, T. J. *J Investig Dermatol* **1975**, *64*, 190–195.
- (70) Sato, S.; Kim, S. W. *International Journal of Pharmaceutics* **1984**, *22*, 229–255.
- (71) C. Bertin J.C. Pittet, P. Beau, P. Pineau, M. Massonneau, C. Robert, J. Hopkins, H. Z. *J Cosmet Sci* **2001**, *59*, 199–210.
- (72) B.J. Bernes *Dynamic Light Scattering*; Wiley, U. S. of A., Ed.; 1976.
- (73) Pershan, P. *191r lab manual*; Physics, H., Ed.; 1982; pp. A-7-1 – A-7-6.
- (74) Demidov, A. A.; Braginskaya, O. V; Rubin, L. B. *Journal of Applied Spectroscopy* **1984**, *41*, 1210–1213.
- (75) N.C. Santos and M.A.R.B. Castanho *Biophysical. J.* **1996**, *71*, 1641–1646.
- (76) Dukhin B.V., S. S. & D. “*Electrokinetic Phenomena*”, ; Sons, J. W. and, Ed.; 1974.
- (77) Lyklema, J. *Fundamentals of Interface and Colloid Science*; 1995; Vol. 2, pp. 3–208.
- (78) Glatter, O. *Journal of Applied Crystallography* **1977**, *10*, 415–421.
- (79) Svergun, D. I.; Semenyuk, A. V; Feigin, L. A. *Acta Crystallographica Section A* **1988**, *44*, 244–250.
- (80) Orthaber, D.; Bergmann, A.; Glatter, O. *Journal of Applied Crystallography* **2000**, *33*, 218–225.
- (81) Pencer, J.; Hallett, F. R. *Physical Review E* **2000**, *61*, 3003–3008.
- (82) Balgavý, P.; Dubničková, M.; Kučerka, N.; Kiselev, M. A.; Yaradaikin, S. P.; Uhríková, D. *Biochimica et Biophysica Acta (BBA) - Biomembranes* **2001**, *1512*, 40–52.
- (83) Schmiedel, H.; Jörchel, P.; Kiselev, M.; Klose, G. *The Journal of Physical Chemistry B* **2000**, *105*, 111–117.
- (84) Pabst, G.; Rappolt, M.; Amenitsch, H.; Laggner, P. *Physical Review E* **2000**, *62*, 4000–4009.
- (85) Engelhardt, H.; Duwe, H. P.; Sackmann, E. *J. Physique Lett.* **1985**, *46*, 395–400.
- (86) Wiener, M. C.; Suter, R. M.; Nagle, J. F. *Biophysical Journal* **1989**, *55*, 315–325.
- (87) Pabst, G.; Koschuch, R.; Pozo-Navas, B.; Rappolt, M.; Lohner, K. *Journal of Applied Crystallography* **2003**, *63*, 1378–1388.
- (88) Barnes, H. A. *A Handbook of Elementary Rheology*; Institute of Non-Newtonian Fluid Mechanics, U. of W., Ed.; 2000.
- (89) Martin, J. B.; Reddy, B. D.; Griffin, T. B.; Bird, W. W. *Engineering Structures* **1987**, *9*, 171–176.

- (90) Bleasdale G. J. T., T. A. . T. *In Organized Solutions*; Friberg Lindman, B., Eds.; M. Dekker: New York, S. E., Ed.; 1992; Vol. 44.
- (91) Malmsten, M. *Soft Matter* **2006**, *2*, 760–769.
- (92) Soussan, E.; Cassel, S.; Blanzat, M.; Rico-Lattes, I. *Angew. Chem Int. Ed.* **2009**, *48*, 274–288.
- (93) Hiwale, P.; Lampis, S.; Conti, G.; Caddeo, C.; Murgia, S.; Fadda, A. M.; Monduzzi, M. *Biomacromolecules* **2011**, *12*, 3186–3193.
- (94) Zha, L.; Banik, B.; Alexis, F. *Soft Matter* **2011**, *7*, 5908–5916.
- (95) Cuomo, F.; Lopez, F.; Ceglie, A.; Maiuro, L.; Miguel, M. G.; Lindman, B. *Soft Matter* **2012**, *8*, 4415–4420.
- (96) Liong, M.; Lu, J.; Kovoichich, M.; Xia, T.; Ruehm, S. G.; Nel, A. E.; Tamanoi, F.; Zink, J. I. *ACS Nano* **2008**, *2*, 889–896.
- (97) Sun, C.; Lee, J. S. H.; Zhang, M. *Adv. Drug Deliv. Rev.* **2008**, *60*, 1252–1265.
- (98) Bhattacharyya, M. S.; Hiwale, P.; Piras, M.; Medda, L.; Steri, D.; Piludu, M.; Salis, A.; Monduzzi, M. *J. Phys. Chem. C* **2010**, *114*, 19928–19934.
- (99) Caboi, F.; Murgia, S.; Monduzzi, M.; Lazzari, P. *Langmuir* **2002**, *18*, 7916–7922.
- (100) R. Angius D. Berti, P. Baglioni, M. Monduzzi, S. M. *J. Phys.: Condens. Matter* **2006**, S2203.
- (101) Murgia, S.; Caboi, F.; Monduzzi, M. *Chem. Phys. Lipids* **2001**, *110*, 11–17.
- (102) Murgia, S.; Lampis, S.; Angius, R.; Berti, D.; Monduzzi, M. *J. Phys. Chem. B* **2009**, *113*, 9205–9215.
- (103) Shah, J.; Sadhale, Y.; Chilukuri, D. M. *Adv. Drug Deliv. Rev.* **2001**, *47*, 229–250.
- (104) Manconi, M.; Isola, R.; Falchi, A. M.; Sinico, C.; Fadda, A. M. *Colloids and surface B* **2007**, *57*, 143–151.
- (105) S. Murgia, S. Lampis, P. Zucca, E. S. and M. M. *J. Am. Chem. Soc.* **2010**, 16176–16184.
- (106) Peetla, C.; Stine, A.; Labhasetwar, V. *Mol. Pharm.* **2009**, *6*, 1264–1276.
- (107) Marques, E. F. *Langmuir* **2000**, *16*, 4798.
- (108) Tayebi, L.; Vashaee, D.; Parikh, A. N. *Chem. Phys. Chem.* **2012**, *13*, 314–322.
- (109) Gradzielski, M. *Curr. Opin. Colloid Interface Sci.* **2004**, *9*, 149–153.
- (110) Brandl, M.; Reszka, R. In *Proc Int Symp Control Release Bioact Mater*; 1995; Vol. 22, pp. 472–473.
- (111) Brandl, M.; Bachmann, D.; Reszka, R.; Drechsler, M. Unilamellar liposomal preparations with high active substance content **2002**.
- (112) Qi, N.; Tang, X.; Lin, X.; Gu, P.; Cai, C.; Xu, H.; He, H.; Zhang, Y. *Inter. J. Pharm.* **2012**, *427*, 234–241.
- (113) Tian, W.; Schulze, S.; Brandl, M.; Winter, G. *J. Controlled Rel.* **2010**, *142*, 319–325.
- (114) Puglia, C.; Trombetta, D.; Venuti, V.; Saija, A.; Bonina, F. *J. Phar. Pharmacol.* **2010**, *56*, 1225–1232.
- (115) Foldvari, M. *Journal of microencapsulation* **1996**, *13*, 589–600.
- (116) Carafa, M.; Marianucci, C.; Di Marzio, L.; Rinaldi, F.; Di Meo, C.; Matricardi, P.; Alhaique, F.; Coviello, T. *Journal of Phar. & Pharmaceut. Sci.* **2011**, *14*, 336–346.
- (117) Pavelic; Skalko-Basnet, N.; Filipovic-Grcic, J.; Martinac, A.; Jalsjenjak, I. *J. Contr. Rel.* **2005**, *106*, 34–43.
- (118) Elsayed, M. M. a; Abdallah, O. Y.; Naggar, V. F.; Khalafallah, N. M. *International journal of pharmaceutics* **2007**, *332*, 1–16.

- (119) Gonzalez-Rodriguez, M. L.; Rabasco, A. M. *Expert Opinion in Drug Delivery* **2011**, *8*, 857–871.
- (120) Cevc, G.; Shatzlein, A.; Richardsen, H. *Biochim. Biophys. Acta* **2002**, *1564*, 21–30.
- (121) Touitou, E.; Alkabes, M.; Dayan, N. *Pharm. Res.* **1997**, *S14*, 305–306.
- (122) Touitou, E.; Dayan, N.; Bergelson, L.; Godin, B.; Eliaz, M. *J. Control. Rel.* **2000**, *65*, 403–418.
- (123) Choi, M. J.; Maibach, H. I. *Skin Pharmacol. Physiol.* **2005**, *18*, 209–219.
- (124) Manosroi, A.; Khanrin, P.; Lohcharoenkal, W.; Werner, R. G.; Gotz, F.; Manosroi, W.; Manosroi, J. *Int. J. Pharm.* **2010**, *392*, 304–310.
- (125) Geusens, B.; Gele, M. Van; Braat, S.; Smedt, S. C. De; Stuart, M. C. A.; Prow, T. W.; Sanchez, W.; Roberts, M. S.; Sanders, N. N. *Advanced Functional Matererials* **2010**, *20*, 4077–4090.
- (126) Sinico, C.; Fadda, A. M. *Expert Opinion on Drug Delivery* **2009**, *6*, 813–825.
- (127) Neubert, R. H. H. *European Journal of Pharmaceutics and Biopharmaceutics* **2011**, *77*, 1–2.
- (128) Song, Y.-K.; Kim, C.-K. *Biomaterials* **2006**, *27*, 271–280.
- (129) Murgia, S.; Falchi, A. M.; Mano, M.; Lampis, S.; Angius, R.; Carnerup, A. M.; Schmidt, J.; Diaz, G.; Giacca, M.; Talmon, Y.; Monduzzi, M. *The journal of physical chemistry. B* **2010**, *114*, 3518–25.
- (130) Pabst, G. *Biophysical Reviews and Letters* **2006**, *1*, 57–84.
- (131) Greespan, P.; Mayer, E. P.; Fowler, S. D. *journal of cellular Biology* **1985**, *100*, 965–973.
- (132) Siegel, D. P.; Burns, J. L.; Chestnut, M. H.; Talmon, Y. *Biophysical Journal* **1989**, *56*, 161–169.
- (133) Lasic, D. D.; Joannic, R.; Keller, B. C.; Frederik, P. M.; Auvray, L. *Advances in colloid and interface science* **2001**, *89-90*, 337–49.
- (134) Dawson, K. A. *Curr. Opin. Colloid Interface Sci.* **2002**, *7*, 218–227.
- (135) Trappe, V.; Sandkühler, P. *Curr. Opin. Colloid Interface Sci.* **2004**, *8*, 4500–4949.
- (136) Briggs, J.; Chung, H.; Caffrey, M. *Journal De Physique Li* **1996**, 723–751.
- (137) Fujimoto, Y.; Onoduka, J.; Homma, K. J.; Yamaguchi, S.; Mori, M.; Higashi, Y.; Makita, M.; Kinoshita, T.; Noda, J.; Itabe, H.; Takanoa, T. *Biological and Pharmaceutical Bulletin* **2006**, *29*, 2174–2180.
- (138) Engelbrecht, T. N.; Schroeter, A.; Haub, T.; Neubert, R. H. H. *Biochimica et Biophysica Acta (BBA) - Biomembranes* **2011**, *1808*, 2798–2806.
- (139) Yen, C.-L. E.; Stone, S. J.; Koliwad, S.; Harris, C.; Farese, R. V. *Journal of Lipid Research* **2008**, *49*, 2283–2301.
- (140) Diaz, G.; Batetta, B.; Sanna, F.; Uda, S.; Reali, C.; Angius, F.; Melis, M.; Falchi, A. *Histochemistry and Cell Biology* **2008**, *129*, 611–621.
- (141) Ferreira, H.; Lúcio, M.; Lima, J. J. L. F. C.; Matos, C.; Reis, S.; Lucio, M. *Analytical and bioanalytical chemistry* **2005**, *382*, 1256–64.
- (142) Gradzielski, M. *Curr. Opin. Colloid Interface Sci.* **2011**, *16*, 13–17.
- (143) Cross, M. M. *J. Colloid Sci.* **1965**, *20*, 417–437.
- (144) Pusey, P. N.; Van Megen, W. *Nature* **1986**, *320*, 340–342.
- (145) Larson, R. G. *The Structure and Rheology of Complex Fluids*; Oxford University Press: New York, 1999.
- (146) Van der Vorst, B.; Van den Ende, D.; Mellema, J. *J. Rheol.* **1995**, *39*, 1183–1200.
- (147) Brown, M. F.; Thurmond, R. L.; Dodd, S. W.; Otten, D.; Beyer, K. *J. Am. Chem. Soc.* **2002**, *124*, 8471–8484.

- (148) Carboni, M.; Falchi, A. M.; Lampis, S.; Sinico, C.; Manca, M. L.; Schmidt, J.; Talmon, Y.; Murgia, S.; Monduzzi, M. *Advanced Healthcare Materials* **2012**, n/a–n/a.
- (149) Pan, J.; Tristram-Nagle, S.; Kučerka, N.; Nagle, J. F. *Biophys. J.* **2008**, *94*, 117–124.
- (150) Zhang, R.; Suter, R. M.; Nagle, J. F. *Phys. Rev. E* **1994**, *50*, 5047–5060.
- (151) Karande, P.; Mitragotri, S. *Biochimica et Biophysica Acta* **2009**, *1788*, 2362–2373.
- (152) Karande, P.; Jain, A.; Ergun, K.; Kispersky, V. *Proc. Nat Academy of Science USA* **2005**, *102*, 4688–4693.
- (153) Park, T. G.; Yong Lee, H.; Sung Nam, Y. *Journal of Controlled Release* **1998**, *55*, 181–191.
- (154) Schwendeman, S. P. *Critical reviews in therapeutic drug carrier systems* **2002**, *19*, 73–98.
- (155) Santo, V. E.; Duarte, A. R. C.; Gomes, M. E.; Mano, J. F.; Reis, R. L. *The Journal of Supercritical Fluids* **2010**, *54*, 320–327.
- (156) P., R. R.; A., P. V. *Hydration forces between phospholipid bilayers*; Elsevier: Amsterdam, PAYS-BAS, 1989; Vol. 988.
- (157) McIntosh, T. J.; McDaniel, R. V.; Simon, S. A. *Biochimica et Biophysica Acta (BBA) - Biomembranes* **1983**, *731*, 109–114.
- (158) Weissmann Bloomgarden, D., Kaplan, R., Cohen, C., Hoffstein, S., Collins, T., Gottlieb, A. Nagle, D., G. *Proc. Natl. Acad. Sci. U.S.A.* **1975**, *72*, 88–92.
- (159) Petrache, H. I.; S. Tristram-Nagle; D. Harries; N. Kučerka; J. F. Nagle; Parsegian., V. A. *J. Lipid Res.* **2006**, *47*, 302–309.
- (160) Jiang, Z.-L.; Huang, G.-X. *Clinica Chimica Acta* **2007**, *376*, 136–141.
- (161) M. Colilla M. Vallet-Regí, M. M. *Int. J. Nanomed.* **2008**, *4*, 403–414.
- (162) Hiwale, P.; Lampis, S.; Murgia, S.; Monduzzi, M. *Journal of Dispersion Science and Technology* **2012**, null–null.